FAILURE PROCESSES IN METAL MATRIX COMPOSITES

GENERAL ELECTRIC COMPANY

PREPARED FOR

AIR FORCE MATERIALS LABORATORY

21 DECEMBER 1973

AD · 773 · 192

REPORT DOCUMENTATION PAGE

READ INSTRUCTIONS
BEFORE COMPLETING FORM

1. REPORT NUMBER	2. GOVT ACCESSION NO.	3. RECIPIENT'S CATALOG NUMBER
AFML-TR-73-290		

4. TITLE *(and Subtitle)*

FAILURE PROCESSES IN METAL
MATRIX COMPOSITES

5. TYPE OF REPORT & PERIOD COVERED

Interim Report – Phase I
1 July 1972 to 1 October 1973

6. PERFORMING ORG. REPORT NUMBER

R73AEG428

7. AUTHOR(s)

J.E. Alexander and
R.G. Carlson

8. CONTRACT OR GRANT NUMBER(s)

F33615-72-C-1713

9. PERFORMING ORGANIZATION NAME AND ADDRESS

Materials & Process Technology Laboratories
General Electric Company
Cincinnati, Ohio 45215

10. PROGRAM ELEMENT, PROJECT, TASK AREA & WORK UNIT NUMBERS

11. CONTROLLING OFFICE NAME AND ADDRESS

Materials and Ceramic Division (LLC)
AFML, WPAFB, Ohio 45433

12. REPORT DATE

December 21, 1973

13. NUMBER OF PAGES

135

14. MONITORING AGENCY NAME & ADDRESS*(if different from Controlling Office)*

15. SECURITY CLASS. *(of this report)*

None

15a. DECLASSIFICATION/DOWNGRADING SCHEDULE

16. DISTRIBUTION STATEMENT *(of this Report)*

Approved for Public Release; Distribution Unlimited

17. DISTRIBUTION STATEMENT *(of the abstract entered in Block 20, if different from Report)*

18. SUPPLEMENTARY NOTES

19. KEY WORDS *(Continue on reverse side if necessary and identify by block number)*

Composites	Tensile	Torsion
Boron	Rupture	Shear
Aluminum	Fatigue	
Failure Mechanisms	Compression	
Metal Matrix	Impact	

20. ABSTRACT *(Continue on reverse side if necessary and identify by block number)*

Boron/Aluminum composites containing 50 v/o of 5.6 mil diameter B in two composite matrix materials (2024Al and 6061Al) consolidated from commercially available and continuous rolled bonded (CRB) tapes, have been evaluated in tensile, fatigue, compression, shear, torsion and rupture tests. Failure modes have been delineated and an extensive number of salient observations made. The information contained in this report will advance the state-of-the art in metal matrix composite, enhance the technology base and aid in future evaluation of failure responses in aluminum composites.

DD $_{1\ JAN\ 73}^{FORM}$ 1473   EDITION OF 1 NOV 65 IS OBSOLETE

IR-1713-(V)

FAILURE PROCESSES
IN
METAL MATRIX COMPOSITES

J. E. Alexander and R. G. Carlson

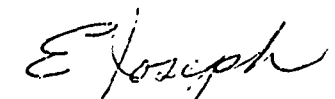Technical Report - Phase I

FOREWORD

This Phase I interim report covers the work performed on contract number F33615-72-C-1713. The work was performed by the Material and Process Technology Laboratories (MPTL) of the General Electric Company's Aircraft Engine Group. This program was sponsored by the Air Force Materials Laboratory under the technical direction of Mr. Erwin Joseph, Air Force Materials Laboratory, Metals Composite Branch, LLC, Wright Patterson Air Force Base, Ohio.

Personnel contributing to this program are Dr. R. G. Carlson, Program Manager, and Mr. J. E. Alexander, and Mr. G. P. Brandenburg as principal investigators, at GE/MPTL. Mr. R. L. Mehan performed the basic failure investigations at Space Science Laboratories, General Electric. Messrs, A. C. Losekamp and J. R. Sharkey are recognized for their work in quality assurance and general support of this program.

Publication of this report does not constitute the Air Force approval of the program's findings or conclusions. It is published principally for the exchange and stimulation of ideas.

This report covers the work performed during the period of 1 July 1972 to 1 October 1973 under Project 7351, Task 735107.

This technical report has been reviewed and is approved.

E. Joseph, Act Chief
Metals Composites Board
Metal & Ceramic Division

iii/iv

TABLE OF CONTENTS

LIST OF ILLUSTRATIONS

LIST OF TABLES

I. INTRODUCTION

It is currently being demonstrated that boron/aluminum composite material can be of significant benefit to the aerospace vehicles where light weight materials with high strength and stiffness are required. A major area of concern was to better understand the failure processes in metal matrix composites. In addition it was deemed beneficial to have an in depth characterization of the composite material behavior while being subjected to various types of loading.

The materials to be studied in this program were commercially available 50 v/o 5.6 mil boron reinforced 2024 and 6061 aluminum. The materials were purchased in diffusion bonded [22/0/-22/0]8 panels and in monolayer tapes. The main effort of evaluation was applied to tensile, axial and flexural fatigue and stress rupture testing. Compression, double lap shear and torsion creep properties were also evaluated. Of special importance to the use of these materials in aircraft engine blading are their response to cyclic thermal exposure and hard body ballistic impact. The effects of thermal exposure and impact on the materials properties mentioned above were also investigated. These efforts served or a basis for the more detailed material evaluation.

The basic failure mechanical in metal matrix filamentary composites was performed at General Electric's Space Sciences Laboratory using acoustic emission, in conjunction with other advanced techniques. A cursory analytical evaluation of composite material behavior determined by computer programs developed at GE/MPTL was performed to aid in the investigation.

This work is thought to be a complete and thorough evaluation of the two composite systems of concern. The information contained in this report should significantly advance the state-of-the-art in metal-matrix composites, enhance the technology base and aid in the understanding of failure processes in metal-matrix composites.

II. MATERIAL PROCUREMENT AND QUALITY ASSURANCE

A. Material Requirements and Vendor Quality Control

The Failure Processes in Metal-Matrix Composites Program is primarily concerned with the evaluation of preconsolidated, diffusion bonded 5.6 mil diameter B/2024 Al matrix tape and panels as well as preconsolidated, diffusion bonded 5.6 mil diameter B/6061 Al matrix tape and panels. Additionally, 5.6 mil diameter B/2024 Al matrix and 5.6 mil diameter B/6061 Al matrix composite products produced by the General Electric developed Monolayer Boron Aluminum (MBA), Continuous Roll Bonding (CRB) process are being used for evaluation to obtain comparative information. A list of program material requirements is given in Table I.

All required 5.6 mil diameter B/6061 Al matrix material, except the CRB tape, was ordered from Amercom, Inc., Northridge, California. The material obtained consisted of two pounds of 45-50 v/o, 5.6 mil diameter B/6061 Al matrix tape, consisting of nine (9) monolayer tapes each being 0.0075 inch thick x 8.5 inches wide x 36.5 inches long. Additionally, fifteen 8-ply panels 0.0588 inch thick x 5.6 inches wide x 7.0 inches long with a filament orientation of $[22/0/-22/0]_8$ were received in two separate lots. For the purpose of definition, a lot will be defined as that group of individual tapes or sets of panels consolidated during the same pressing operation. Thus, two separate lots of panels would have been consolidated during two separate pressing operations. Vendor reported quality control results for the consolidated diffusion bonded 5.6 mil diameter B/6061 Al matrix material is presented in Table II. All material was visually inspected for surface flaws and workmanship and determined to be acceptable. Visual inspection was made for possible internal defects by surface pattern examination. No gross irregularities were detected.

All of the required 50 v/o 5.6 mil diameter B/2024 Al matrix material, except the CRB tape, was purchased from AVCO Corporation, Lowell, Massachusetts. To meet program requirements for the 2024 Al matrix material, three pounds of monolayer tape and twenty 8-ply panels with a fiber orientation of $[22/0/-22/0]_8$ were ordered. The required monolayer tape was received in three separate shipments of 0.8, 2.0 and 0.2 pounds each. The tape consisted of 84 separate pieces measuring approximately 0.0065 inch x 7.25 inches x 8.50 inches. The vendor reported quality control data for the monolayer tape products is presented in Table III. The 8-ply panels with a fiber orientation of $[22/0/-22/0]_8$ were received in four lots totaling 21 separate panels. Each panel was nominally 0.051 inch x 5.0 inch x 7.0 inch. Vendor reported quality control results for the consolidated panels are presented in Table IV. All material was visually inspected for surface flaws and workmanship and determined to be acceptable.

3

TABLE I. <u>MATERIAL REQUIREMENTS FOR FAILURE PROCESSES IN</u>
<u>METAL-MATRIX COMPOSITES PROGRAM</u>

A. <u>Baseline Data</u>

1. <u>8-Ply Panels (5 inches x 7 inches)</u>

50 v/o 5.6 mil dia. B/2024 Al [0]	1 panel
50 v/o 5.6 mil dia. B/6061 Al [0]	1 panel

B. <u>Basic Failure Studies</u>

1. <u>Monolayer Tapes (5 inches x 7 inches)</u>

1 v/o 5.6 mil dia. B/2024 Al [0]	8 tapes
25 v/o 5.6 mil dia. B/2024 Al [0]	8 tapes
50 v/o 5.6 mil dia. B/2024 Al [0]	8 tapes
1 v/o 5.6 mil dia. B/6061 Al [0]	8 tapes
25 v/o 5.6 mil dia. B/6061 Al [0]	8 tapes
50 v/o 5.6 mil dia. B/6061 Al [0]	8 tapes

2. <u>8-Ply Panels (5 inches x 7 inches)</u>

50 v/o 5.6 mil dia. B/2024 Al [0]	1 panel
50 v/o 5.6 mil dia. B/6061 Al [0]	1 panel
50 v/o 5.6 mil dia. B/2024 Al [22/0/-22/0]	1 panel
50 v/o 5.6 mil dia. B/6061 Al [22/0/-22/0]	1 panel

C. <u>Airfoil and Dovetail Related Testing</u>

1. <u>Monolayer Tapes (8 inches x 8 inches, minimum)</u>

45-50 v/o 5.6 mil dia. B/2024 Al [0]	3 pounds
45-50 v/o 5.6 mil dia. B/6061 Al [0]	2 pounds

2. <u>8-Ply Panels (5 inches x 7 inches)</u>

45-50 v/o 5.6 mil dia. B/2024 Al [22/0/-22/0]	19 panels
45-50 v/o 5.6 mil dia. B/6061 Al [22/0/-22/0]	14 panels

3. <u>Wire Mesh/2024 Al Products</u>

3-inch x 4-inch tapes (2024 Al/150 mesh/2024 Al)	260 tapes
3-inch x 4-inch panels (2024 Al/150 mesh/2024 Al)	9 panels

TABLE II. VENDOR QUALITY CONTROL RESULTS OF 5.6 MIL DIAMETER B/6061 Al MATRIX MATERIAL RECEIVED FROM AMERCOM, INC.

Vendor Identification No.	QA Specimen No.	v/o B	Tensile Load (Lbs)	UTS (ksi)
Monolayered Tape				
2402-P	2402-1	45	515	187[a]
2403-P	2404-1	45	560	198[a]
2404-P	2407-1	45	520	186[a]
2405-P				
2406-P				
2407-P				Avg. 190
2408-P				
2409-P				
2410-P				
8 Ply Panels[b]				
2412P-(1-12)	2412-1	45	3625	165[c]
	2412-2	45	3525	160[c]
				Avg. 163
2485P-(1-3)	2485-1	45	2975	144[c][d]

(a) Specimens 0.375 inch wide x 7.0 inches long with 3-inch gauge length.
(b) [22/0/-22/0]
(c) Specimens 0.375 inch wide x 9.0 inches long with 3-inch gauge length.
(d) Specimen slipped in grips twice during test. Sample taken from plate edge with large thickness variation indicating unconsolidated material. This sample not representative of material from lot 2485P.

5

TABLE III. VENDOR QUALITY CONTROL RESULTS OF 5.6 MIL
DIAMETER B/2024 Al MATRIX MONOLAYER TAPE RECEIVED FROM
AVCO CORPORATION

Vendor Lot No.	Boron Spool No.	Boron Tensile Strength (ksi)	Composite Ultimate Tensile Strength (ksi)
OM-96	C-10-411	512	184
			178
			195
			Avg. 186
OM-97	C-21-415	506	N/A[a]
OM-98	C-21-415	506	220
			219
			188
			Avg. 209
OM-99	C-21-415	506	177
			186
			207
			Avg. 190
OM-100	C-13-368	587	180
			190
			193
			Avg. 188
OM-101	C-13-368	587	N/A[b]

(a) [0]

(b) N/A - Not Available

6

TABLE IV. VENDOR QUALITY CONTROL RESULTS OF 5.6 MIL DIAMETER B/2024 Al MATRIX

$[22/0/-22/0]_8$ RECEIVED FROM AVCO CORPORATION

Vendor Identification			v/o B	E_1 (psi x 10^6)	E_2 (μsi x 10^6)	ϵ_f [a] (%)	UTS (ksi)
Lot No.	Panel No.	Sample No.					
105	5	1	50	28.3	22.9	.72	172
105	5	2	50	29.6	20.4	.80	176
105	5	3	50	29.4	21.1	.84	189
107	3	1	50	26.2	22.6	.85	200
107	3	2	50	25.9	23.3	.87	207
107	3	3	50	27.0	22.1	.72	166 [b]

(a) Fracture Strain, i.e., 0.0072 in/in = 0.72%

(b) Sample taken from plate edge with large thickness variation (.049" - .053") indicating unconsolidated material. This sample not representative of material from Lot 107.

7

B. Quality Assurance

Throughout Phase I of the subject program, all B/Al materials used were commercially available composite tapes and panels, with the exception of the composite material fabricated by GE/MPTL for the initial work at the Space Sciences Laboratory-GE to identify fundamental failure mechanisms using the acoustical emission techniques in B/Al composite material. Additionally, the test specimens fabricated from 150 mesh stainless steel wire cloth and 2024 Al foil plys were fabricated by GE/MPTL. For the purpose of defining starting material quality, a quality assurance plan was established. The plan, as outlined in the Quality Assurance Plan Data Sheet, Appendix A, was rigidly followed to assure that high quality composite material be used in specimen machining and testing. As each lot of commercial material was received, it was assigned a quality control number for future identification.

Nondestructive evaluation included ultrasonic through-transmission C-scan (TTUCS), low energy X-ray radiography and ultrasonic thickness direction velocity measurements. A typical C-scan of an Amercom panel is shown in Figure 1. Ultrasonic thickness direction velocity measurements for commercially available as well as GE/MPTL composite material are found in Table V and Table VI. Typical X-ray radiographs of Amercom tapes and panels are found in Figures 2 and 3. The above evaluation techniques indicated that all material was of acceptable quality for use in this program.

Destructive evaluation of composite materials consisted of boron filament tensile tests, B/Al tape tensile tests, and volume percentage constituent checks. To determine presence of filament degradation due to diffusion bonding, the aluminum matrix is dissolved and the remaining filaments are pulled in tension. Results are presented in Tables VII, VIII, and IX. Tape tensile tests were performed as a quality control measure using a specimen design as shown in Figure 4. The strengths from these quality measurements, Table X are somewhat lower than were expected in light of the excellent filament tensile strengths obtained. The lower strengths are deemed to be attributable to the difficulties in performing reliable tests on monolayed tape. However, the tapes were of acceptable quality level to be used in the fabrication of shear and compressive creep specimens. Volume percent of composite constituents was determined by weight analyses and results are given in Table XI. Metallographic examination of B/Al composite materials used in this program indicated bonding and filament arrays were acceptable as previously shown by NDE evaluation. Typical photomicrographs are presented in Figures 5, 6, and 7.
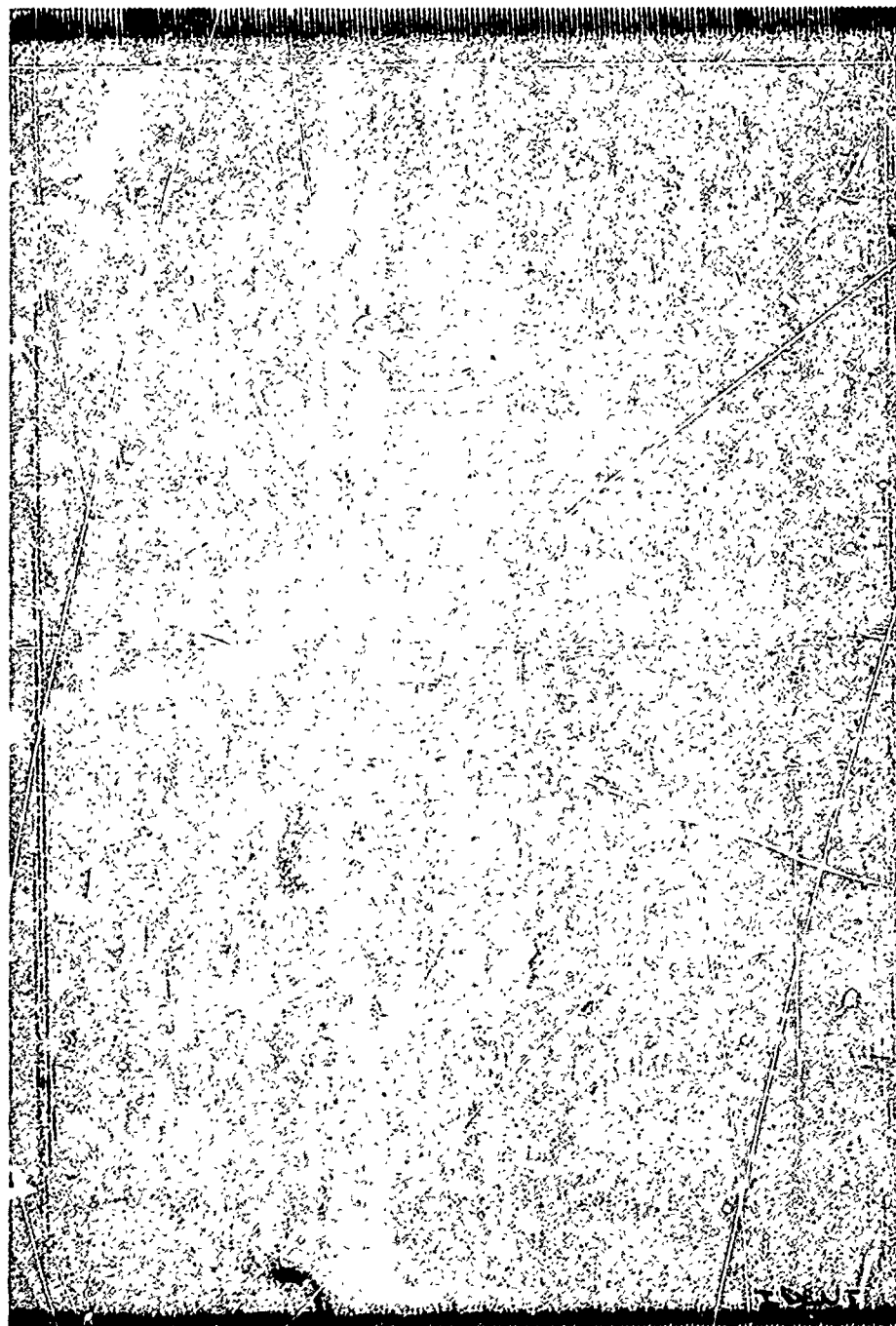
Figure 1   Typical C-Scan of Amercom 8 Ply Panel

9

TABLE V. RESULTS OF ULTRASONIC THICKNESS DIRECTION VELOCITY MEASUREMENTS ON AVCO AND GE 8-PLY PANELS[a]

Vendor Lot No.	Identification Panel No.	GE Identification No.	Aluminum Matrix Alloy	Boron Diameter (In.)	Volume Percent Boron	Density (g/cc)	Modulus of Elasticity (psi x 10^6)[b]
103	1	FAV 5262-E1	2024	0.0056	50	2.620	21.73
103	2	FAV 5262-E2	2024	0.0056	50	2.620	22.71
103	3	FAV 5262-E3	2024	0.0056	50	2.620	22.69
103	4	FAV 5262-E4	2024	0.0056	50	2.620	24.95
103	5	FAV 5262-E5	2024	0.0056	50	2.620	22.71
105	1	FAV 5262-F1	2024	0.0056	50	2.616	23.00
105	2	FAV 5262-F2	2024	0.0056	50	2.616	22.04
105	3	FAV 5262-F3	2024	0.0056	50	2.616	28.13
105	4	FAV 5262-F4	2024	0.0056	50	2.616	22.39
105	5	FAV 5262-F5	2024	0.0056	50	2.616	---
106	1	FAV 5262-G1	2024	0.0056	50	2.635	28.17
106	2	FAV 5262-G2	2024	0.0056	50	2.635	26.91
106	3	FAV 5262-G3	2024	0.0056	50	2.635	25.24
106	4	FAV 5262-G4	2024	0.0056	50	2.635	23.85
106	5	FAV 5262-G5	2024	0.0056	50	2.635	26.26
106	6	FAV 5262-G6	2024	0.0056	50	2.635	28.32
107	1	FAV 5262-H1	2024	0.0056	50	2.635	23.22
107	2	FAV 5262-H2	2024	0.0056	50	2.635	27.37
107	3	FAV 5262-H3	2024	0.0056	50	2.635	---
107	4	FAV 5262-H4	2024	0.0056	50	2.635	25.16
107	5	FAV 5262-H5	2024	0.0056	50	2.635	24.10
-	-	I5062-5	2024	0.0056	50	2.86	26.68
-	-	I5062-6	2024	0.0056	50	2.86	20.17

(a) Avco Panels at $[22/0/-22/0]_8$; GE Panels at $[0]_8$
(b) Single Results

TABLE VI. RESULTS OF ULTRASONIC THICKNESS DIRECTION VELOCITY MEASUREMENTS

ON AMERCOM AND GE 8-PLY PANELS[a]

Vendor Identification No.	GE Identification No.	Aluminum Matrix Alloy	Boron Diameter (In.)	Volume Percent Boron	Density (g/cc)	Modulus of Elasticity (psi x 106)
2412P1	FAM 4266-A1	6061	0.0056	45+	2.58	17.97
2412P2	FAM 4266-A2	6061	0.0056	45+	2.58	18.26
2412P3	FAM 4266-A3	6061	0.0056	45+	2.58	18.41
2412P4	FAM 4266-A4	6061	0.0056	45+	2.58	18.60
2412P5	FAM 4266-A5	6061	0.0056	45+	2.58	18.44
2412P6	FAM 4266-A6	6061	0.0056	45+	2.58	19.97
2412P7	FAM 4266-A7	6061	0.0056	45+	2.58	18.61
2412P8	FAM 4266-A8	6061	0.0056	45+	2.58	16.16
2412P9	FAM 4266-A9	6061	0.0056	45+	2.58	20.08
2412P10	FAM 4266-A10	6061	0.0056	45+	2.58	18.49
2412P11	FAM 4266-A11	6061	0.0056	45+	2.58	22.37
2412P12	FAM 4266-A12	6061	0.0056	45+	2.58	20.14
2485P1	FAM 4266-B1	6061	0.0056	45+	2.58	18.74
2485P2	FAM 4266-B2	6061	0.0056	45+	2.58	20.76
2485P3	FAM 4266-B3	6061	0.0056	45+	2.58	18.74
--	I 5066-4	6061	0.0056	50	2.82	19.65
--	I 5066-5	6061	0.0056	50	2.82	21.69

(a) Amercom Panels at $[22/0/-22/0]_8$ GE Panels at $[0]_8$

(b) Average of 3 Results

(c) Single Results

11
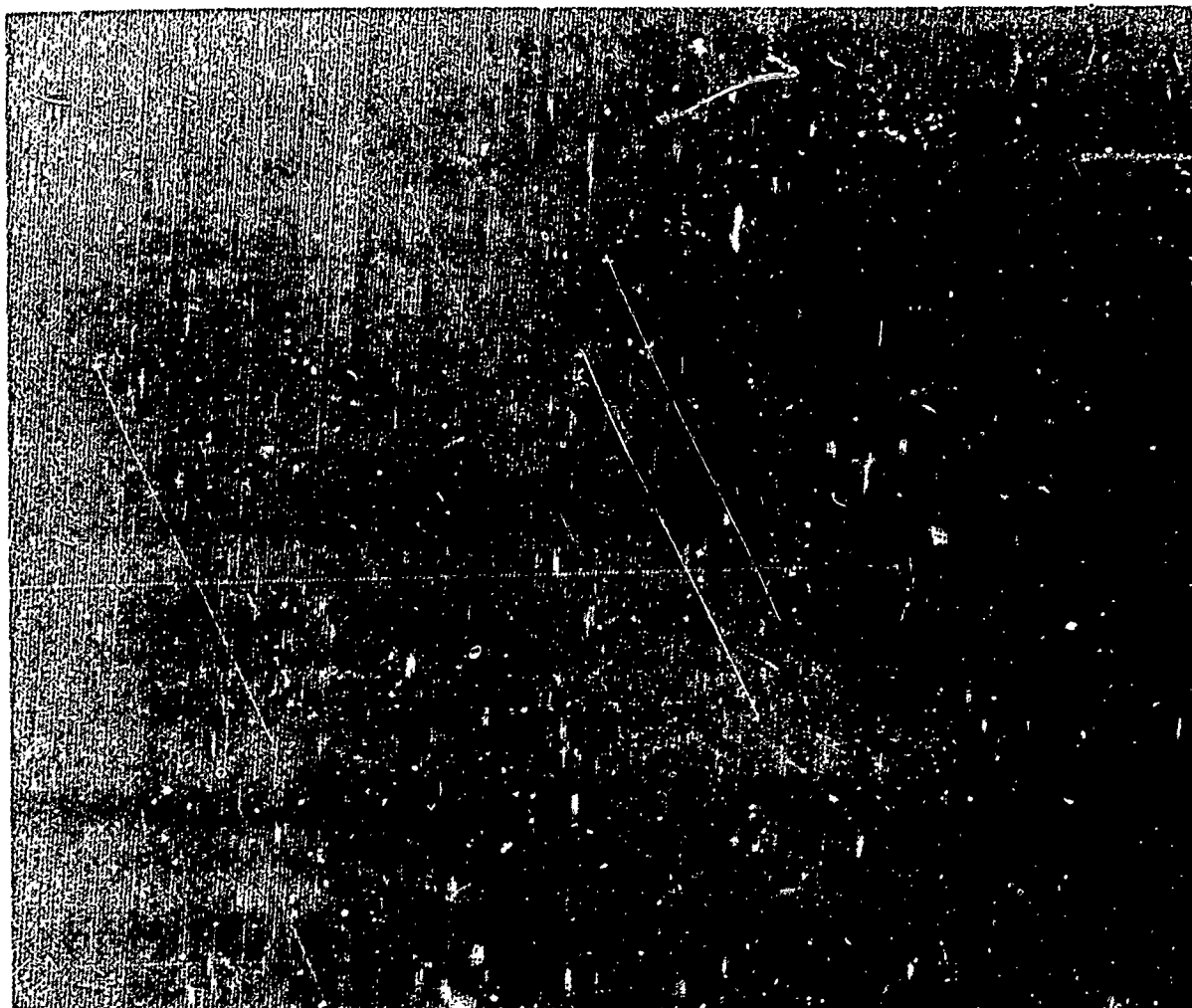
Figure 2   Typical X-Ray Radiography of Amercom Tape

Figure 3   Typical X-Ray Radiography of Amercom 8 Ply Panel

TABLE VII. BORON FILAMENT TENSILE RESULTS[a]

Amercom Inc. Material

GE Identification No.		Test Lot No.	Vendor Identification No.	Strength (ksi)	Standard Deviation (ksi)	Coefficient of Variation (%)
Panels						
FAM	4266-A1	1055	2412P-1	529.9	40.5	7.6
	-A2	1056	2412P-2	453.9	21.5	4.7
	-A3	1057	2412P-3	456.0	10.5	2.3
	-A4	1058	2412P-4	531.0	26.3	5.0
	-A5	1059	2412P-5	493.7	37.0	7.5
	-A6	1060	2412P-6	465.7	18.9	4.0
	-A7	1061	2412P-7	513.6	26.5	5.2
	-A8	1062	2412P-8	540.0	24.7	4.5
	-A9	1063	2412P-9	466.9	18.9	4.0
	-A10	1064	2412P-10	481.5	30.9	6.4
	-A11	1065	2412P-11	509.6	30.8	6.0
	-A12	1066	2412P-12	500.6	17.5	3.5
	-B1	1067	2485P-1	542.8	37.8	7.0
	-B2	1068	2485P-2	525.4	32.4	6.2
	-B3	1069	2485P-3	526.2	19.3	3.7
Tapes						
FAMT	466-C1	1070	2402P	506.7	16.8	3.3

[a] 1" gauge
1"/minute head rate
10 tests per lot

14

TABLE VIII. BORON FILAMENT TENSILE RESULTS[a]

AVCO Corporation Material

GE Identification No.		Test Lot No.	Vendor Identification No.	Strength (ksi)	Standard Deviation (ksi)	Coefficient of Variation (%)
Panels						
FAV	5262-E1	1036	OM-103-1	469.0	43.2	9.2
	-E2	1037	OM-103-2	495.0	41.0	8.3
	-E3	1038	OM-103-3	523.0	59.0	11.3
	-E4	1039	OM-103-4	503.5	31.5	6.2
	-E5	1040	OM-103-5	466.1	27.2	5.8
	-F1	1041	OM-105-1	482.4	46.1	9.6
	-F2	1042	OM-105-2	462.9	54.7	11.8
	-F3	1043	OM-105-3	514.8	31.2	6.1
	-F4	1044	OM-105-4	527.0	18.7	3.6
	-G1	1045	OM-106-1	553.8	41.3	7.5
	-G2	1046	OM-106-2	561.5	37.8	6.7
	-G3	1047	OM-106-3	538.8	39.2	7.3
	-G4	1048	OM-106-4	554.6	35.2	6.3
	-G5	1049	OM-106-5	553.0	34.4	6.2
	-G6	1050	OM-106-6	560.7	29.4	5.2
	-H1	1051	OM-107-1	573.3	26.6	4.6
	-H2	1052	OM-107-2	545.0	31.4	5.8
	-H4	1053	OM-107-4	531.5	33.0	6.2
	-H5	1054	OM-107-5	535.1	33.6	6.3
Tapes						
FAVT	562-A1	1106	OM-96-1	495.8	20.7	4.2
	-F1	1107	OM-99-1	549.0	83.5	15.2
	-D1	1108	OM-101-1	537.6	33.1	6.1

[a] 1" gauge
1"/minute head rate
10 tests per lot

15

TABLE IX. BORON FILAMENT TENSILE RESULTS[a]

GE Materials

GE Identification No.	Test Lot No.	Strength (ksi)	Standard Deviation (ksi)	Coefficient of Variation (%)
Panels				
I 5062-5	1000	527.0	43.0	8.1
I 5062-6	1001	542.4	43.2	7.9
I 5066-4	1018	553.0	55.3	9.9
I 5066-5	1019	503.1	50.9	10.1
Tapes				
I 5062-7A	1002	542.4	43.2	8.1
-7B	1003	551.0	49.9	9.1
-7C	1004	553.8	43.9	7.9
-7D	1005	574.1	39.5	6.9
-7E	1006	584.7	51.7	8.8
-7F	1007	568.0	47.1	8.3
-7G	1008	592.8	37.6	6.3
-7H	1009	469.4	60.6	12.9
I 2062-1A	1010	529.0	43.4	8.2
-1B	1011	498.6	57.3	11.5
-1C	1012	538.4	61.0	11.3
-1D	1013	514.8	68.9	13.4
-1E	1014	535.1	68.2	12.7
-1F	1015	511.6	55.3	10.8
-1G	1016	550.2	59.8	10.9
-1H	1017	487.6	39.7	7.9
I 5066-3A	1020	563.1	47.6	8.4
-3B	1021	531.5	105.3	19.8
-3C	1022	518.5	60.8	11.7
-3D	1023	576.1	49.8	8.6
-3E	1024	544.9	53.9	9.9
-3F	1025	539.2	62.0	11.5
-3G	1026	520.9	61.2	11.8
-3H	1027	546.9	62.7	11.5
I 2066-1A	1028	418.6	78.8	18.8
-1B	1029	507.1	60.9	12.0
-1C	1030	518.1	42.7	8.2
-1D	1031	544.5	42.2	7.8
-1E	1032	520.9	55.7	10.7
-1F	1033	544.5	32.6	6.0
-1G	1034	471.8	36.9	7.8
-1H	1035	496.9	60.1	12.1

[a] 1" gauge
1"/minute head rate
10 tests per lot

16
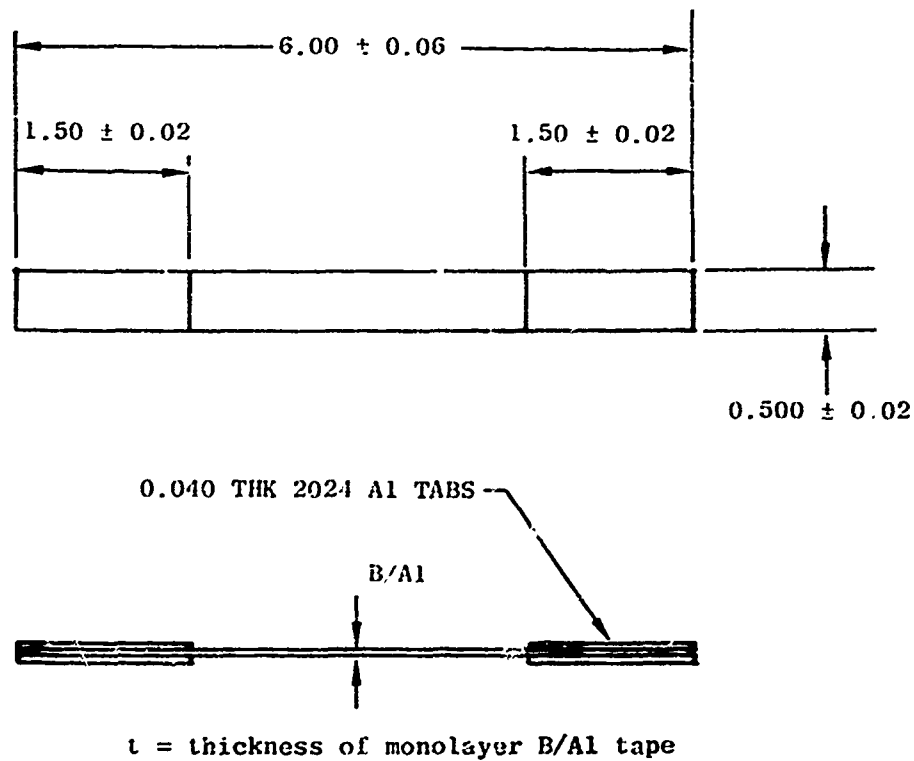
Figure 4   Monolayer Tape Tensile Test Specimen Configuration

TABLE X. MONOLAYER TAPE TENSILE RESULTS

GE Identification No.	Vendor Identification No.	Matrix Alloy	Nominal Volume (%)	Ultimate Tensile Strength (ksi)
FAMT-466-C1 (B-3)	2402 P	6061 Al	45	176.2
FAMT-466-C1 (B-4)	2402 P	6061Al	45	180.1
FAVT-562-A1 (A-7)	OM 96	2024 Al	50	171.5
FAVT-562-F1 (A-10)	OM 99	2024 Al	50	172.4
FAVT-562-D1 (A-11)	OM 101	2024 Al	50	166.5

TABLE XI. RESULTS OF VOLUME PERCENTAGE CHECKS ON COMPOSITE MATERIAL BY VENDORS

Vendor	Identification No.	Composite Form	Matrix Material	Nominal v/o B	Measured v/o B	Filaments per Inch
General Electric - MPTL	I-5066-5	Panel	6061 Al	50	48.9	---
	I-5062-6	Panel	2024 Al	50	48.0	---
	I-0066-2F	Tape	6061 Al	1	1.5	5
	I-0062-2D	Tape	2024 Al	1	0.9	3
	I-2066-1H	Tape	6061 Al	25	26.2	56
	I-2062-1H	Tape	2024 Al	25	30.1	60
	I-5066-3H	Tape	6061 Al	50	43.6	147
	I-5062-7E	Tape	2024 Al	50	50.8	154
Amercom, Inc.	FAM -4266-A3	Panel	6061 Al	45+	46.8	---
	-A5	Panel	6061 Al	45+	46.6	---
	-A6	Panel	6061 Al	45+	46.4	---
	-A7	Panel	6061 Al	45+	47.7	---
	FAMT- 466-C1	Tape	6061 Al	45	46.1	141
	-E1	Tape	6061 Al	45	45.8	142
	-G1	Tape	6061 Al	45	45.8	141
AVCO Corporation	FAV -5262-F5	Panel	2024 Al	50	49.9	---
	-G3	Panel	2024 Al	50	51.7	---
	-H1	Panel	2024 Al	50	50.8	---
	FAVT- 552-A2	Tape	2024 Al	50	51.7	124
	-B3	Tape	2024 Al	50	51.7	124
	-C12	Tape	2024 Al	50	51.5	120
	-D4	Tape	2024 Al	50	50.0	124
	-G1	Tape	2024 Al	50	51.1	121

19

TRANSVERSE   5G395   LONGITUDINAL   5G396

50 V/O 5.6 MIL B/2024 Al
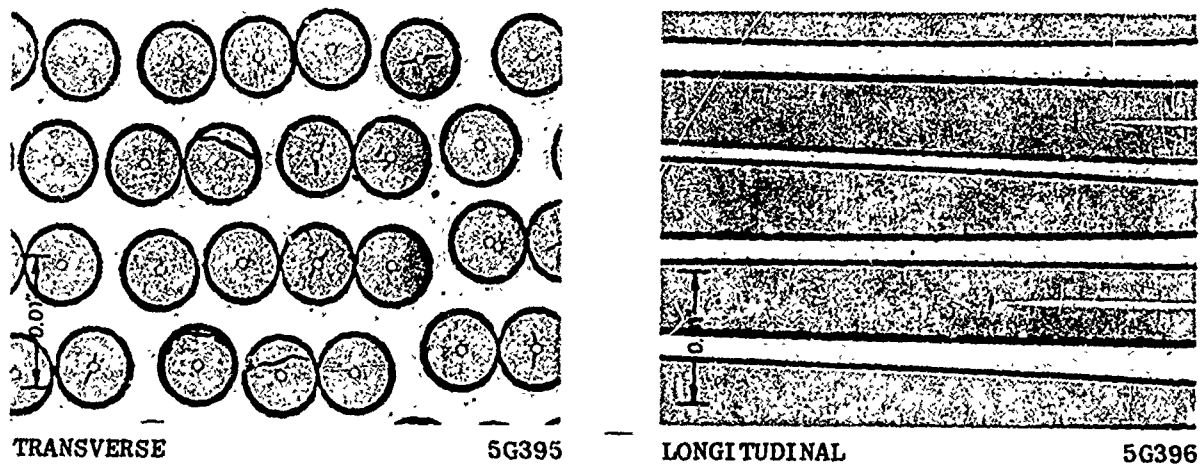
LONGITUDINAL   5G398
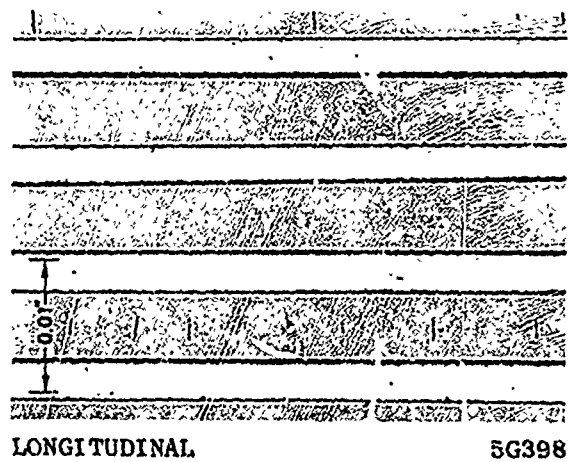
50 V/O 5.6 MIL B/6031 Al

Figure 5   Typical Microstructure of GE-MPTL $[0]_8$
            Boron/Aluminum Composite Material Fabricated
            Using the MBA/CRB Process
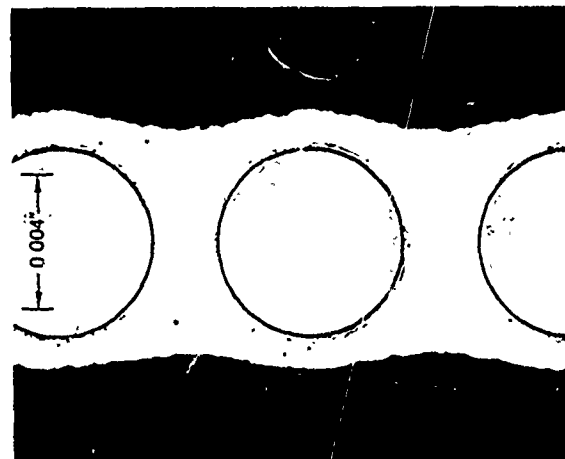
TRANSVERSE   5G409

$[0]_1$
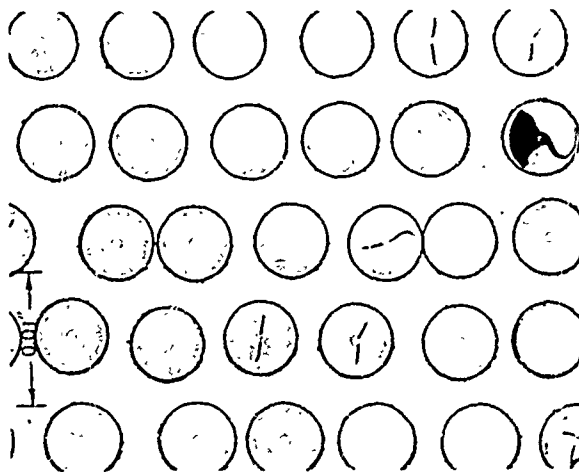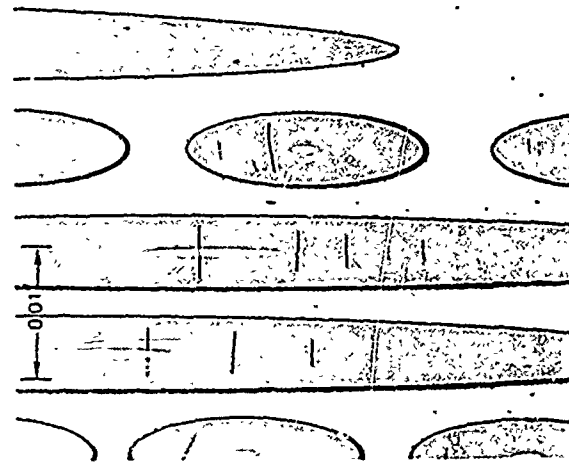
TRANSVERSE   5G393   LOGITUDINAL   5G394

$[22/0/-22/0]_8$

Figure 6   Typical Microstructures of 45+V/O 5.6 MIL B/6061Al
            Composite Products Produced by Amercom, Incorporated

TRANSVERSE   5G408

$[0]_1$
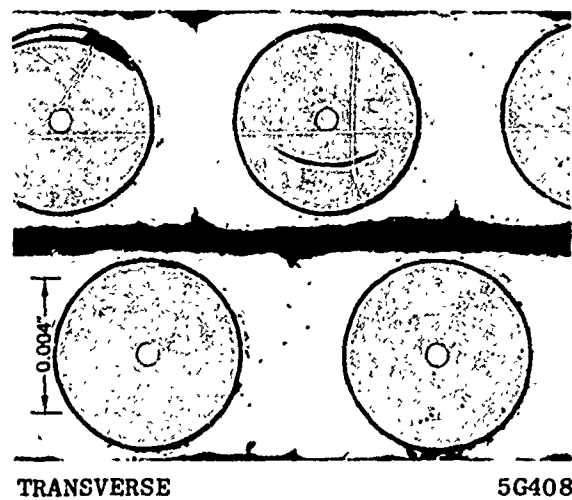
TRANSVERSE   5G400   LONGITUDINAL   5G401
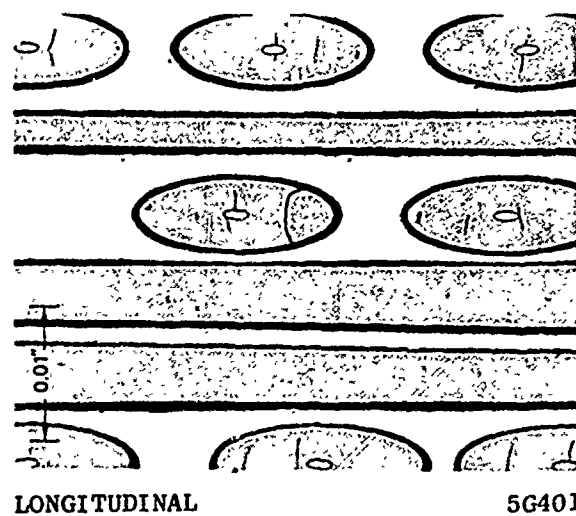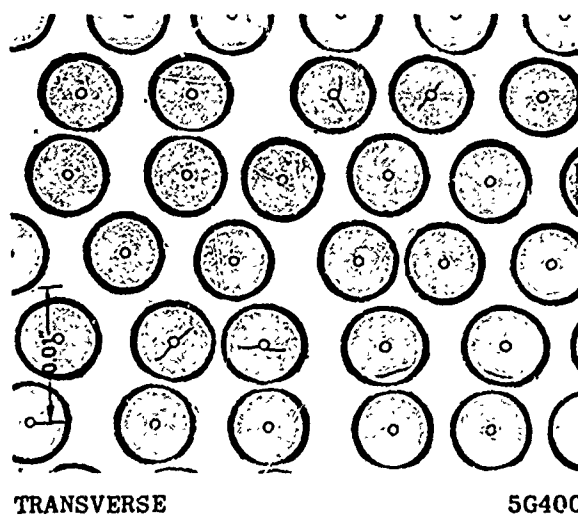
$[22/0/-22/0]_8$

Figure 7   Typical Microstructures of 50 V/O 5.6 MIL B/2024 Al Composite
Products Produced by Avco Corporation

22

III. SPECIMEN DESIGN AND FABRICATION

A. Specimen Design

A number of factors were considered in the design of the specimen configurations. The standard specimen, shown in Figure 8 was used for tensile testing of only the $[0]_8$ specimens fabricated in M&PTL to obtain baseline test data. One factor in the selection of this specimen geometry, as well as the others to be described later, was the gentle introduction of the stress into the gage region by a smooth load transition, i.e., the "bow tie" shape. Also of concern was the stress intensification at the specimen grip sections. The average grip stress must be significantly lower than in the gage region. If the knurled grips "bite" into the grip region, filament crushing and fragmentation can result. To minimize the crushing action, metal tabs were bonded to the specimen either during fabrication or as part of the consolidation process. The specimen shown in Figure 8 was formed with an integrally bonded outer layer of stainless steel mesh imbedded into the Al alloy matrix. In specimen preparation, the outer ply layer in the one inch gage was essentially removed. Still another factor is specimen alignment. Accurate alignment of the tensile axis is essential and probably is even of greater importance in composite material specimens. To assure proper alignment, end-notches, to accommodate 0.125-inch diameter pins were machined into each end of the specimen.

Figure 9 shows the transverse tensile specimen geometry used in obtaining the baseline data on only the $[90]_8$ specimens. In our recent study on transverse test configuration, this geometry was found to yield the most reproducible data. Extra care is needed in machining of the edges to minimize filament fracturing. As in the case of the standard tensile specimen shown in Figure 8, this specimen also contains the stainless steel mesh integrally bonded into the outer aluminum alloy layers of the grip regions.

Figure 10 is the specimen configuration similar to Figure 8, but without the outer ply containing the stainless steel mesh. This specimen was used in the majority of the program testing including tensile, tensile fatigue, rupture and torsion creep. The grip regions were reinforced with metal sheets suitably bonded to the test specimen tab surfaces.

The notched tensile specimen configuration can be seen in Figure 11. This configuration, except for the notch, is identical to the standard specimen shown previously in Figure 10. The notch stress concentration factor of $K_t = 3.0$ was determined analytically as given by Peterson. [1]

The double lap shear creep specimens, Figure 12, were machined from three previously consolidated panels which were stacked and diffusion bonded. The gap in the center was obtained by cutting the middle panel prior to the final bonding operation.

The compressive creep specimen, Figure 13, is a one-half inch cube. One side of the cube was marked in order to assure that the accurately aligned top and bottom were used as the faying surface.

23

(C7212696)

├──►◄──┤
1/2

Figure 8   Machined Longitudinal Tensile Test Specimens Utilizing
            Protective Outer Surface of Stainless Steel Mesh.
            Specimens of This Configuration Were Used for Base
            Line Data Acquisition.

(C7212695)

|←→| 1/2
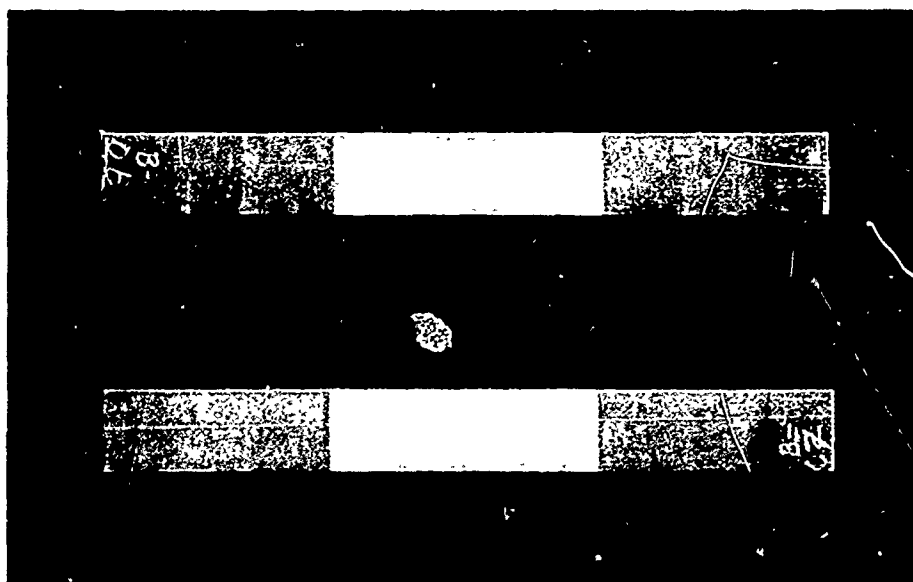
Figure 9   Machined Transverse Tensile Specimens Utilizing
            Protective Outer Surface of Stainless Steel Mesh.
            Specimens of This Configuration Were Used for
            Base Line Data Acquisition

(C7212697)

Figure 10   Typical Machined Specimens Used for Tensile,
             Tensile Fatigue, and Stress Rupture Testing.   No
             Protective Outer Surface of Stainless Steel Mesh Exists

26

1/2

.375
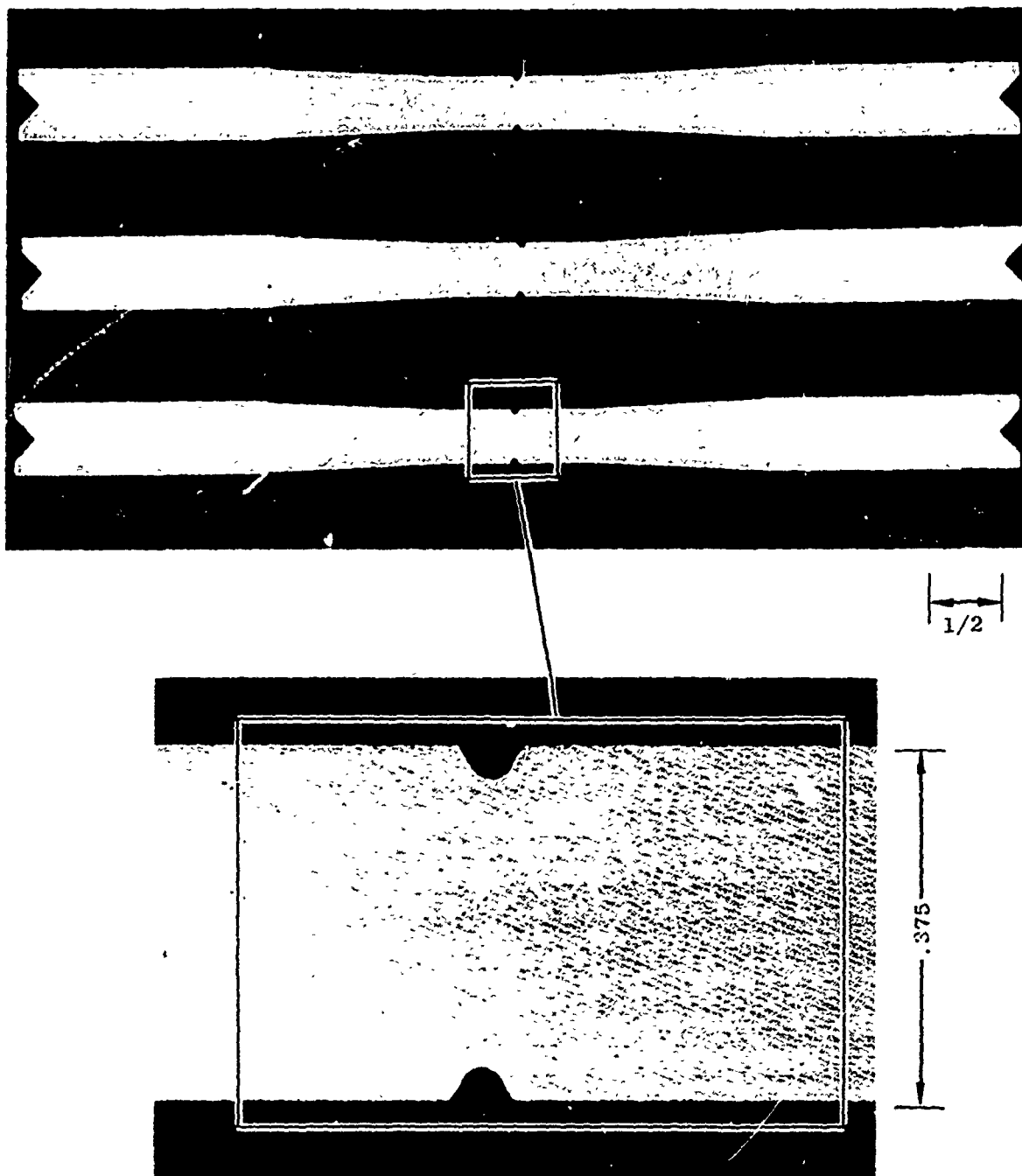
(C7212698)

(C7212699)

Figure 11   Typical Machined Specimen to be Used for Notched
             Tensile & Notched Tensile Fatigue Testing. No
             Protective Outer Surface of Stainless Steel Mesh Exists
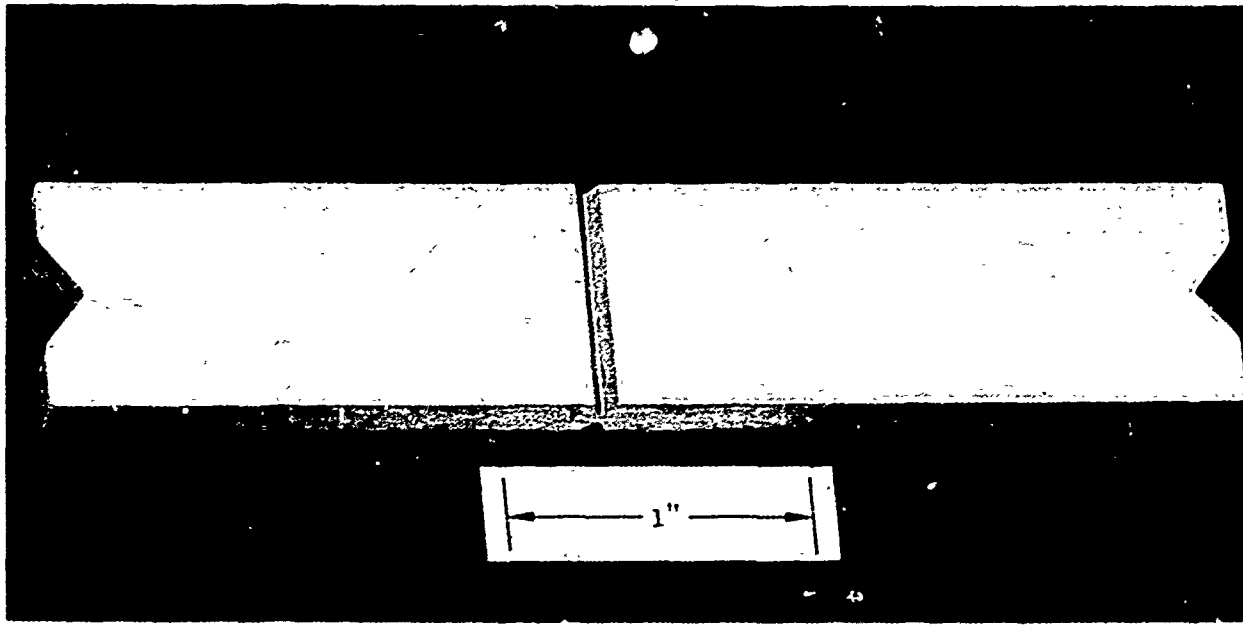
Figure 12   Double Lap Shear Creep Specimen
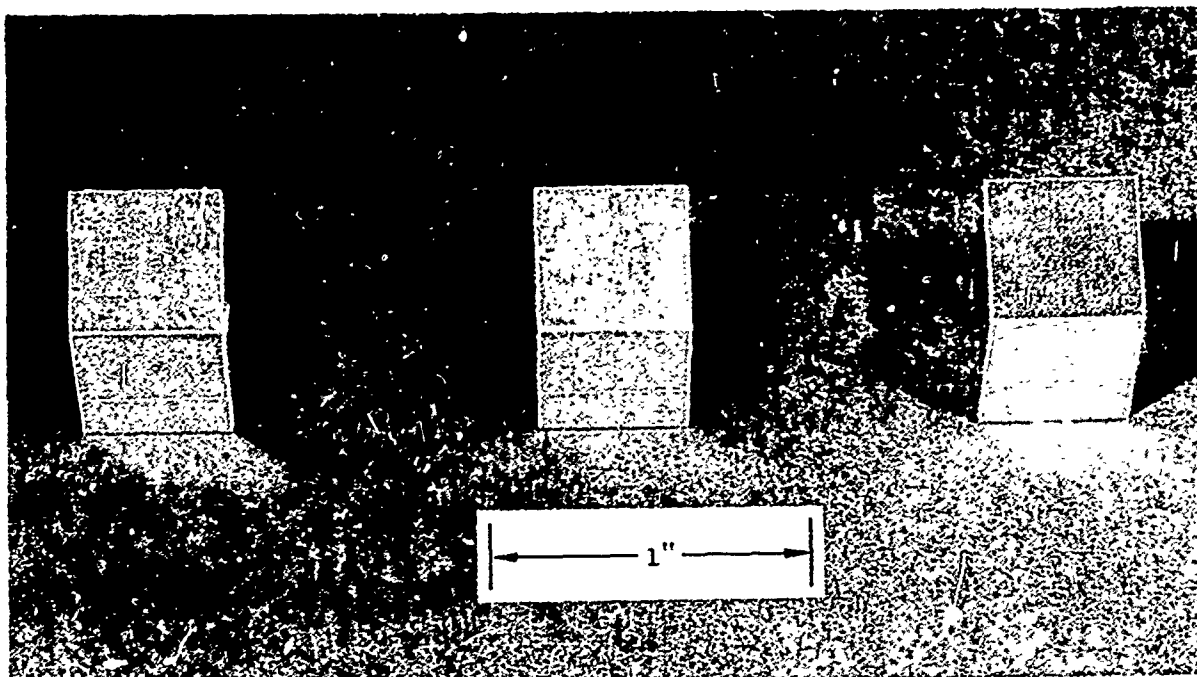
Figure 13   Compression Test Specimen

B. Specimen Fabrication

Due to the nature of the specimen design for the compressive creep and double lap shear creep tests additional consolidation was required at General Electric's M&PTL. In the design for the compressive creep specimens, individual monolayer tapes were used in multiple ply layups and these stacked plys subsequently vacuum hot pressed to a consolidated thickness of greater than 0.600 inch, nominally. To achieve this required before-machining thickness of approximately 0.600 inch, the number of monolayer tapes required for the B/2024 Al, B/6061 Al and wire mesh/2024 Al systems are, respectively, 96, 80, and 140. Consolidation of the wire mesh/2024 Al system was completed, at the pressing parameters of 930°F/30 min/5 ksi. The measured thickness of this panel was 0.658 inch, and although slightly greater than the calculated value of 0.600, this panel was quite acceptable for the manufacture of compression test specimens. The B/2024 and B/6061 Al compression panels were also vacuum hot pressed utilizing the standard compaction parameters for the respective B/2024 and B/6061 systems. The measured thicknesses for the B/2024 and B/6061 panels were 0.564 inch and 0.548 inch respectively. These panel thicknesses, although slightly less than the calculated value of 0.600 inch, were also acceptable for manufacture of the compression test specimens.

Through-transmission ultrasonic C-scans of the panels for compressive creep specimens indicated excellent bonding with no areas present for possible rejection.

Fabrication of panels required for the double lap shear creep specimens, Figure 12, required a two step process. First, individual 8 ply panels were formed. For the B/6061 Al and B/2024 Al systems 8-ply panels received from Amercom, Inc. and AVCO Corporation were utilized. For the wire mesh/2024 Al system additional panel consolidation was required by GE. Nine panels were consolidated, each panel consisting of 13 layers of wire mesh/2024 Al monolayer tape. Each tape consisted of a sandwich layup of 0.0015 inch 2024 Al/150 mesh stainless steel/0.0015 inch 2024 Al pre-consolidated by hot rolling to give an individual thickness of about 0.0047 inches. The panels were then subsequently consolidated at 940°F/30 min/5 ksi. The second step required to obtain panels for the double lap shear creep specimens necessitates an additional consolidation of a three panel layup. The layup consist of another sandwich type layup where the upper and lower panels full size and the center panel sectioned into two pieces and separated, laterally, a distance equal to that required in the design of the double lap shear creep specimen. Mating surfaces were roughened and cleaned prior to final consolidation.

Consolidation of the various material systems was performed utilizing the standard consolidation parameters for the respective material systems. Through transmission ultrasonic C-scans (gray scale) of the consolidated sandwich panels indicate the bond between separate panels to be excellent and the void area between the center panels to be uniform across the width of the sandwich panel. No translation movement occurred during the consolidation cycle.

C. Special Considerations

1. Ballistic Impact

A major requirement for compressor blade material is the ability to withstand high velocity impact damage. As an integral part of this program the effects of this blade type damage on standard specimens were evaluated. Steel ball projectiles were impacted into one of the test specimen edges to conduct the experiments. Based on conditions which govern the angle of impact between the projectile and the blade leading edge[2] in conjunction with the specimen geometry, a 60° incidence angle (γ) was selected. A schematic illustration of the specimen arrangement is shown in Figure 14. The 0.175 inch diameter steel ball impacted the specimen edge at approximately 1000 fps and induced an edge notch with an estimated stress concentration factor (K_t) of about 2.0.

Twenty four 8-ply specimens were ballistically impacted at 1000 fps prior to tensile testing. No fracturing occurred during the ballistic impact. Typical through transmission ultransonic C-scans (TTUCS) with gray scale are shown in Figure 15. These C-scan traces indicate a slight degree of irregularity near the edge of the impact, but there was no detectable delamination. Additional inspection utilizing red dye penetrant observations revealed no crack indications.

2. Cyclic Thermal Exposure

Another major requirement for composite compressor blade material is that it be able to withstand numerous severe fluctuations in temperature. In order to determine the effect of cyclic thermal exposure on the materials being evaluated in this program, compressive creep and axial fatigue specimens were cycled from -60F to 540F for two thousand (2000) cycles.

Figure 16 shows the test specimen bundle, instrumented with seven thermocouples (two for control, one for record, and four for distribution) and wrapped in aluminum foil. Heat up was accomplished by compressed air flowing through the test chamber from a stainless steel heat exchanger in a muffle furnace. When specimens reach the maximum temperature, the heated air solenoid valve was closed and liquid nitrogen gas solenoid valve opened allowing liquid nitrogen to be drawn from a pressurized dewar. Both heated air and nitrogen gas were baffled and diffused into test chamber to provide uniform heating and cooling rates. If heating or cryogenic sources failed for any reason, the system would stop cycling and the specimens would return to room temperature. A schematic for the thermal cycling setup is shown in Figure 17. A typical time-temperature trace is shown in Figure 18. The specimens were visually examined after 10, 100 and 500 cycles, and with C-scan and dimensional analysis after 1000 and 2000 cycles. No evidence of delamination, distortion, or severe discoloration was evident after thermal cycling. The specimens were tested and results discussed in a later section.

31
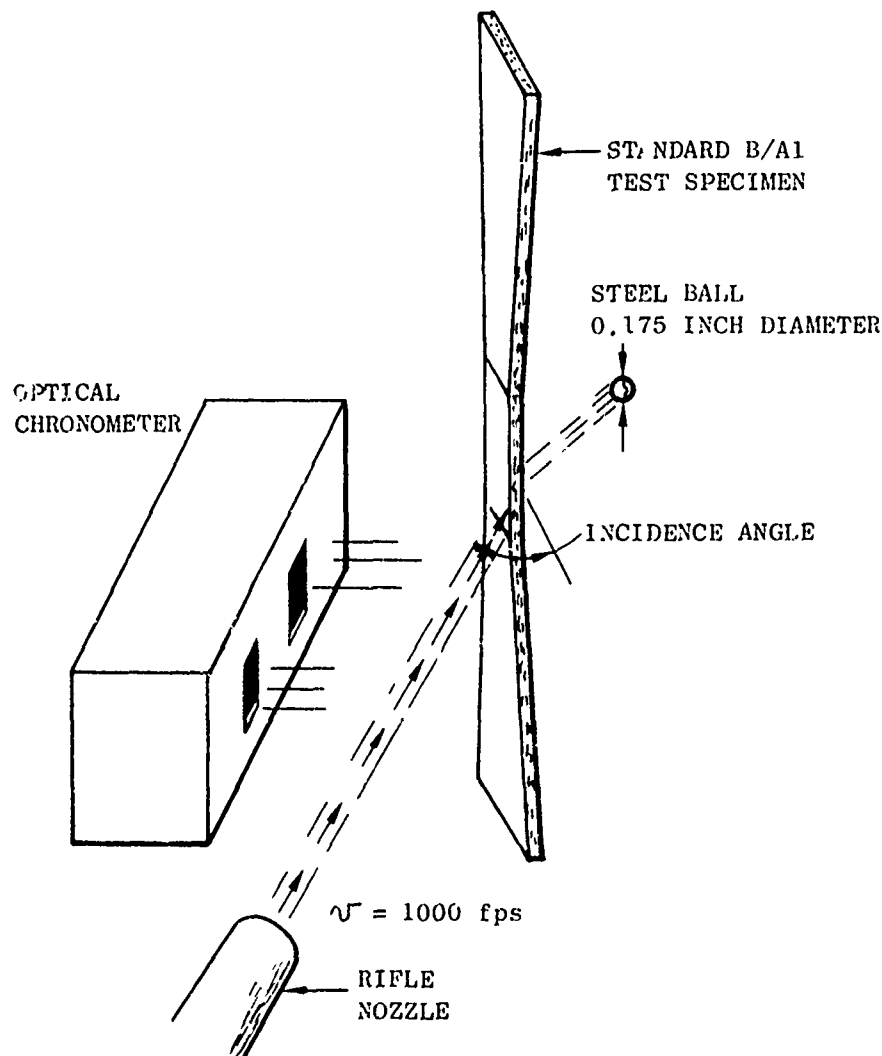
Figure 14 Schematic Illustration of the Impact Test Setup For
Impacting the Standard Specimen Edge with a 0.175 inch
Diameter Steel Ball

A32   A38   B30   B33

2024 Al MATRIX   2024 Al MATRIX   6061 Al MATRIX   6061 Al MATRIX

AVCO MATERIAL   AMERCOM MATERIAL
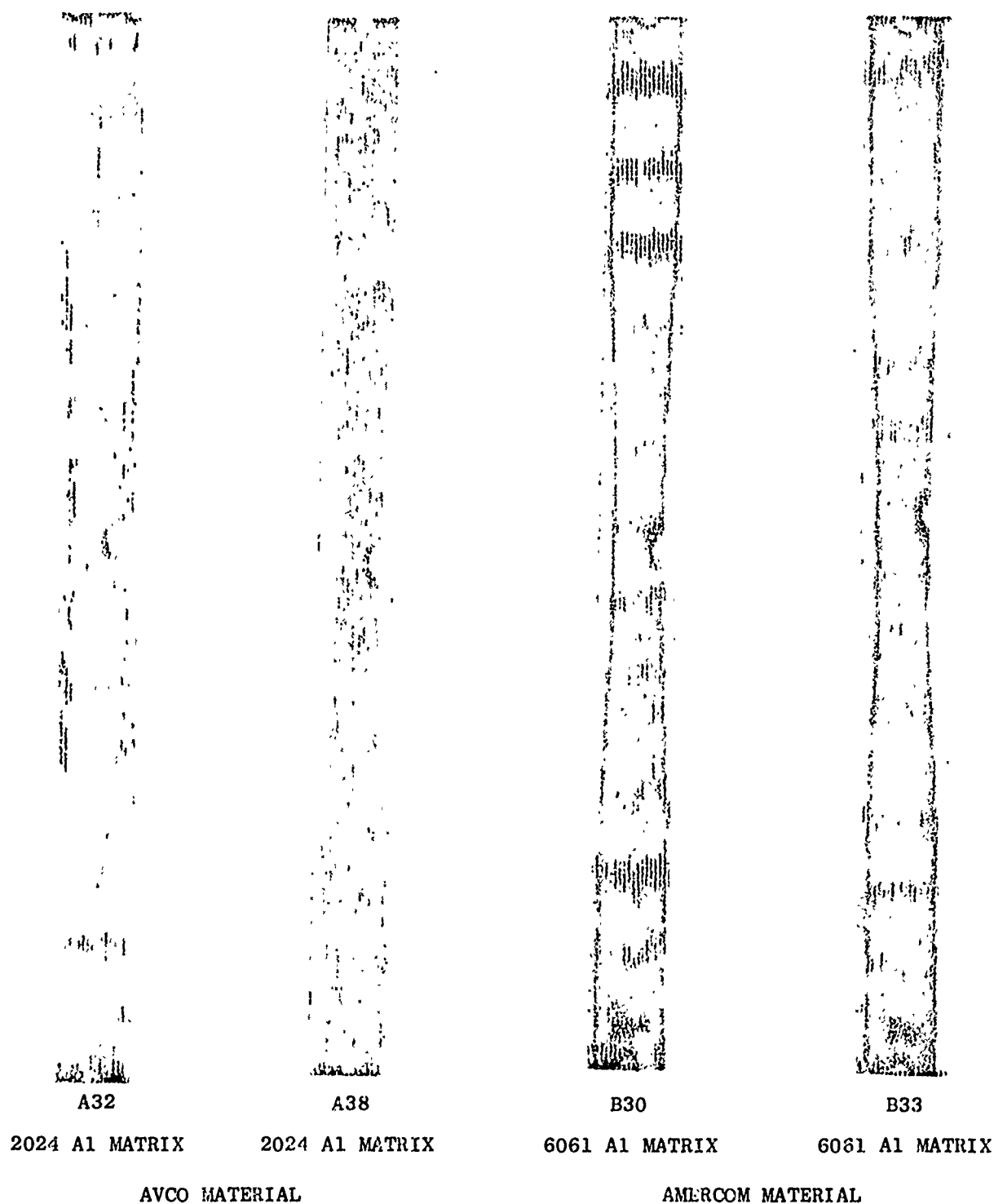
Figure 15   Typical Through Transmission "C" Scans of B/Al Specimens Ballistically Impacted at 1000 fps on Right Center Section of Gauge Region

STANDARD SPECIMENS

COMPRESSIVE
CREEP SPECIMENS

ALUMINA SUPPORT
BLOCKS

THERMOCOUPLE
LEAD WIRES
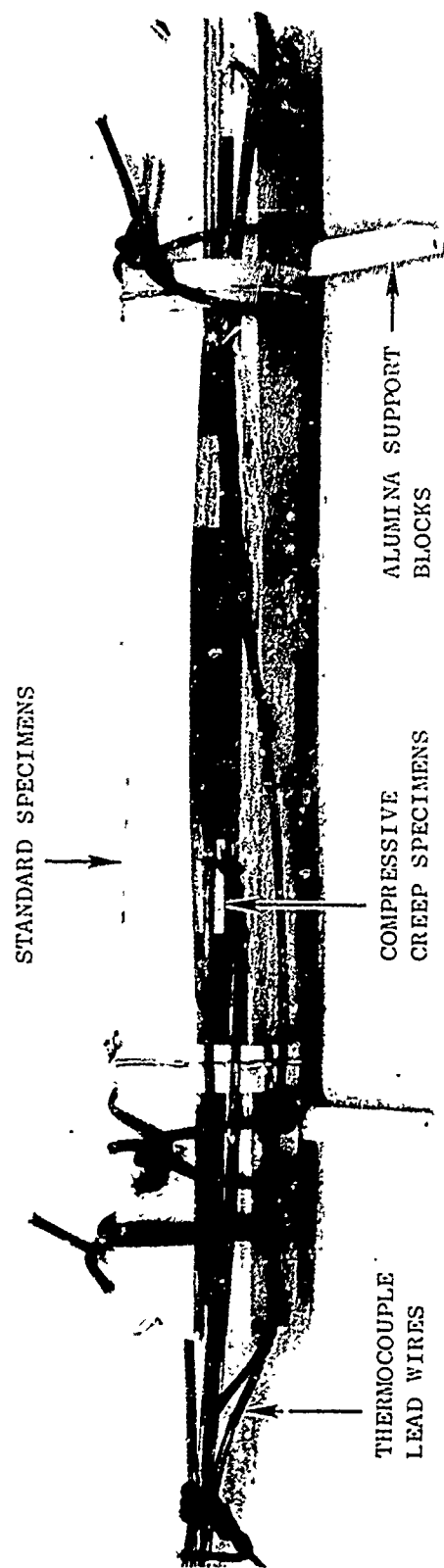
Figure 16   Specimen Bundle for Cyclic Thermal Exposures
Prior to Wrapping in Aluminum Foil

34
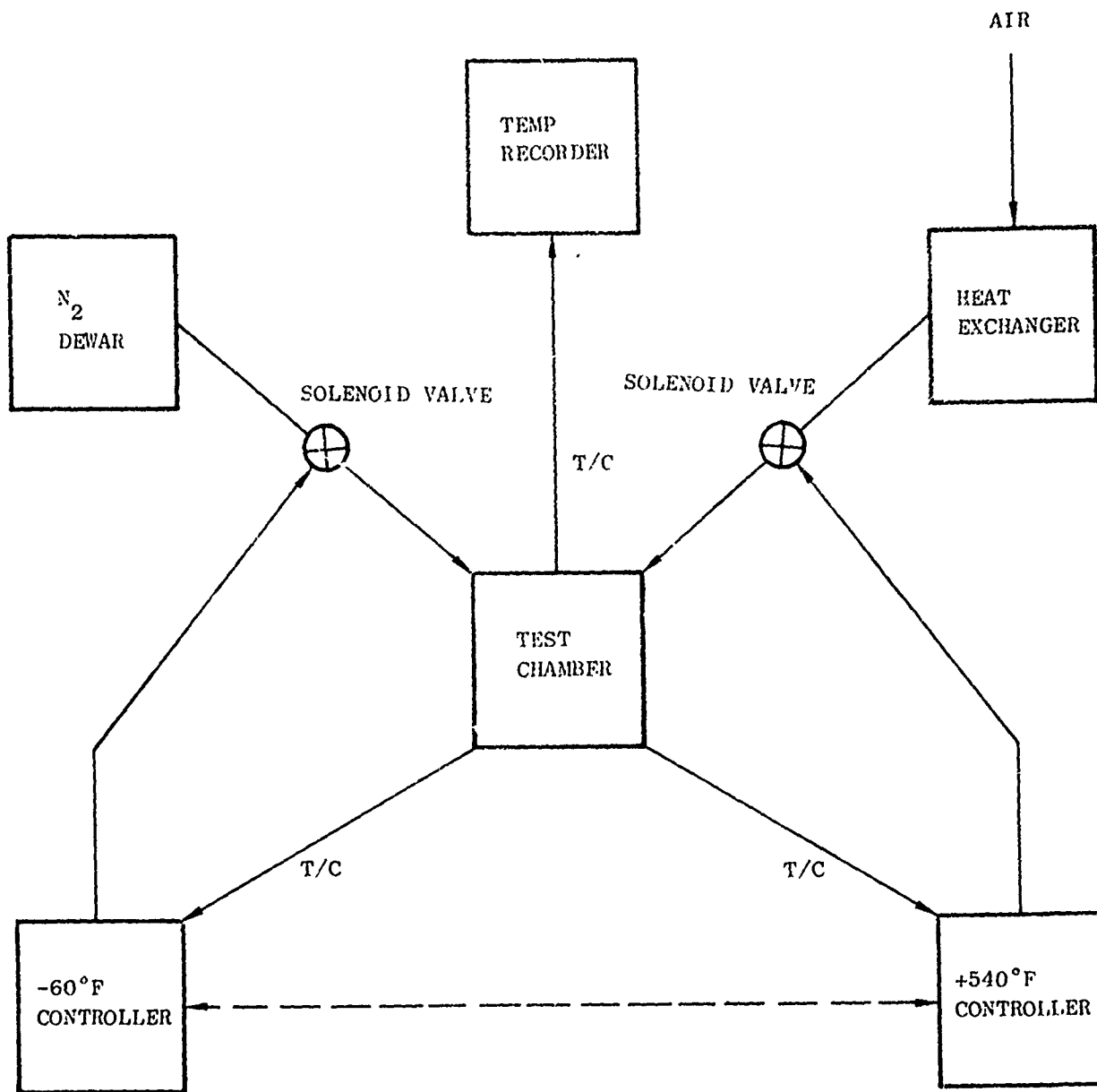
Figure 17   Schematic of Thermal Cycle Test Setup
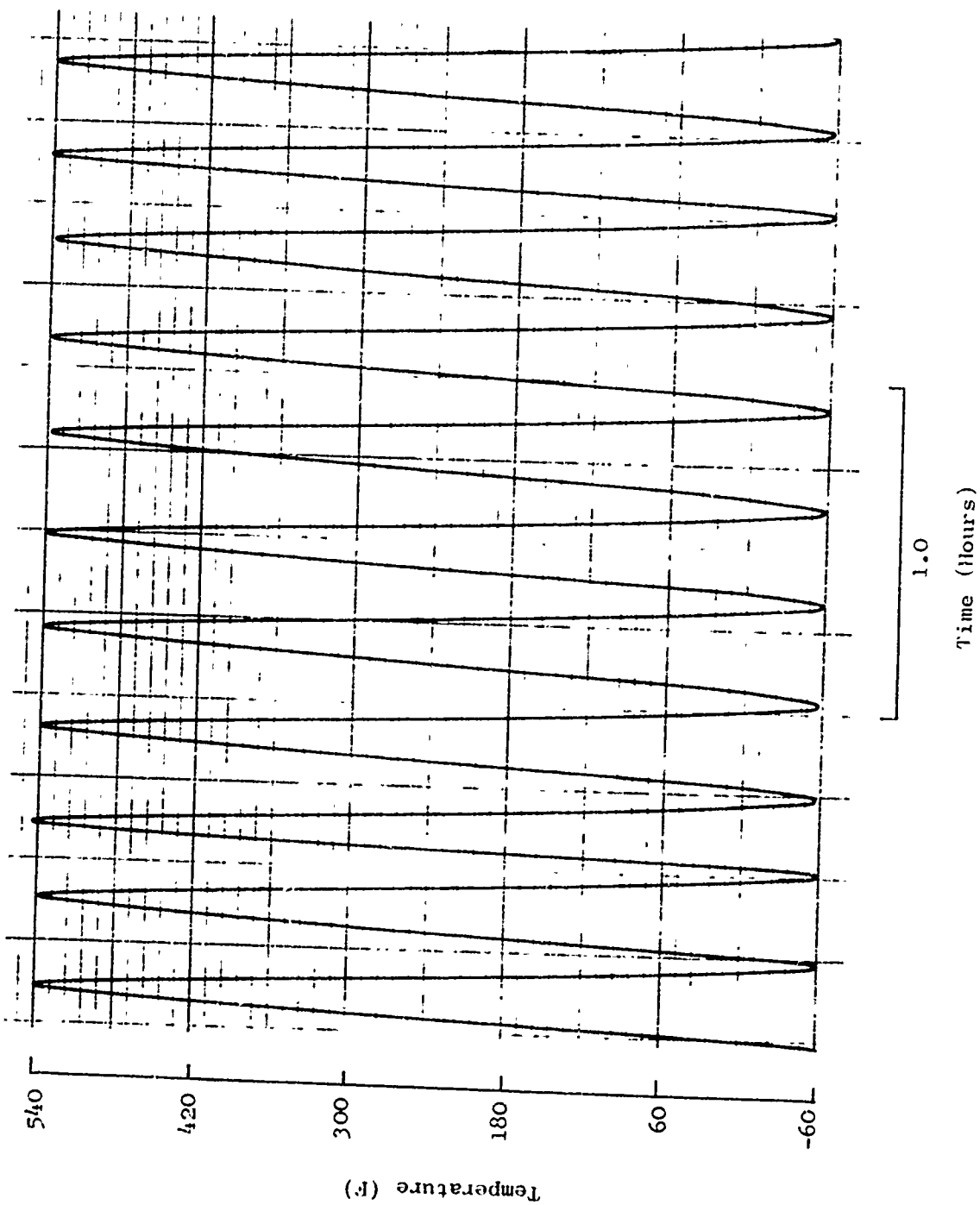
Figure 18 Time Temperature Trace for Cyclic Thermal Exposure (Cycles 85-95)

36

IV. BASIC FAILURE STUDIES

The purpose of this portion of Failure Processes in Metal Matrix Composites was to investigate basic failure mechanisms of B/Al using acoustic emission, X-ray radiography, metallography and fractography. To do this, monolayer tapes of 1, 25, and 50 volume percentage boron as well as 50 v/o [22/0/-22/0]$_8$ panel specimens were used. The 1 and 25 v/o B/2024 and B/6061 tapes were manufactured at GE/MPTL, while the 50 v/o tapes included those also manufactured at GE/MPTL along with those purchased from Amercom and AVCO.

Acoustic Emission - In general, when a material is being stressed, various events associated with its deformation (crack growth, etc) each have an audio signature (acoustic emission) which can be detected and analyzed using sophisticated electronic techniques.

For the acoustic emission tests on B/Al composites, a modification in the electronic circuitry was made in order that a filament or filament/matrix failure would be counted only once. In the usual case, an individual acoustic event is counted for as many times as the amplitude of the damped sinusoidal signal exceeds the pre-set discrimination level. The modification consisted of using the gate output of a Tektronic 545B oscilloscope set to trigger at a signal level greater than ± 150 mv. Using a sweep rate of 0.5 msec/cm, this insured that most events would be counted only once. The gain level in the preamplifier was maintained at 40 db.

One problem that is always of major concern in applying acoustic emission techniques is the avoidance of spurious noise induced in the grips. Previous work performed on carbon/epoxy specimens had shown that such spurious emissions could completely mask failure events occurring in the specimen. To check-out various gripping methods and end tab attachments, 0.016-inch thick and 0.5-inch wide steel specimens were used. At the amplifier gains used to monitor acoustic events in B/Al (40 db), the only noise detectable from the steel specimen would be produced by the grips and end tabs. It was found that 2024 Al end tabs bonded to the steel using an epoxy consisting of a 50-50 mixture of Versamid 140 and Epon 815 with the specimen and end tab assembly held in wedge grips with serrated faces produced few, if any, emissions at an attenuation level of 40 db. It seems probable that all or most of the emissions detected in B/Al specimens are due to the composite.

A typical record of both the load-deflection values are shown in Figure 19, the 55 or so individual acoustic events recorded up to failure are assumed to be filament fractures.

Fracture of Single Fiber Specimens - In order to examine in detail the effect of a fiber fracture on the interface and surrounding matrix, single filament specimens were prepared. They were fabricated by diffusion bonding single filaments in both a 2024 and 6061 matrix, with the processing conditions such that the filament-matrix bond should be the same in both these low volume fraction specimens (of the order of 1%), as the 50 v/o specimens.

37
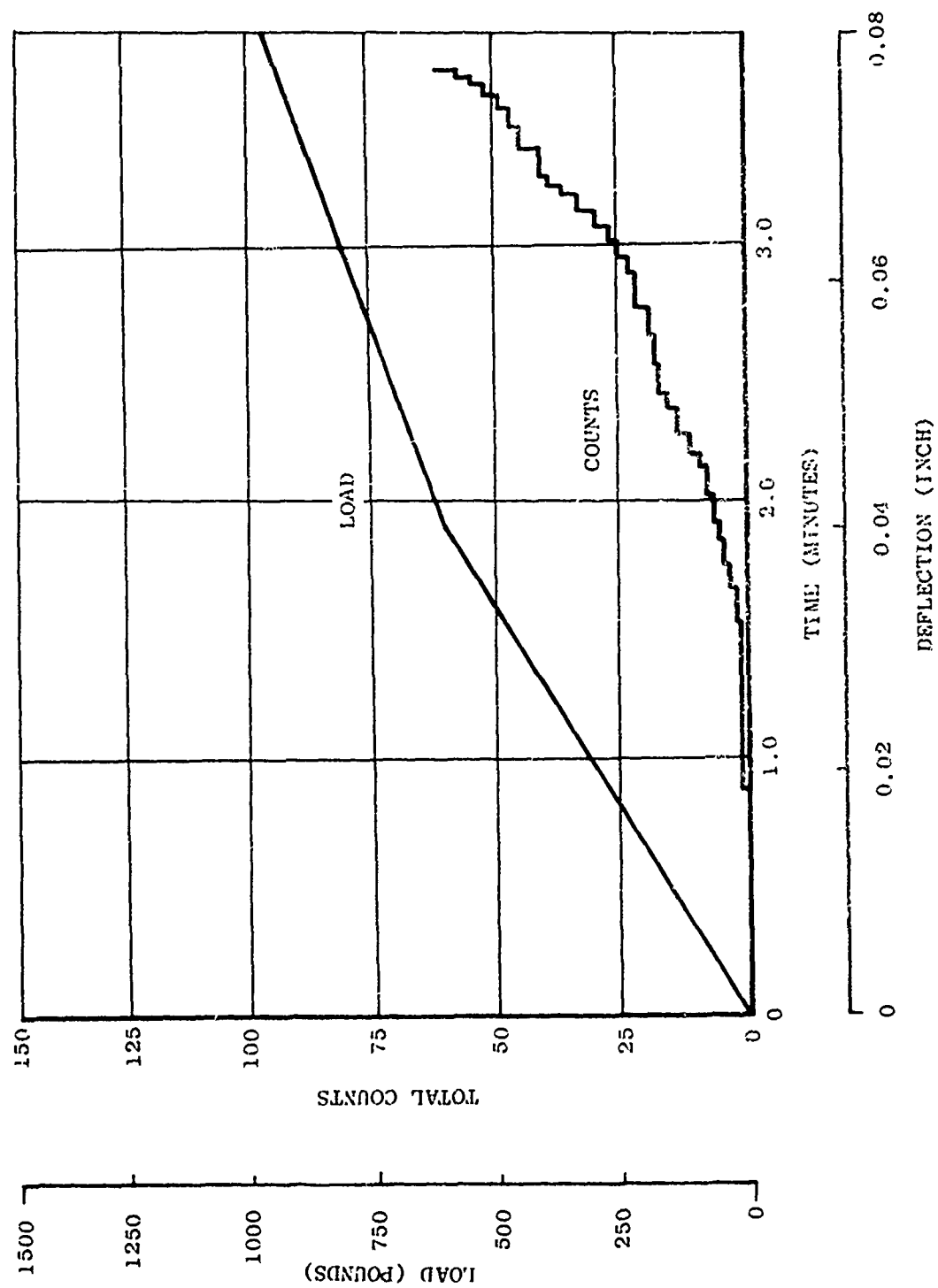
Figure 19   Acoustic Emission and Deflection Record of a Monolayer B/Al Tape Specimen Tested in Tension

38

The results from these two individual specimen tests were somewhat surprising. When testing the 2024 single filament specimen, an extraordinarily large number (on the order of 300) acoustic events were obtained. The origin of these events became clear when the broken filaments were etched out, as shown in Figure 20. The filaments were broken into small fragments and were fractured both longitudinally and transversely. It is inferred this occurred because the filament was well bonded to the matrix, and the Poisson induced matrix compressive stress was sufficient to fragment the filament. Separate experiments, consisting of leaching out untested single filament specimens and tensile testing them, indicated they probably were not damaged during fabrication. These data are presented in Table XII.

The behavior of a single filament specimen in a 6061 matrix was somewhat different, as shown in Figure 21. In this case, no filament fracture occurred prior to the "composite" fracture. This is evident from Figure 21, and it may be noted that the specimen displayed no acoustic activity prior to fracture. One possible rationale for the observed differences between the two individual tests, one with the 6061 Al matrix and the other with the 2024 Al matrix could be due to the filament-matrix bond. This presumed lack of filament-matrix bond could be specific to these two individual tests and not generally representative since a strength difference was not noted in the 50 v/o longitudinal specimens.

A cursory metallographic examination was made of the bond between the fiber and matrix in each of these systems. Taper sections leading to a 5000x tip magnification were used, and they are shown in Figure 22. There is no discernable difference in the interface between the two specimens.

Uniaxial Monolayer Fracture Behavior - Specimens of 50 v/o B/Al tape were subjected to a tensile load while concurrently recording acoustic events, and were then unloaded. In order to determine the nature of these events, experiments involving leaching away the aluminum matrix were used to reveal the degree of filament damage incurred by the specimen. Prior to leaching, one side of the specimen was coated with RTV to provide stiffness to the specimen after the matrix had been removed.

The results of these experiments are summarized in Figures 23 through 25. It may be noted that in all cases a particular filament failed more than once, and in one case (Figure 25) only one filament broke, giving rise to 15 acoustic events. In general some discrepancies between the number of events and filament fragments were noted and may be due to: (a) not all filament fragments were recovered, (b) the energy of the break was too low to trigger the Tektronix 545B oscilloscope, or (c) two breaks occurred so closely together so that only one was counted.

It may be seen, then, that cumulative fracture in the sense that individual filaments fail randomly throughout the specimen does not occur in the B/Al monolayer specimens examined to date. Rather, a few weak filaments fail several times.

A summary of 50 v/o B/Al tape testing is found in Table XIII. By observing acoustic events and tensile strength in the [0] specimens, it can be seen that acoustic events are not strictly a direct proportion to tensile strength. This observation along with the leaching experiments discussed previously leads to the conclusion that acoustic events prior to composite failure are failures of a few weak filaments each fracturing in several places. This is in contradiction of work performed by Herring (3) who found random filament failures throughout the specimen. The fact that his material was degraded in strength due to processing may account for the difference in failure mode.

39

TYPICAL LEACHED OUT FRAGMENTS

|—————————|
0.1 in.

Unloaded After 340
Acoustic Events

Failure Begins @ .35% Strain

Load, Pounds (y-axis: 0, 20, 40, 60)

Deflection, in. (x-axis: 0, .01, .02, .03)
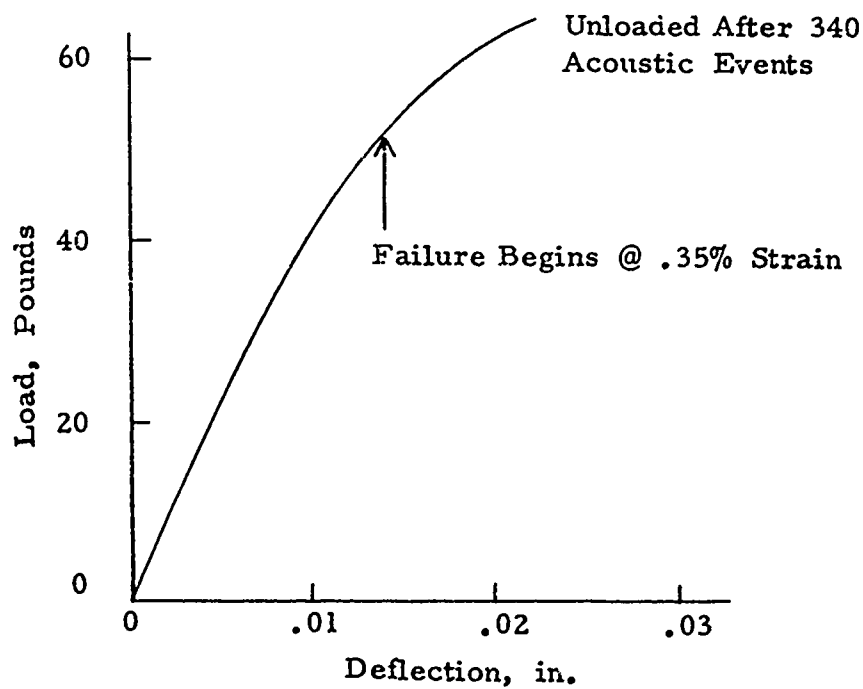
Figure 20   Filament Fragments Recovered from a Single Filament Composite in
a 2024 Matrix Which Displayed 340 Acoustic Events Before Unloading

40

TABLE XII.   TENSILE STRENGTHS OF FILAMENTS LEACHED
FROM THE 2024 Al MATRIX

SOURCE OF FILAMENT	FILAMENT STRENGTH[a] (ksi)
50 v/o Monolayer	577
	600
	610
	619
	560
	595
Single Filament Specimen	576
	556

[a] Two inch gage length
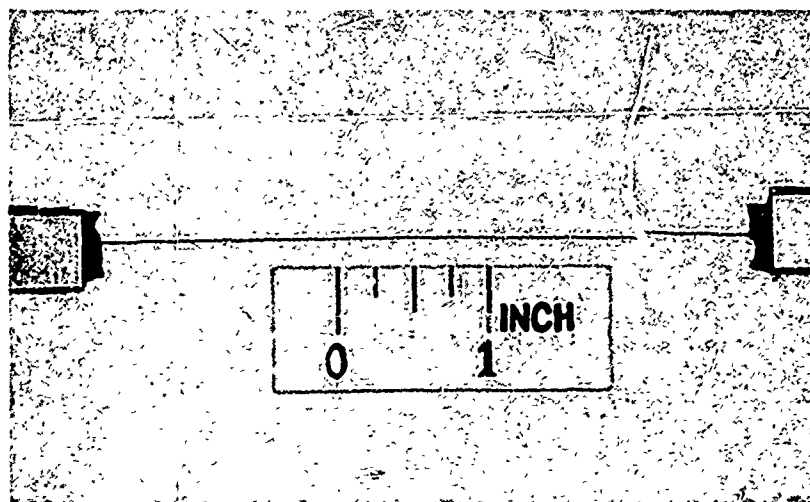
LEACHED OUT SPECIMEN

Failure @ about 0.5% Strain
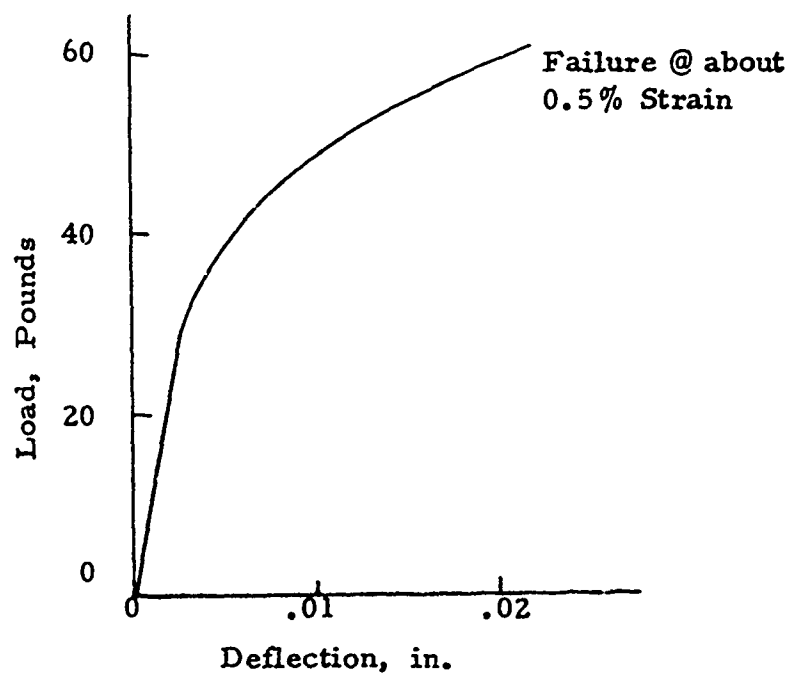
Figure 21   Photograph Showing Lack of Filament Breakage of a
Single Filament Specimen in a 6061 Matrix
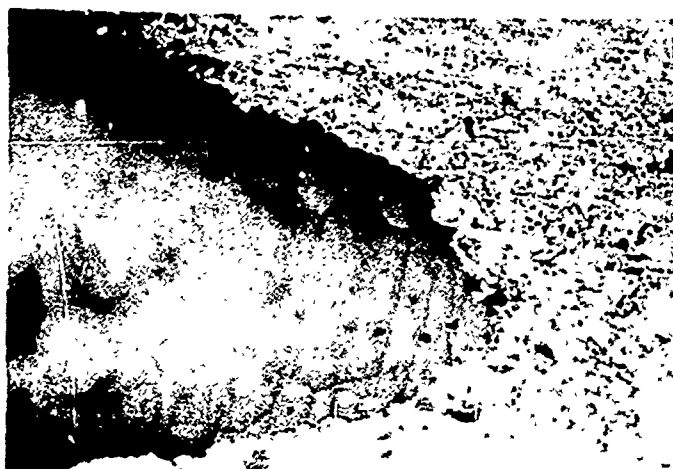
6061 MATRIX   5 μm
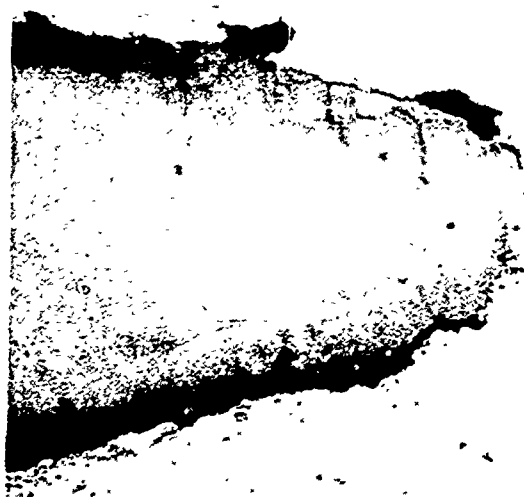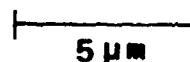
2024 MATRIX   5 μm
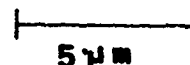
Figure 22   Taper Section of Single Filament Specimens.
The Magnification Refers to the Tip

43
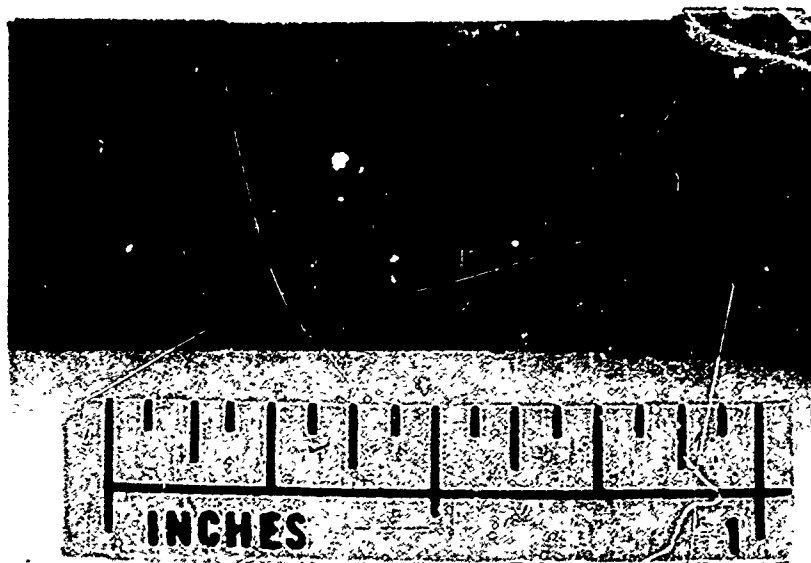
ETCHED SPECIMEN AFTER TEST
THERE ARE TWO BROKEN FILAMENTS
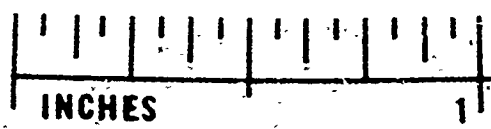
FILAMENT PORTIONS RECOVERED - 12

Figure 23   Photograph of Specimen 255-2 Unloaded Prior to
Failure With 18 Acoustic Events Recorded

44
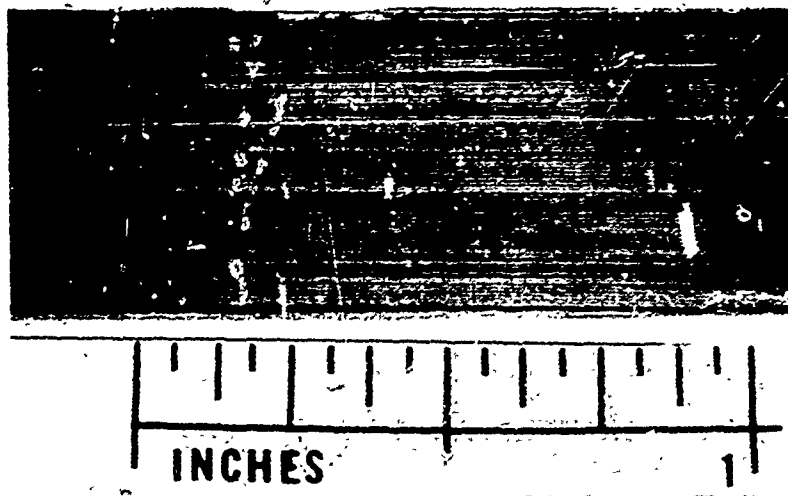
ETCHED SPECIMEN AFTER TEST
THERE ARE SIX BROKEN FILAMENTS
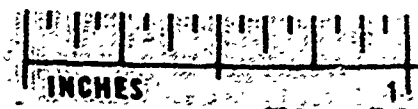
FILAMENT PORTIONS RECOVERED -- 25

Figure 24   Photograph of Specimen 255-4 Unloaded Prior to
Failure With 40 Acoustic Events Recorded
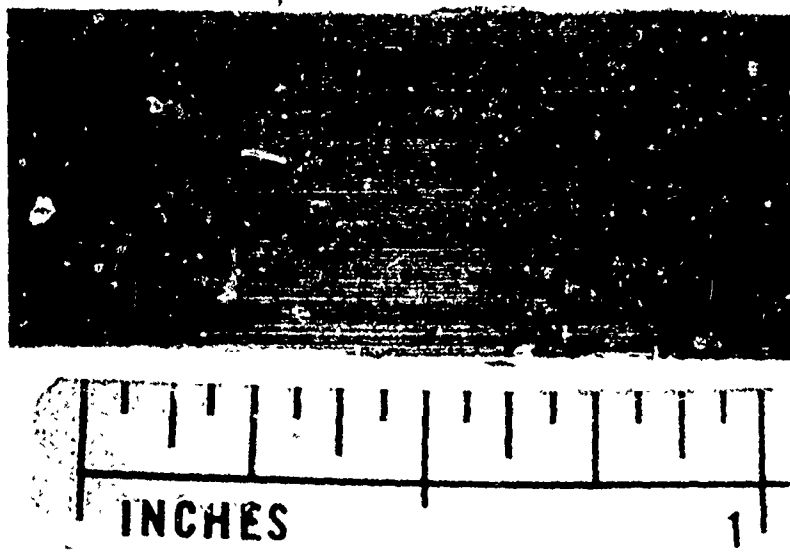
ETCHFD SPECIMEN AFTER TEST
THERE IS ONE BROKEN FILAMENT AT THE EDGE

FILAMENT PORTIONS RECOVERED - 7

Figure 25   Photograph of Specimen 255-6 Unloaded Prior to Failure
With 15 Acoustic Events Recorded

TABLE XIII. TENSILE RESULTS ON MONOLAYER TAPE SPECIMENS
CONTAINING 50 v/o BORON

Source	Filament Orientation	Matrix	Modulus (10^6 psi)	UTS (ksi)	Acoustic Events
Amercom	[0]	6061	27.9	178	92
	[0]	6061	29.0	152	65
	[0]	6061	-	175	15
	[0]	6061	-	158	22
	[0]	6061	-	169	40
	[0]	6061	-	129	45
AVCO	[0]	2024	34..	123	-
	[0]	2024	-	63.8	16
	[0]	2024	-	161	63
	[90]	2024	20.5	21.5	-
	[90]	2024	-	14.6	-
	[90]	2024	-	13.2	-
GE/MPTL	[0]	2024	31.4	194	35
	[0]	2024	33.0	211	50
	[22]	2024	20.6	26.4	0
	[22]	2024	23.3	31.6	~ 3
	[90]	2024	21.9	10.6	0
	[90]	2024	-	9.8	0
	[0]	6061	-	218	-
	[0]	6061	-	228	34
	[0]	6061	-	197	-
	[0]	6061	-	219	60
	[0]	6061	-	195	38
	[0]	6061	-	212	29
	[22]	6061	-	15.6	-
	[22]	6061	-	16.5	-

Summarizing, in uniaxial monolayer tapes, a few weak filaments fail several times each to account for the observed acoustic emissions on tensile loading. Composite failure occurs in essentially a non-cumulative manner with the aluminum matrix failing in plastic flow after gross filament failure. Also, it should be noted that an individual filament failure does not cause a matrix crack to reach the surface, a distance of only 0.001 inch, as was observed in boron/epoxy specimens. This is attributed to the ability of the metal matrix to plastically deform. A limited number of tests have been performed on 25 v/o B/Al specimens in a 6061 matrix, as shown in Table XIV. A typical fracture is shown in Figure 26. Because less energy is released, specimen distortion and local buckling does not occur as in the 50 v/o case, Figure 27. Interestingly, the number of filament breaks (as detected by acoustic emissions) is about the same for the 20 v/o as the 50 v/o material. This behavior, as well as the slightly lower strength compared to the 50 v/o material (corrected for volume fraction) needs to be investigated further.

One interesting fact was noted for the case of the notched specimens. In the case where the specimens were unloaded prior to fracture, severe distortion in a ruffle-like pattern along specimen edges occurred. The explanation for this phenomenon probably lies in the presence of local plastic shear strain in the aluminum adjacent to the notch, caused by the necessity of the aluminum to transfer load from the cut fibers into the uncut ones. Because of this load transfer, there is an area in the specimen center on either side of the notch where the filaments are stressed to an equal amount, and the specimen can fail at any plane in this area. As shown in Figure 28, the above explanation or a similar one must hold, because the specimen failed away from the minimum cross-section.

Off-Axis Tests - Monolayer tape specimens tested with the filaments in the [90] orientations are also listed in Table XIII.

Typical fractures for these specimens are shown in Figure 29. In the [90] case no acoustic emissions were detected during the test at the attenuation level used (40 db), indicating no filament splitting. Examination of the fracture surface showed, not surprisingly, that the specimen failed at the boron-aluminum interface. For the [22] specimen, failure in two out of three cases occurred in the specimen center, which indicates that the shear coupling term introduced by the grips did not affect the strength. The failure again occurred at the filament matrix interface. However, in two cases some acoustic emissions were detected during the test prior to failure. By etching out the filaments and carefully examining them, it was possible to determine these events were not due to filament splitting or breakage in the gage length. Thus, this indicated acoustic activity was due either to events taking place in filaments under the end tabs, or were caused by interface failures.

Elastic Behavior - For completeness, it was considered of interest to determine the four independent elastic constants for this orthotropic lamina system. The combination of 50 v/o B in 2024 aluminum was chosen, using MBA tape manufactured by General Electric Company. Duplicate specimens were tested in the [0], [22], and [90] direction with opposed strain gages affixed to the specimens in the center. Each set of gages were recorded in one of two X-Y recorders, and the Y-axis of each recorder was connected to the load cell. For the [22] specimen, the length-to-width ratio was large enough (approximately 11) to avoid any large non-uniform deformation in the center of the specimen caused by the shear coupling introduced by the grips[4].

48

TABLE XIV.   TENSILE RESULTS ON GE/MPTL 25 v/o$^{(a)}$ B/Al
MONOLAYER TAPE SPECIMENS

Matrix	UTS (ksi)$^{(b)}$	Acoustic Events
6061	64.6	25
6061	69.3	42
6061	68.0	17
2024	93.8	15
2024	92.4	9

(a)   Nominal

(b)   B/2024 - 30.1 v/o
       B/6061 - 26.2 v/o
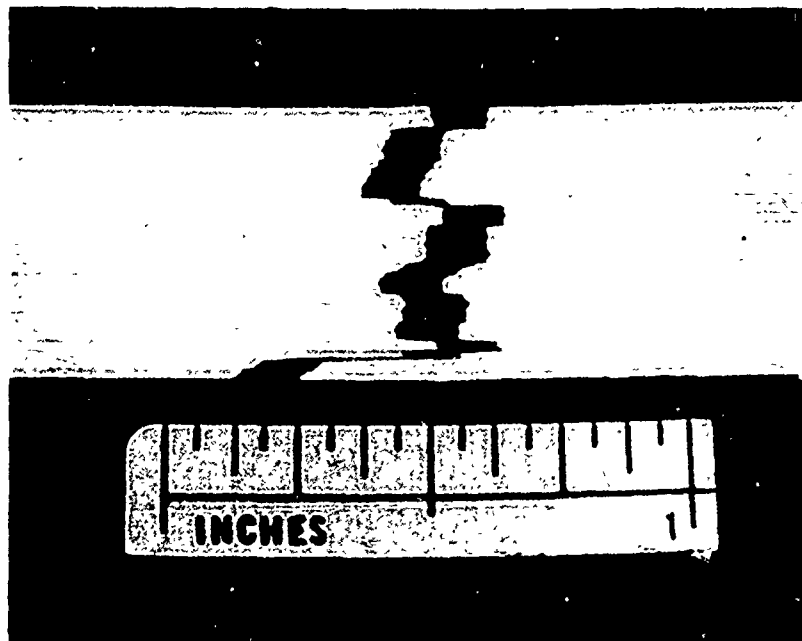
Figure 26 Fracture Appearance of a 20 V/O B/Al Monolayer
Tape With a 6061 Matrix
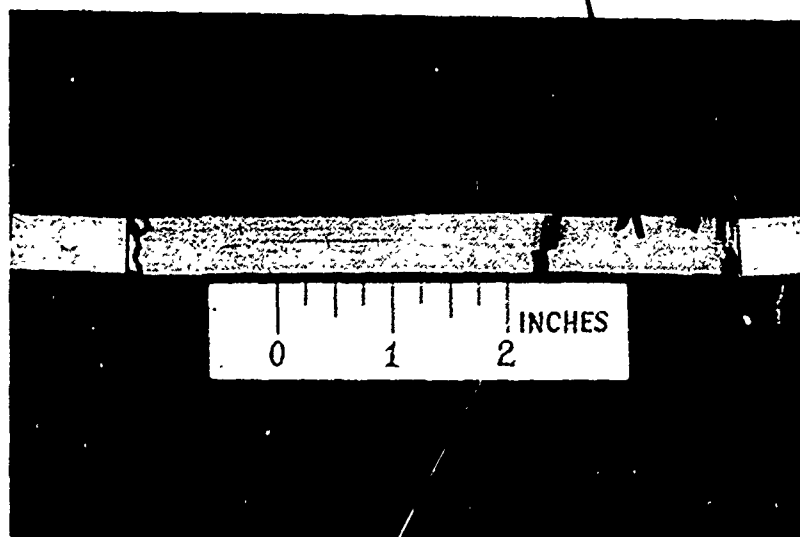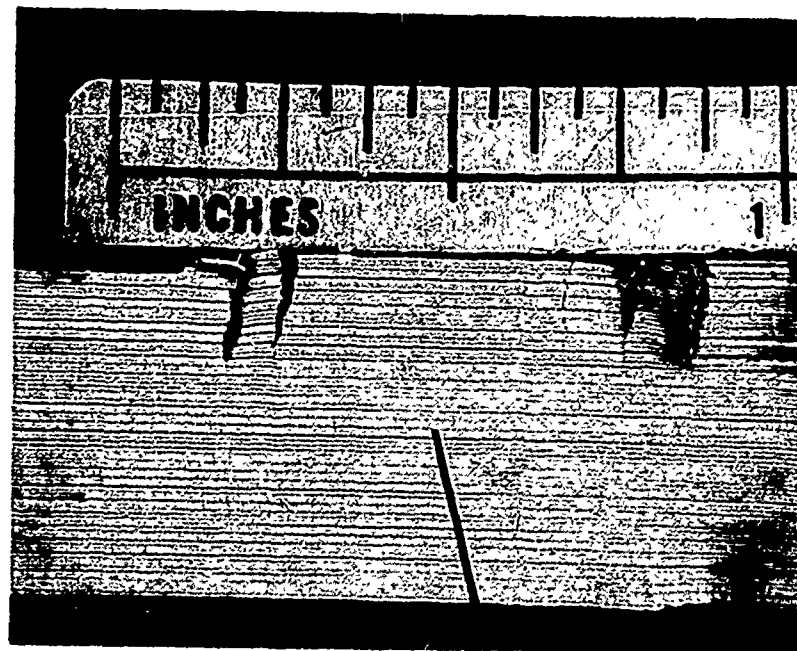
Figure 27   Failure Appearance of a 50% B/Al Monolayer
Tape Specimen. Approximately 34 Filament
Breaks Were Detected Acoustically Prior to
Failure.

51
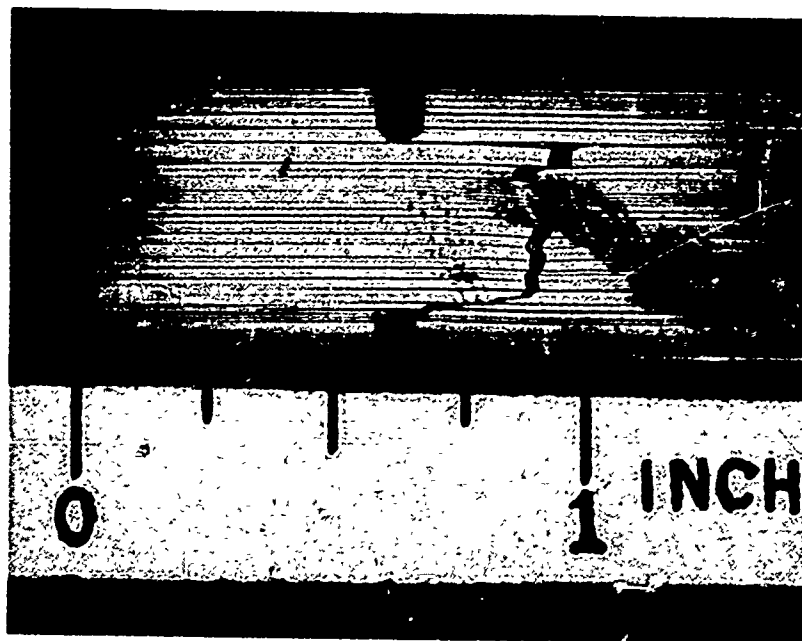
Figure 28   Failure Observation After Tensile Testing of a
Notched Monolayer B/Al Tape Specimen. There Were
5 to 6 Filament Breaks Detected Acoustically Prior
to Failure.
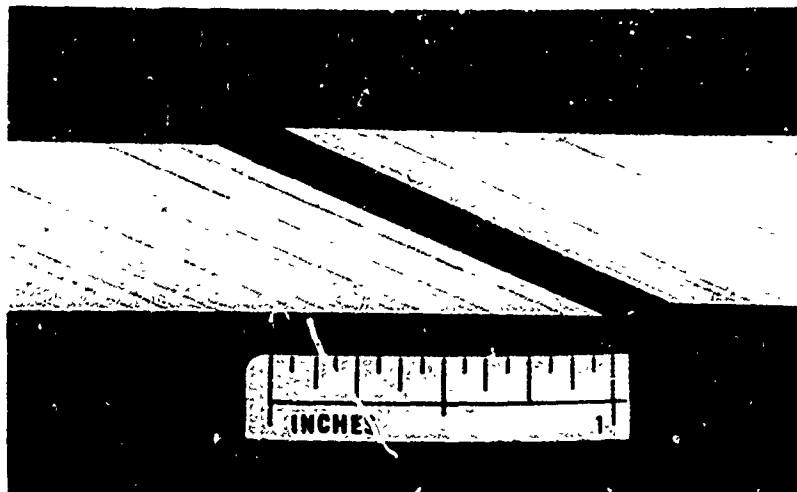
FILAMENT ORIENTATION – 22°
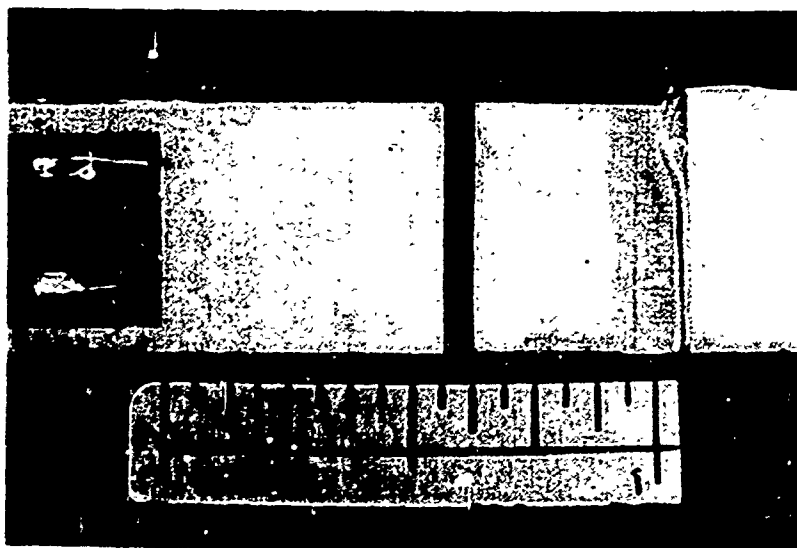
FILAMENT ORIENTATION – 90°

Figure 29   Failure of Two 50 V/O Composites With the Boron Filaments
Oriented With Respect to the Filament Axis

Typical data obtained in these three directions are shown in Figures 30, 31, and 32. Macroscopic yielding in the aluminum when tested in the [0] direction takes place at a composite stress around 55,000 psi, and is evidenced by a knee in the curve. The cause for the small degree of non-linearity just prior to failure is not known, and was not present in all the specimens. In the [22] specimens, plastic flow in the aluminum is much more pronounced, and the aluminum begins to yield at about 13,000 psi. The slopes of the elastic portions of the stress-strain curves in both the longitudinal and transverse direction are represented by the stiffness terms C_{ij} referred to a set of axis rotated [22] with respect to the specimen axis.

The results for the [90] specimens are given in Figure 32. Although a large amount of plastic deformation takes place in the aluminum, it is severely localized and not detected by the strain gages, so the resulting stress-strain curves in both directions appear elastic. The transverse strain was very low (less than 50 μ-in at failure), and at the gain setting used in the recorder this movement was not detected. Consequently, the term ν_{21} was calculated from the relation

$$\frac{\nu_{21}}{E_{22}} = \frac{\nu_{12}}{E_{11}} \tag{1}$$

where E_{11}, E_{22}, ν_{12}, and ν_{12} are the longitudinal and transverse moduli and Poisson's ratio, respectively.

The data in Figures 30 through 32 may be used to calculate the four independent elastic constants. Using the transformation equations, (5)

$$\bar{s}_{11} = \frac{m^4}{E_{11}} - \frac{2m^2 n^2}{E_{11}} \nu_{12} + \frac{n^4}{E_{22}} + \frac{m^2 n^2}{G_{12}}$$

$$\bar{s}_{12} = \frac{m^2 n^2}{E_{11}} - (m^4 + n^4) \frac{\nu_{12}}{E_{11}} + \frac{m^2 n^2}{E_{22}} - \frac{m^2 n^2}{G_{12}} \tag{2}$$

where S_{ij} are elastic compliances, G_{12} the shear modulus, and m and n direction cosines. Using the values obtained from [0] and [90] specimens, E_{11}, E_{22}, and ν_{12} can be measured. Then two values for G_{12} may be obtained from each of the equations in (2), with the result that $G_{12} = 5.91 \times 10^6$ psi $\pm 8\%$. It was found that the four independent elastic constants, based on these limited data, were:

$$E_{11} = 32.2 \times 10^6 \text{ psi}$$

$$E_{22} = 21.9 \times 10^6 \text{ psi}$$

$$G_{12} = 5.91 \times 10^6 \text{ psi} \tag{3}$$

$$\nu_{12} = 0.147$$

54

$$\mathcal{V}_{12} = 0.147$$

Transverse (2)

Axial (1)

$$E_{11} = 32.2 \times 10^6 \text{ psi}$$
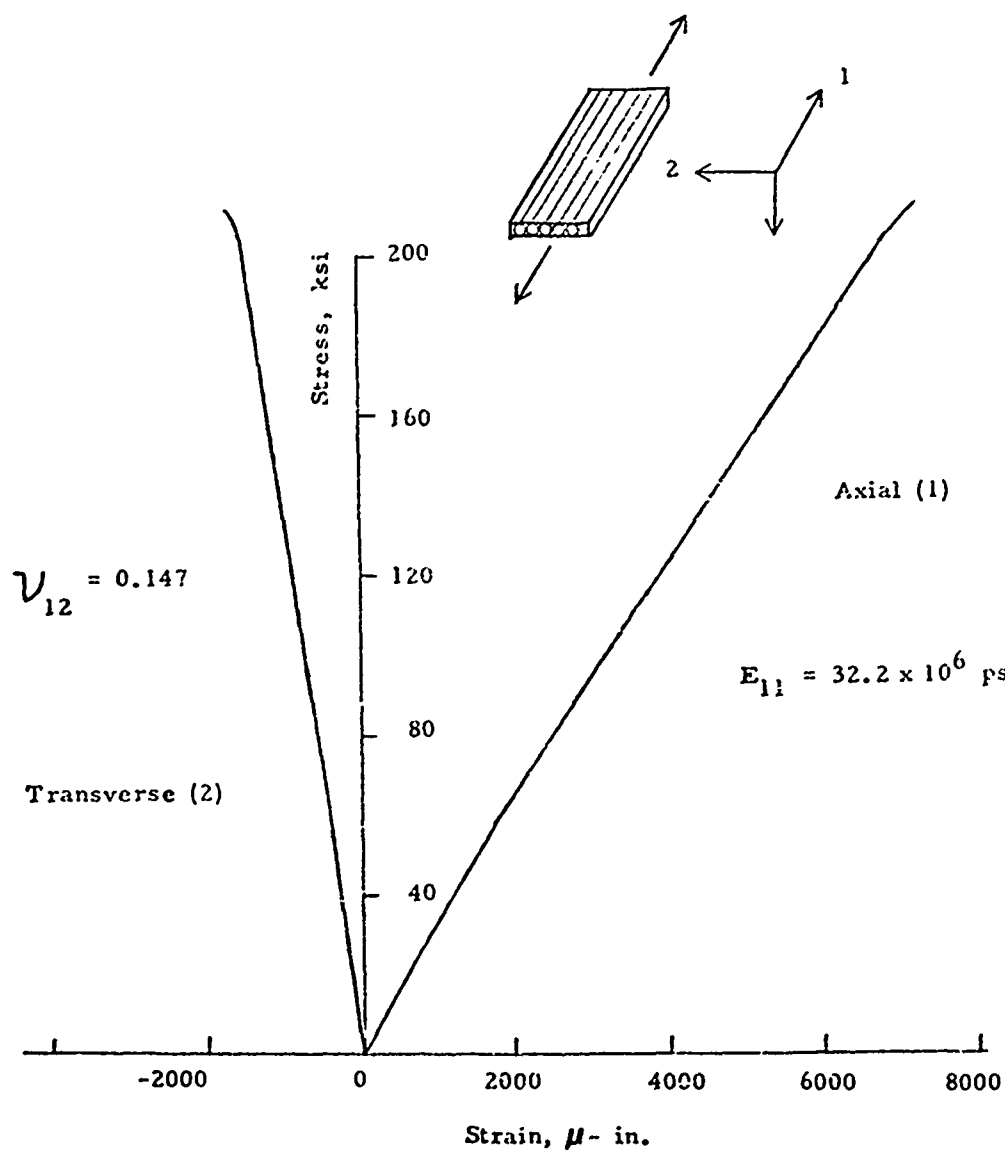
Figure 30 Stress-Strain Curves for 0-degree 50 V/O
Monolayer Tape

Stress, ksi

40

30

Axial (1)

Transverse (2)

20

$\overline{C}_{11}$ = 21.9 × 10^6 psi

$\overline{C}_{12}$ = 75.8 × 10^6 psi

10

2

1

-1000   0   1000   2000   3000   4000

Strain, μ- in.
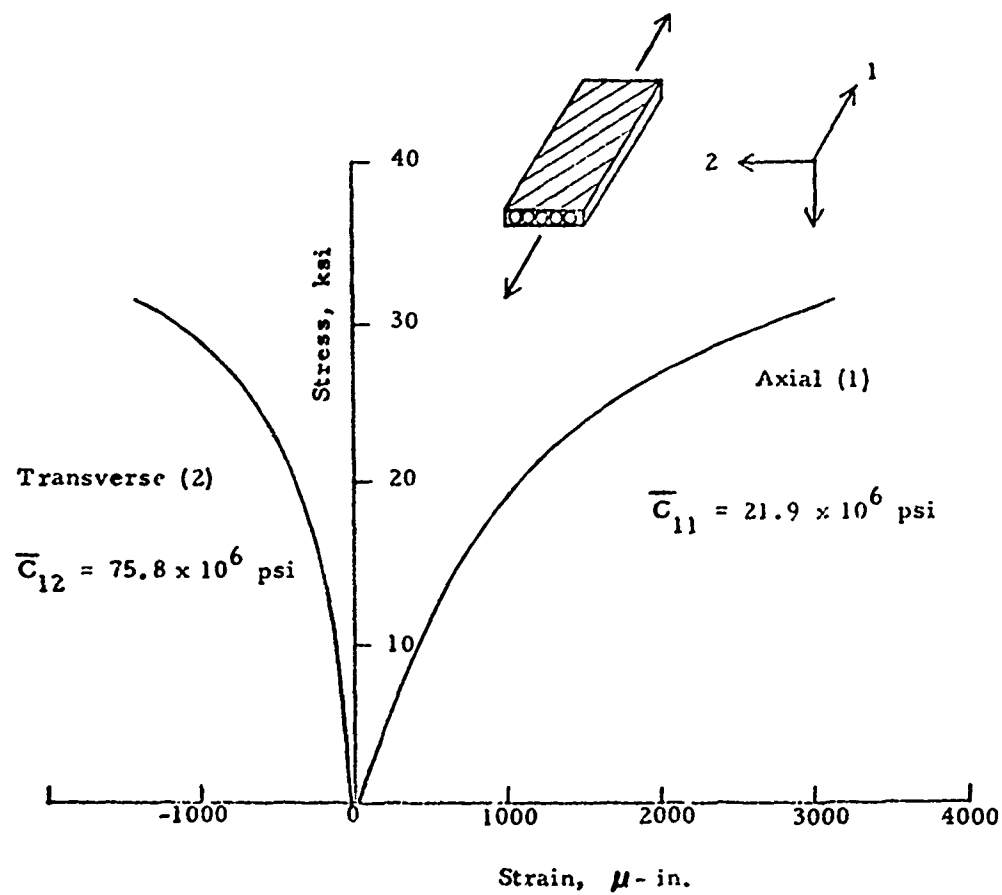
Figure 31 Stress-Strain Curves for 22-Degree 50 V/O
Monolayer Tape
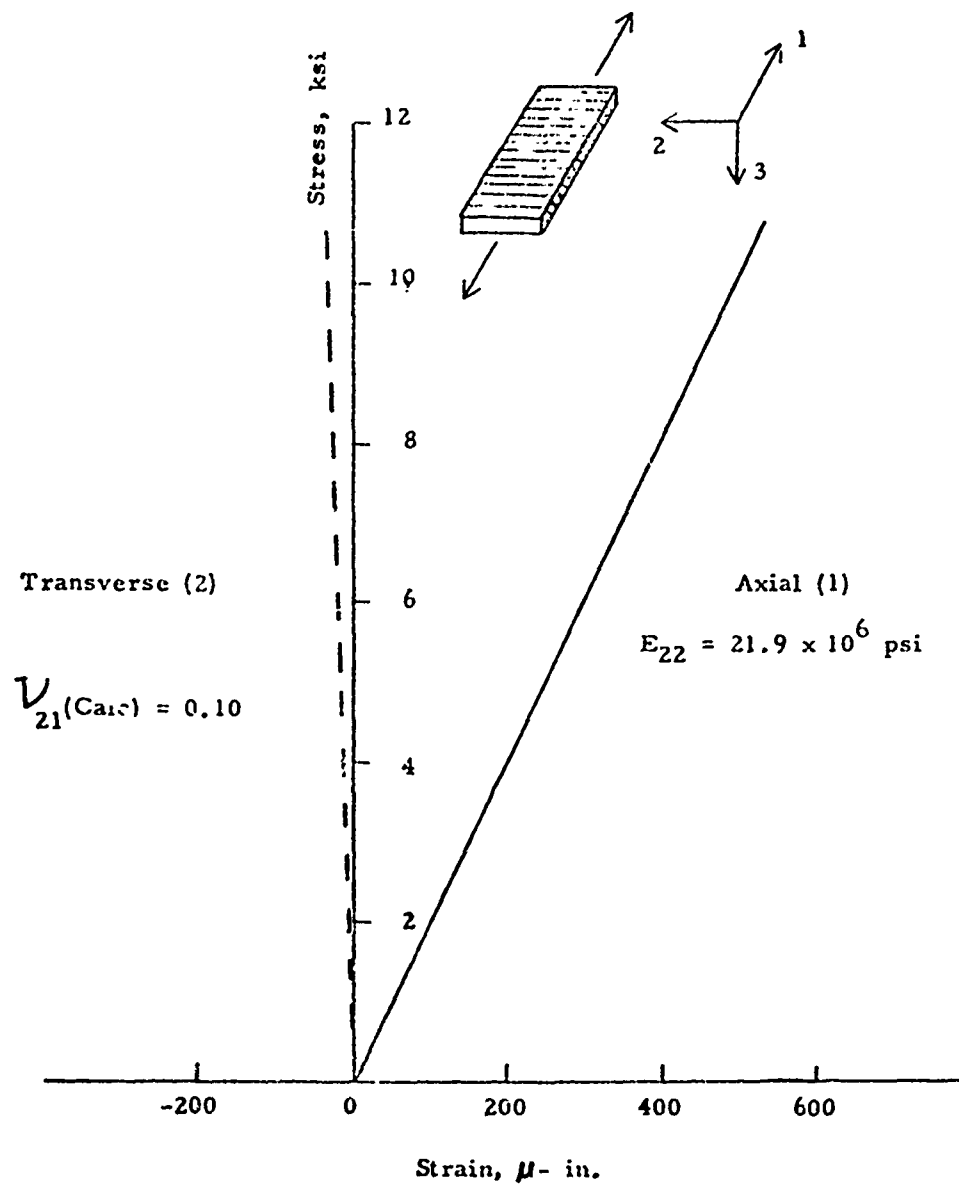
Figure 32 Stress-Strain Curves for 90-degree 50 V/O
Monolayer Tape

Comparing these values to those reported for 50 v/o 4.2 mil filaments (4), it is found that good agreement exists between E_{12} and E_{22}, but G_{12} and ν_{12} are higher for the smaller fibers. The reported values for the smaller fibers are as follows:

$$E_{11} = 33.9 \times 10^6 \text{ psi}$$

$$E_{22} = 20.5 \times 10^6 \text{ psi}$$

$$G_{12} = 8.15 \times 10^6 \text{ psi} \tag{4}$$

$$\nu_{12} = 0.24$$

Whether or not this is representative of the differing fiber diameters is subject to additional work; such work is not in the scope of this program.

Frequency Analysis

Although the basic failure mechanism for the monolayer 45 v/o B/Al tape is reasonably well understood, it was considered of interest to explore the applicability of frequency analysis to the time domain acoustic signal corresponding to a filament fracture. Some earlier work with boron/epoxy composites suggested that there could perhaps be a unique spectrum associated with a filament fracture, but this had not been extended to B/Al.

To perform this work, both an accelerometer and a semiconductor strain gage was affixed to a monolayer B/Al specimen (I-5066) and the acoustic emissions monitored during the test. The tape record of the test was played back at one-quarter of the recording speed (15 ips vs. 3 3/4 ips) into a UA6 Federal spectrum analyzer, and the spectra of the individual filament fracture events was studied.

It was found that the semiconductor strain gage signal was characterized by a high frequency component, about 35-44 KHz, and a low frequency component of about 300 Hz. It is considered likely that these two frequencies correspond to the longitudinal and transverse resonant frequencies of the specimen, which are given by:

$$f = \frac{a_n}{21.1} \frac{h}{\ell^2} \frac{Eg}{\rho} \qquad \text{(Transverse)}$$

$$f = \frac{n}{2} \frac{Eg}{\rho} \qquad \text{(Longitudinal)}$$

when f = frequency, sec^{-1}

     a_n = constant equal to 22.4, 61.7,... for a clamped-clamped beam

     h = thickness, in.

     ℓ = length, in.

$$E = \text{modulus, psi}$$

$$g = \text{gravitational constant} = 386 \text{ in/sec.}$$

$$\rho = \text{density, lb/in}^2$$

$$n = 1, 2, 3, \ldots$$

For a 45 v/o B/Al monolayer specimen, we have $\rho = .095$ lb/in^3
$E = 32 \times 10^6$ psi, $\ell = 5.2$ in. (between grips), and we can compute the following fundamental frequencies:

$$f_o = 131 \text{ Hz} \qquad \qquad \text{(Transverse)}$$

$$f_o = 34.8 \text{ KHz} \qquad \qquad \text{(Longitudinal)}$$

These values are of the correct order of magnitude to account for the observed frequencies.

The spectrum obtained from the accelerometer was considerably more complicated, and was found to consist almost entirely of various resonance modes of the accelerometer. This was not the case for boron/epoxy, where low frequency resonances were detected. It would seem, at the present, that frequency analysis of acoustic events from B/Al composites is not a promising avenue to explore.

V. MATERIAL EVALUATION

A. Tensile

All tensile testing was performed on a 60,000 lb capacity universal testing machine. Strain measurements were obtained with a mechanically averaging LVDT-type, 1-inch extensometer, while load was monitored by a tensile load cell. The outputs from each were fed directly into an X-Y recorder to obtain load-strain curves.

Prior to testing the standard longitudinal tensile specimens to failure, each was cycled three times from 0 to 1000 lbs to properly seat the specimen in the grips and to partially strain harden the aluminum matrix as would be found in a component part having undergone several loading cycles. This method has been found to yield valid, reproducible results. Ballistically impacted and double edge notched specimens were also cycled, but the maximum load was reduced in proportion to the reduction of area due to the notch. Transverse tensile specimens were not cycled. All loading was at a rate of 0.05 in/minute. Elevated temperature testing was conducted using the same set-up, but with the addition of a circulating hot air furnace. Specimens were held fc 12 minutes within ± 5F of test temperature prior to testing, all other parameters being the same.

1. Standard (Smooth) Specimens

In order to obtain baseline data, $[0]_8$ panels were manufactured by the GE-CRB process (6) from which longitudinal and transverse tensile specimens were machined. This baseline tensile data is given in Table XV. Tensile data for the two composite systems being evaluated are given in Table XVI.

One immediate observation that can be made is that in the B/2024 system, the 75F and 600F, but the 75F strength is considerably lower than those quality control results made available by AVCO. Filament strengths at GE/MPTL obtained from the panel in question average 469 ksi which is somewhat lower than other panels supplied. Therefore, it is felt that the 75F strength on the B/2024 tensile tests (i.e., A-2, A-3) is not a fair estimate of that property. To enable comparisons between the two materials being evaluated, a 75F tensile strength is obtained by averaging the two valid tests in Table XVI, along with the five valid QC tests presented by AVCO in Table IV. A vi'. of 179 ksi for the 75F tensile strength of the B/2024 material will be used for the purpose of comparison from this point on.

TABLE XV. BASELINE TENSILE DATA ON CRB PANELS OF $[0]_8$ AND $[90]_8$ 50 v/o BORON REINFORCED 2024 AND 6061 Al

Specimen Number	Matrix Alloy	Filament Orientation	Test Temp (F)	E_1 (10^6 psi)	E_2 (10^6 psi)	UTS (ksi)	ϵ_f (μ in/in)
A-01	2024	[0]	75	32.9	26.7	182	7100
A-02	2024	[0]	75	28.2	21.9	184	8100
A-03	2024	[0]	600	26.3	20.1	185	8900
A-04	2024	[0]	600	22.9	18.3	175	9900
A-06	2024	[90]	75	29.7	-	22.7	1200
A-07	2024	[90]	75	17.3	-	21.9	2300
A-08	2024	[90]	600	11.9	-	9.0	3100
A-09	2024	[90]	600	-	-	9.3	-
B-01	6061	[0]	75	29.8	26.9	208	7800
B-02	6061	[0]	75	28.0	23.5	186	7800
B-03	6061	[0]	600	28.5	18.8	180	8900
B-04	6061	[0]	600	28.5	19.1	179	8300
B-06	6061	[90]	75	16.3	-	19.5	7000
B-07	6061	[90]	75	15.9	-	17.5	5900
B-08	6061	[90]	600	13.9	-	5.2	13000
B-09	6061	[90]	600	14.4	-	5.0	13000

TABLE XVI. TENSILE RESULTS OF $[22/0/-22/0]_s$ ALUMINUM COMPOSITE MATERIALS

Specimen Number	Matrix Alloy	Test Temp (F)	E_1 (10^6 psi)	E_2 (10^6 psi)	ε_f (± in/in)	UTS (ksi)	Avg. UTS (ksi)
A-1	2024	75	28.8	22.2	5000[a]	122[a]	
A-2	2024	75	31.4	23.4	6400	158	179[b]
A-3	2024	77	34.4	23.9	5500	151	
A-4	2024	600	37.0	16.8	7800	145	
A-5	2024	600	25.7	18.3	8100	156	154
A-6	2024	600	25.1	16.6	9200	160	
B-1	6061	75	27.9	19.3	8300	172	
B-2	6061	75	29.8	19.1	8600	173	174
B-3	6061	75	27.2	19.6	8500	177	
B-4	6061	600	21.7	14.3	9100	133	
B-5	6061	600	24.6	14.1	9300	133	132
B-6	6061	600	23.5	15.7	8300	129	

(a) failed in grip region

(b) includes 5 QC results

63

A comparison of smooth longitudinal tensile results indicates that moduli reflect the higher volume percentage reinforcement on the B/2024 material (50 v/o vs 45 v/o for B/6061) while 75F tensile strengths are essentially equal. The 600F tensile strength of the B/2024 is greater primarily due to the greater matrix shear strength at that temperature. The B/6061 material seems to exhibit greater strain to fracture for a given UTS.

The failure mode in tension does not seem to be clearly either one of cumulative or non-cumulative filament fracture. It has been shown that there is a range of stress over which high strength boron filament will fail, with statistically more failures occurring at the higher stresses. Test results indicate that while some individual weaker filaments fail during loading of the composite specimens, the majority of filaments fail in a narrow stress range to cause almost instantaneous, gross failure of the specimen, or in a manner approximating a non-cumulative failure mode.

Composite failure occurs when filament fractures are linked by shear failure in the matrix. Shear lag analysis predicts that the greater the matrix or filament-matrix shear strength, the greater the density of filament fractures allowed without composite failure. Therefore, the greater the matrix shear strength, the flatter the fracture surface and the greater the composite strength.

This analysis becomes considerably more complex when crossplied material is investigated. The interactions between [0] and off axis plies are not well understood and could not be evaluated effectively within the scope of this program.

In general, it was observed that the fracture surfaces of the 75F specimens were relatively flat thereby supporting the above shear lag hypothesis.

Figures 33 and 34 are fracture surfaces of representative B/2024 tensile specimens tested at 75 and 600F. The only difference noted (other than the topography) is the matrix of the specimen tested at 600F has a larger cell structure and globular surface commensurate with the higher temperature exposure. Similar fractography was observed in B/6061 specimens.

2. Double Edge Notched Specimens ($K_t = 3$)

Testing results of the double edge notched specimens, designed to have a notch stress concentration factor of $K_t = 3.0$, are presented in Table XVII. As can be seen, the effective stress concentration (UTS smooth/UTS notched) is considerably less than that value (3.0) for both materials. The effective stress concentration also decreases in both materials at 600F most probably due to the decreased matrix shear strength being unable to transfer the stress any considerable distance, thus making the notch less effective as a stress raiser.

It should be noted that as in the case of the notched monolayer B/Al specimen discussed previously, the fracture did not occur at the notched cross-section, but to one side of it. This observation reinforces the previous observation that the stress concentration caused by a notch, however slight as compared to homogeneous materials, occurs at some distance from the parallel to the notched cross-section.

64
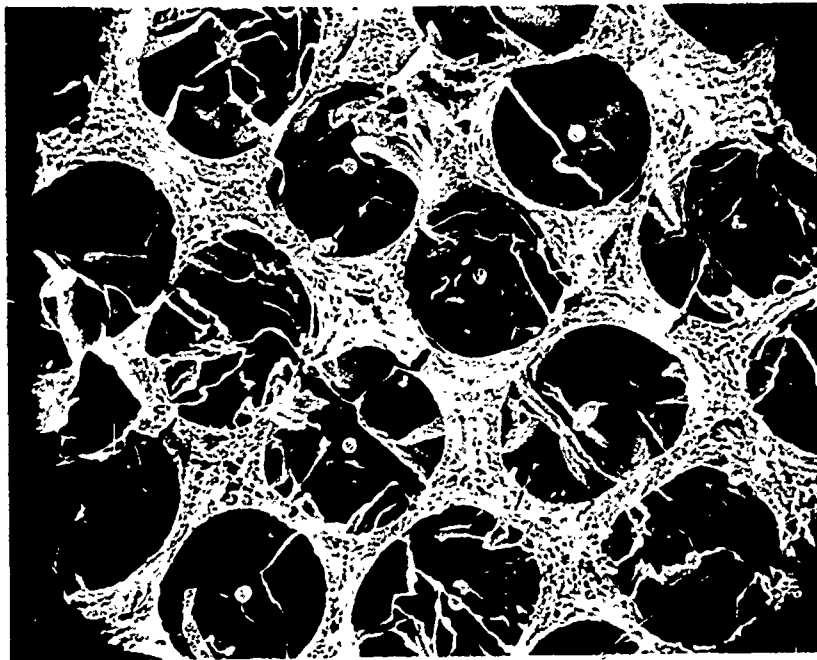
FILAMENTS AND MATRIX AT 143X
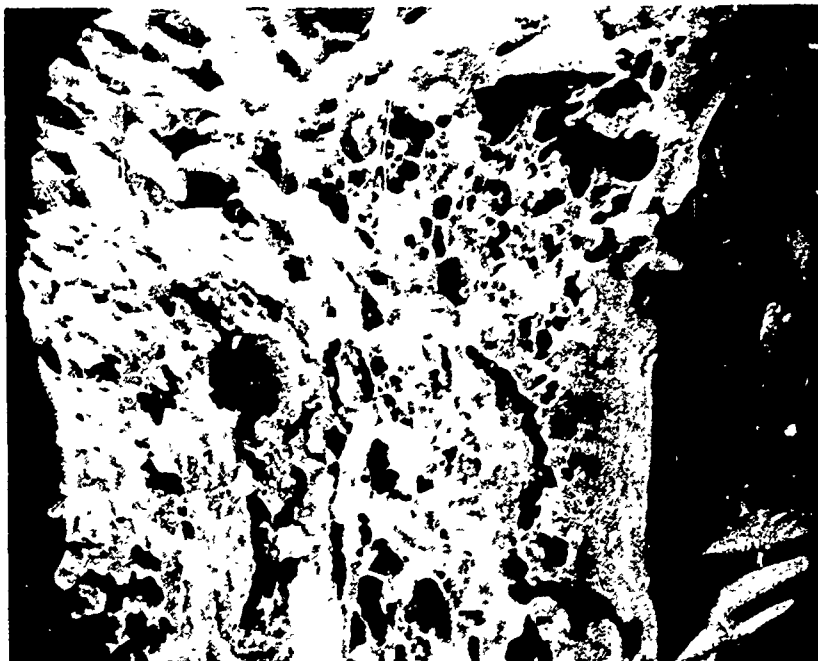
MATRIX AT 1430X

Figure 33   Fracture Surface of a B/2024 Tensile Specimen Tests at 75°F
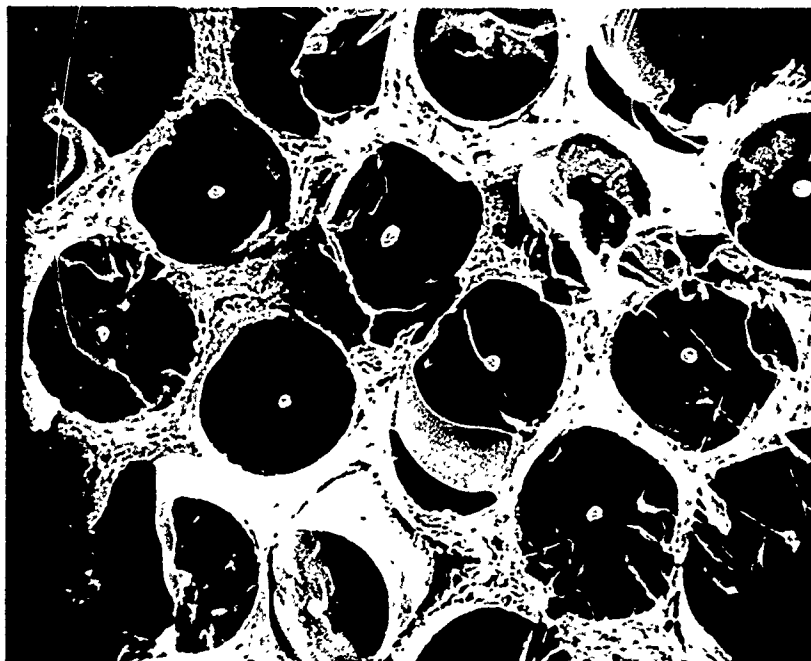
FILAMENTS AND MATRIX AT 145X

MATRIX AT 1450X

Figure 34 Fracture Surface of a B/2024 Tensile Specimen Tested at 600°F

TABLE XVII. TENSILE RESULTS OF DOUBLE EDGE NOTCHED AND BALLISTICALLY IMPACTED [22/0/-22/0]$_2$ 50 v/o 5.6 MIL B REINFORCED 2024 AND 6061 ALUMINUM

	Specimen Number	Matrix Alloy	Test Temp (F)	Notch Depth (in)	UTS Notched (ksi)	K_t (effective)(a)	K_t (analytical)(b)
Double Edge Notched	A-77	2024	75	.038	156	1.15	3.0
	A-78	2024	75	.038	144	1.25	3.0
	A-79	2024	75	.038	151	1.19	3.0
	A-80	2024	600	.038	130	1.19	3.0
	A-81	2024	600	.038	128	1.20	3.0
	A-82	2024	600	.038	137	1.12	3.0
	B-75	6061	75	.038	126	1.33	3.0
	B-76	6061	75	.038	124	1.41	3.0
	B-77	6061	75	.038	109	1.59	3.0
	B-78	6061	600	.038	127	1.04	3.0
	B-79	6061	600	.038	126	1.04	3.0
	B-80	6061	600	.038	129	1.02	3.0
Ballistically Impacted	A-27	2024	75	.056	77.9	2.30	1.7
	A-28	2024	75	.097	62.9	2.85	1.7
	A-29	2024	75	.083	76.7	2.33	1.7
	A-30	2024	600	.107	77.5	2.00	1.7
	A-31	2024	600	.111	72.9	2.13	1.7
	A-32	2024	600	.107	56.2	2.70	1.7
	B-27	6061	75	.037	109	1.59	1.7
	B-28	6061	75	.029	106	1.64	1.7
	B-29	6061	75	.028	112	1.56	1.7
	B-30	6061	600	.077	79.7	1.64	1.7
	B-31	6061	600	.064	95.6	1.37	1.7
	B-32	6061	600	.046	90.7	1.45	1.7

(a) UTS smooth/UTS notched

(b) Stress Concentration Design Factors, R. E. Peterson, John Wiley & Sons, 1953.

3. Ballistically Impacted Specimens

The results of the ballistically impacted specimens, also Table XVII, are more difficult to interpret. Damage to the specimen by hard body ballistic impact is two-fold. First, the 0.175 inch diameter ball causes a notch, in the specimen edge, of approximately its diameter with depth varying from specimen to specimen. Secondly, the impact causes filament damage in the proximity of the impact notch. The extent of peripheral damage cannot be determined quantitatively, but can be related directly to notch depth.

Since the specimen design which imposes a stress concentration of $K_t = 3.0$, determined analytically for homogeneous materials, does not cause an effective stress concentration near that value in the materials evaluated in the program, it is safe to assume that the single edge notch configuration of the ballistically impacted specimens, $K_t \approx 1.7$, will not effectively concentrate stress to any great extent. Therefore, any strength decrease caused by a ballistic impact notch must be caused mainly by damage internal to the material, rather than stress concentration. By assuming effective stress concentration factors for B/2024 and B/6061 composite materials at 75F and 600F, in light of values obtained in the double edge notched testing, Table XVII, it is possible to calculate an effective reduction in cross-section. a*

Since

$$UTS_{smooth} = \frac{P}{t \times w} \quad \text{and}$$

$$UTS_{notched} = \frac{P}{t \times (w-a)}$$

where: P = failure load (lbs)

t = thickness (in)

w = width (in)

and a = apparent notch depth (in),

then $$\frac{UTS_{smooth}}{UTS_{notched}} = \frac{(w-a)}{w} = K_t \text{ (effective)}$$

If a value of $UTS_{smooth}/UTS_{notched}$ were assumed for a particular specimen, since w is fixed, "a" must be replaced with a*. Using this method, an a* was calculated for each specimen using the assumed values listed in Table XVIII.

TABLE XVIII. ASSUMED VALUES OF K_t (EFFECTIVE)

	B/2024	B/6061
75F	1.10	1.20
600F	1.05	1.00

A plot of a vs a*, Figure 35, indicates a good degree of correlation. This theory is further supported in Figure 36, where a transverse cross-section through a ballistic impact notch reveals an area of broken filaments adjacent to the notch.

The purpose of this explanation is to show that the extremely low strengths of the B/2024 ballistically impacted specimens in Table XVII, as compared to the B/6061, is not a deficiency of the material. The strengths in the table are calculated using the apparent notch depth. It can be seen that the notch depths of the B/2024 specimens are considerably greater than the B/6061. This can magnify, as seen in Figure 35, since the effective reduction in cross section increases at a faster rate than does the physically measurable damage.

The conclusion obtained is that hard body ballistic impact has a degrading effect on B/Al, not by causing stress concentrations, but by causing internal filament damage adjacent to the impact making failure at that notch much more likely, and that B/2024 is not more suceptable to ballistic impact damage than is B/6061.

B. Axial Fatigue

All axial fatigue tests of B/2024 and B/6061 composite materials in the standard test specimen configuration were conducted on a Sonntag SF-1-U Universal Fatigue Machine. Dynamic forces were produced by a rotating mass at 30 Hz. The positive mean stress necessary to obtain an A-ratio of 0.95 ($A = \sigma_{alternating}/\sigma_{mean}$) was superimposed on the dynamic load by a preload spring. The machine was dynamically calibrated with standard strain gauge load cells prior to testing. Specimens were gripped in the same manner as tensile specimens.

Elevated temperature tests were monitored with two chromel alumel thermocouples fixed to either side of the gauge section with RTV-106 silicon rubber. Heat was provided by passing air through a heat exchanger and then diffusing the heated air around the specimen.

1. Standard (Smooth) Specimens

Results of standard axial fatigue tests of B/2024 and B/6061 at 75F, 300F and 600F are found in Table XIX. Data are displayed graphically in Figure 37. In testing, a modified stairstep method was employed with run out defined as 10^7 cycles without failure. Several specimens had lives longer than 10^7 cycles, these specimens are denoted by an arrow on the plot of maximum stress vs cycles to failure. A straight line, relationship (on the semi log plot) was assumed to adequately describe those stress levels investigated. It appears that the elevated temperature curves approach the room temperature curves of each composite material, respectively, at short fatigue lives.

Fatigue limits at 10^7 cycles were determined to be the midpoint between the run out stress and the next higher stress investigated. (For the B/6061 material for which no runout was obtained, the fatigue limit was the intersection of the curve best fitting the data and the 10^7 cycle line). These limits in ksi are listed in Table XX.

TABLE XX. FATIGUE LIMITS OF B/Al COMPOSITE MATERIALS

Material	75F (ksi)	300F (ksi)	600F (ksi)
B/2024	91.5	87.5	54
B/6061	92.5	70	45

69
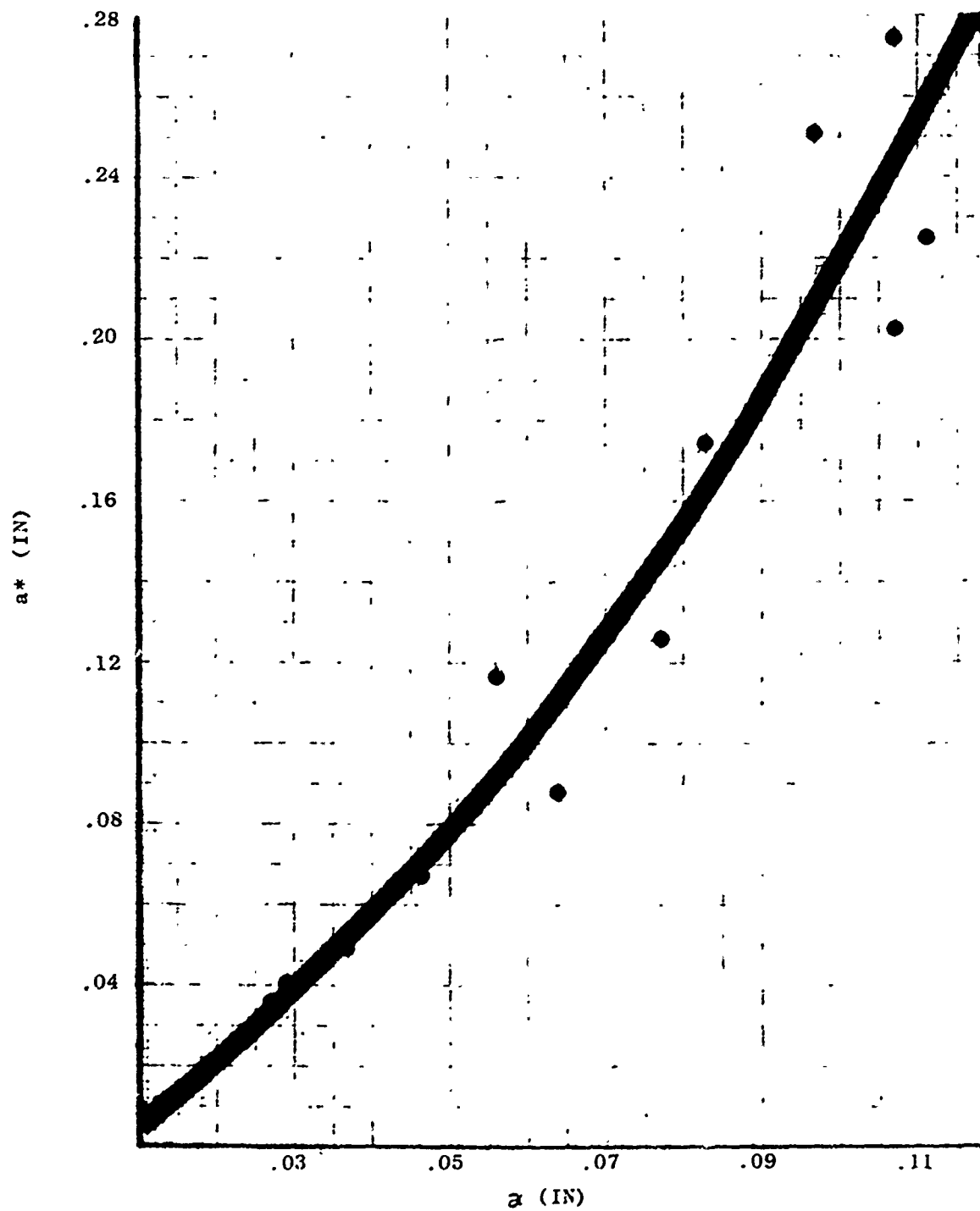
Figure 35   Plot of Apparent Notch Depth (a) Vs. Effective Notch Depth (a*) in Ballistically Impacted $[22/0/-22/0]_8$ B/Al Composite Specimens

TABLE XIX. STANDARD AXIAL FATIGUE (A = 0.95) RESULTS [22/0/-22/0]s 50 v/o 5.6 MIL B/6061 Al COMPOSITE MATERIAL AND 45 - v/o 5.6 MIL B/6061 Al COMPOSITE MATERIAL.

| Specimen Number	Matrix Alloy	Test Temp. (F)	Maximum Stress (ksi)	Cycles (x 10³)	Remarks
A-75	2024	75	88	15228.	Runout
A-7	2024	75	95	3504.	Failure
A-8	2024	75	110	9.	Failure
A-9	2024	75	90	242	Failure
A-10	2024	75	95	192	Grip Failure
A-11	2024	300	85	12241	Runout
A-12	2024	300	90	9425	Failure
A-13	2024	300	100	1570	Failure
A-14	2024	300	85	-	Failed on loading
A-61	2024	600	90	198	Failure
A-15	2024	600	52	10060	Runout
A-16	2024	600	80	1449	Failure
A-17	2024	600	56	5646	Failure
A-18	2024	600	75	532	Failure
A-19	2024	600	70	1040	Failure
A-20	2024	600	60	5843	Failure
B-7	6061	75	95	3682	Failure
B-8	6061	75	90	10000	Runout
B-9	6061	75	100	1991	Failure
B-10	6061	75	105	438	Failure
B-11	6061	300	65	12524	Failure
B-12	6061	300	90	750	Failure
B-13	6061	300	80	1876	Failure
B-14	6061	300	75	6042	Failure
B-15	6061	600	90	174	Failure
B-16	6061	600	80	100	Failure
B-17	6061	600	48	5733	Failure
B-18	6061	600	70	399	Failure
B-19	6061	600	60	2559	Failure
B-20	6061	600	52	5487	Failure
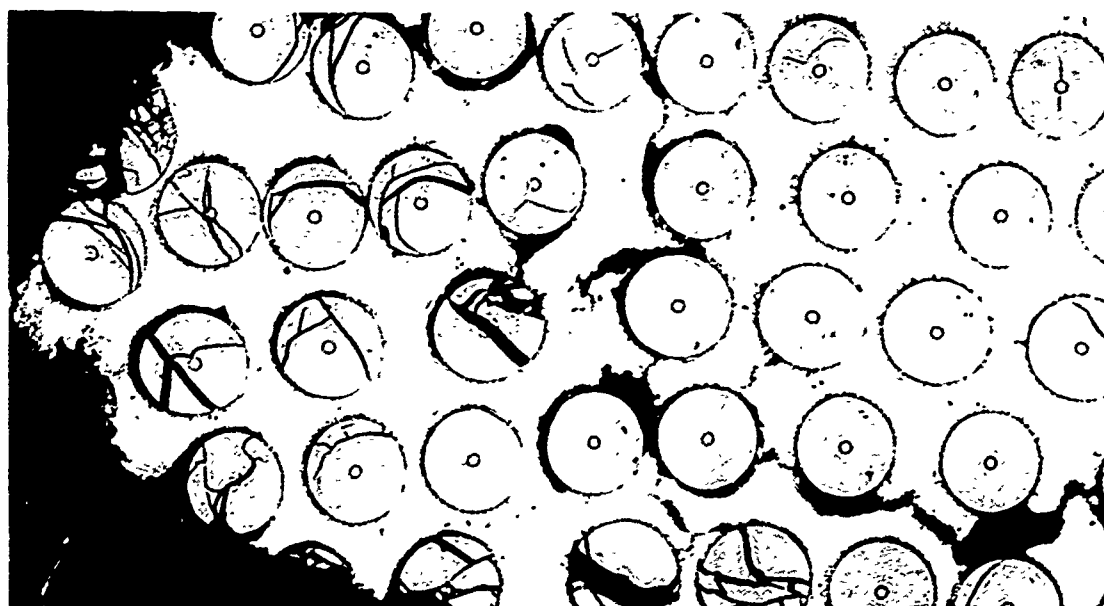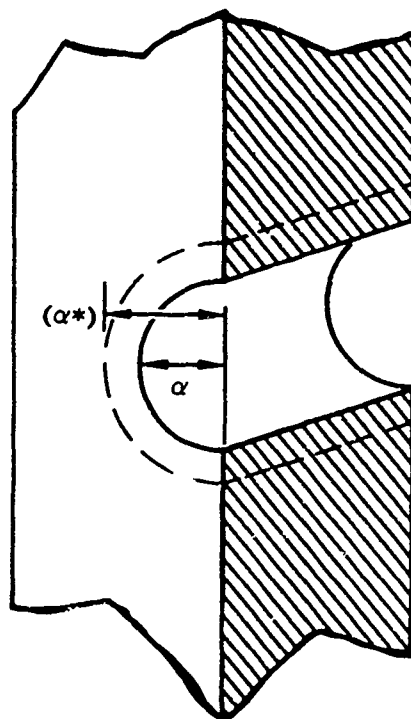
Figure 36   Explanation of Concept of Effective Notch in Ballisti-
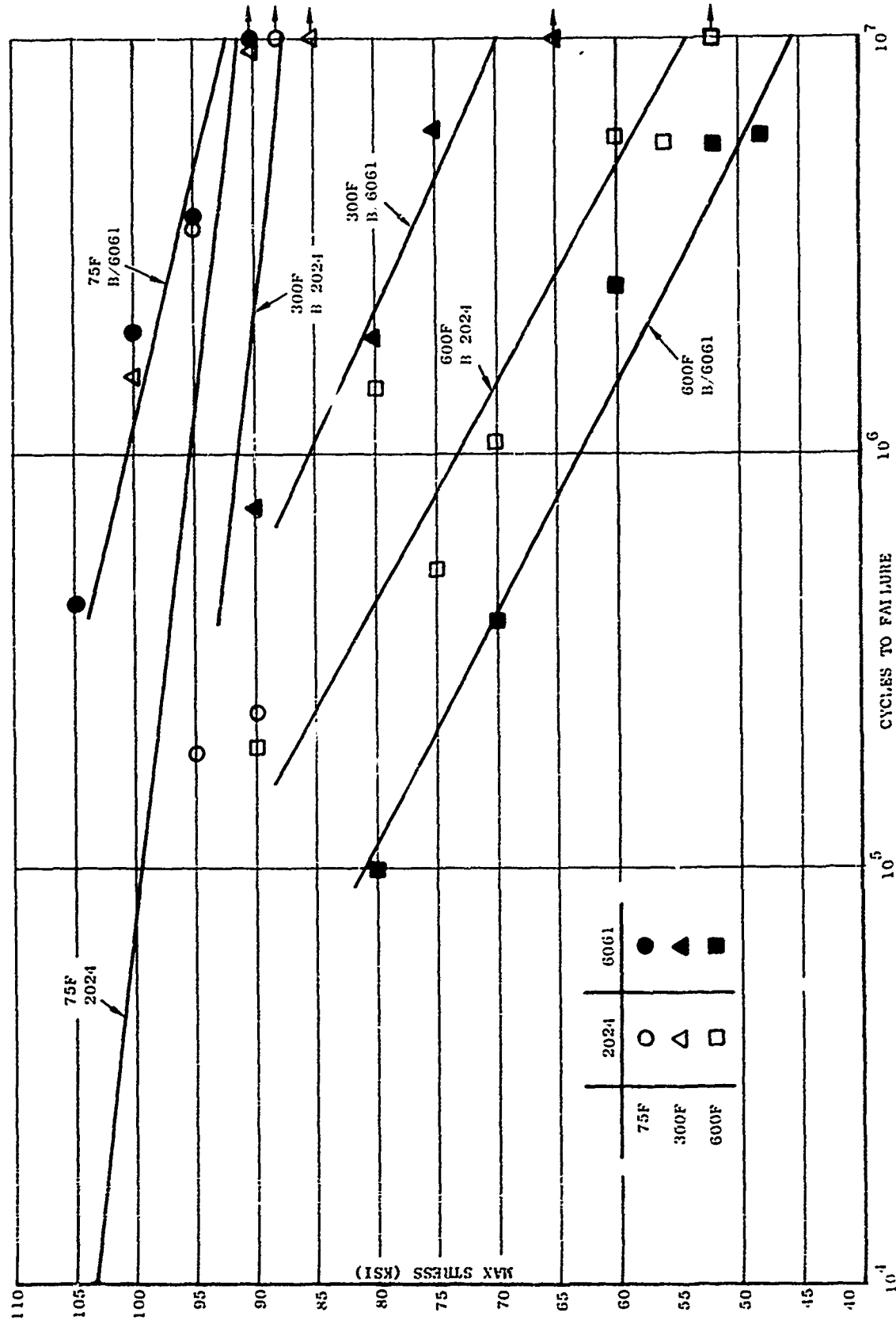cally Impacted $[22/0/-22/0]_8$ B/Al Specimens

Figure 37 Axial Fatigue Results of Standard B/2024 and B/6061 [22/0/-22/0]$_8$ Composite Specimens Tested at 75, 300, and 600F (A=0.95)

73

The axial fatigue specimens are shown in Figures 38, 39, and 40 in the condition they were received from testing vendor. (The dark globules on the gauge section of elevated temperature specimens is the RTV used to hold the thermocouples. This was not removed for fear of damaging the specimens.) The 75F B/2024 specimens exhibit well defined fracture surfaces with no delamination, as can be seen in Figure 38. The 75F B/6061 specimens, on the other hand, have interfilament cracking and delamination along with a well defined fracture surface. At 300F specimens of both systems, Figure 39, look much like those tested at 75F, with a little more delamination and interfilament cracking in the B/6061.

Specimens of both systems tested at 600F had a high degree of delamination. No well defined fracture surface exists as is shown in Figure 40.

The key to the difference in fracture behavior between the two composite systems is most likely in the strengths of the matrix materials involved. Since there is very little use for heat-treatable aluminum alloys in the O-temper, there was scant data available for strength at elevated temperatures. With limited testing at GE/MPTL and considerable engineering judgment, the plot presented in Figure 41 is believed to be a fair representation of the UTS as a function of temperature. (The shear strength is approximately 60% of the UTS at a given temperature.)

The difference in the fracture characteristics at 300F can ostensibly be explained by the fact that the 300F strength of 2024 is greater than the 75F strength of 6061 which is in the range of 20 ksi. This leads one to believe that when the matrix material is lowered into the range of approximately 15 to 20 ksi, there is a change in the axial fatigue failure mechanism from one of transverse crack propagation to one of interply delamination. Delamination continues until one or more [22] plies fail in shear causing over load tensile failure in the remaining plies.

Summarizing, at 75F the B/2024 and B/6061 systems are equally resistant to axial fatigue type loading. At 300F the B/2024 system is clearly superior due to the matrix strength being above the postulated threshold stress for delamination type failure. At 600F both systems are essentially equal with the B/2024 system having a slight advantage due to high matrix strength.

2. Axial Fatigue of Notched Specimens

Results of double edge notched and ballistically impacted axial fatigue tests are listed in Table XXI. As can be seen in Figure 42 notched specimen fatigue lives are in good agreement with smooth specimen curves. This confirms the conclusion reached concerning the notched tensile specimens. That is, machined notches are not effective stress concentrators, at least at low levels of K_t. It is interesting to note that the double edge notch specimens, displayed along with those ballistically impacted in Figure 43 and 44, failed in the same manner as did the edge notched tensile specimens, at a plane parallel to but some distance from the plane of the notch.

The impacted fatigue specimens were evaluated using the concept of effective reduction in cross-section a^*, evolved in analyzing the impacted tensile specimens. Fatigue limits obtained in the same manner as for the smooth specimens are presented in Table XXII.

74

Figure 38   B/Al Axial Fatigue Specimens After Testing at 75F

A-11   A-12   A-13   A-14   B-11   B-12   B-14
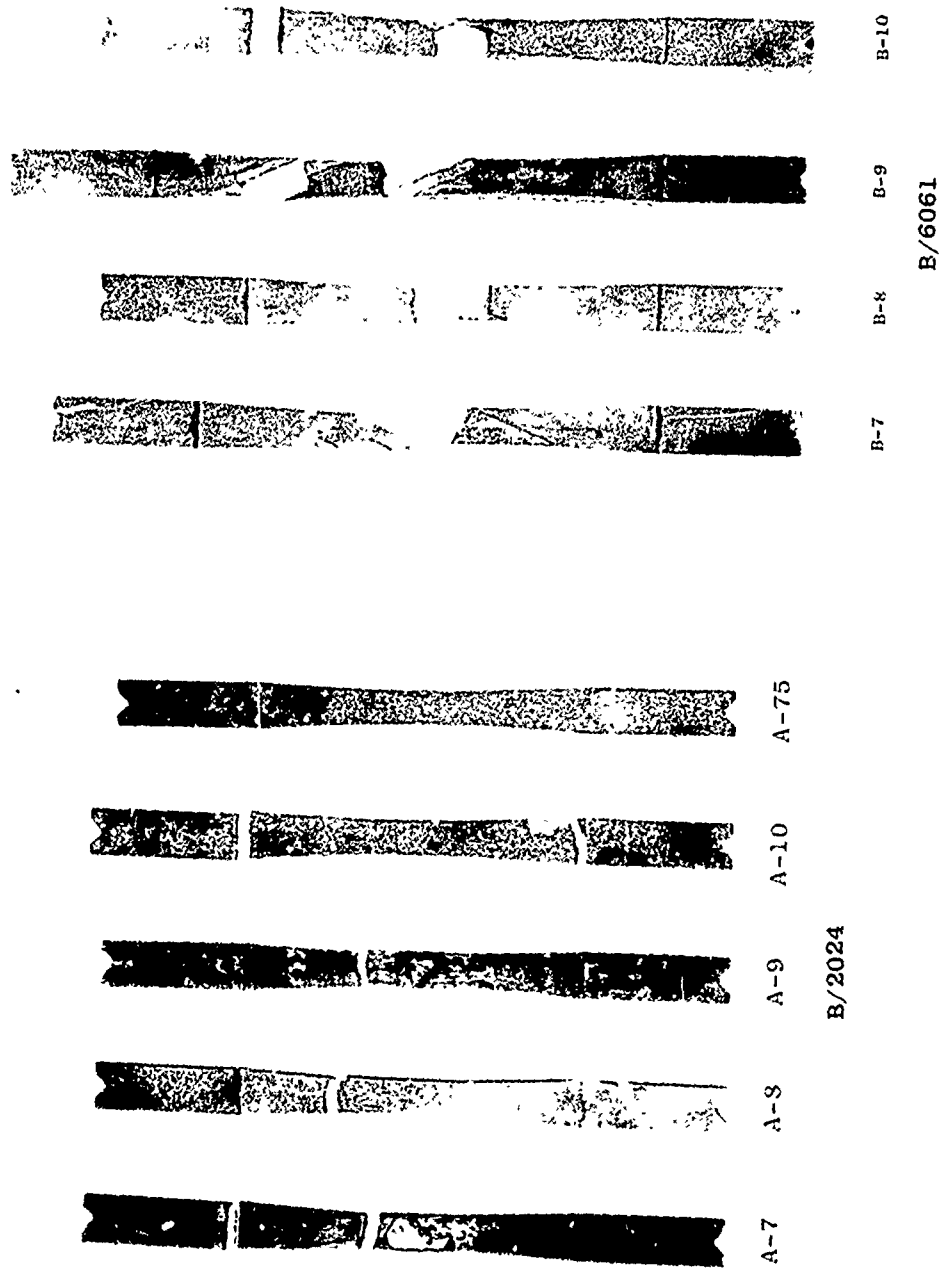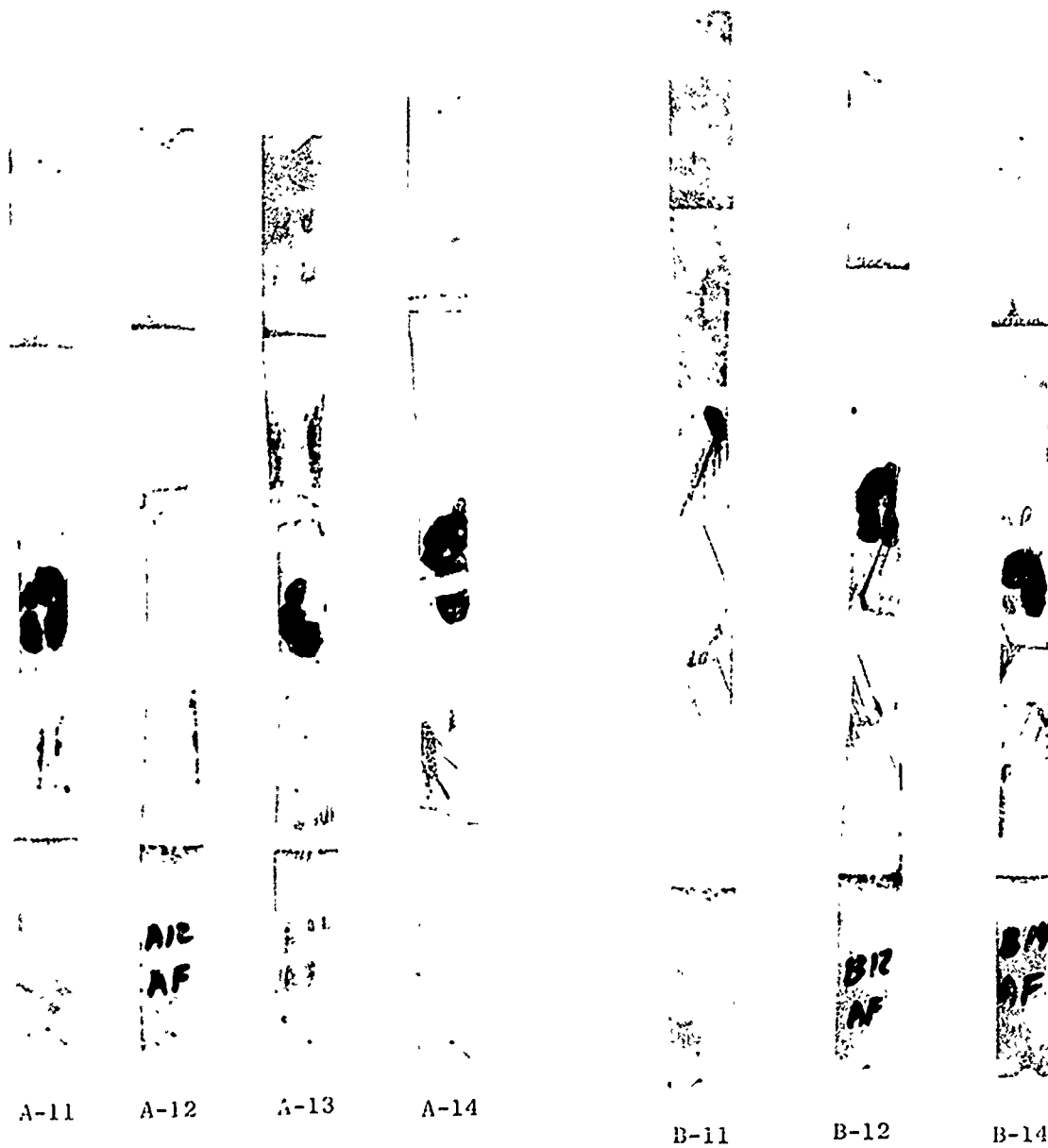
AXIAL FATIGUE

Figure 39   B/Al Axial Fatigue Specimens After Testing at 300F

76

Figure 40 B/Al Axial Fatigue Specimens After Testing

B-20

B-19

B-18   B-17   B/6061

B-16

B-15

A-20

A-19   B/2024

A-18

A-17

A-16

A-15

77
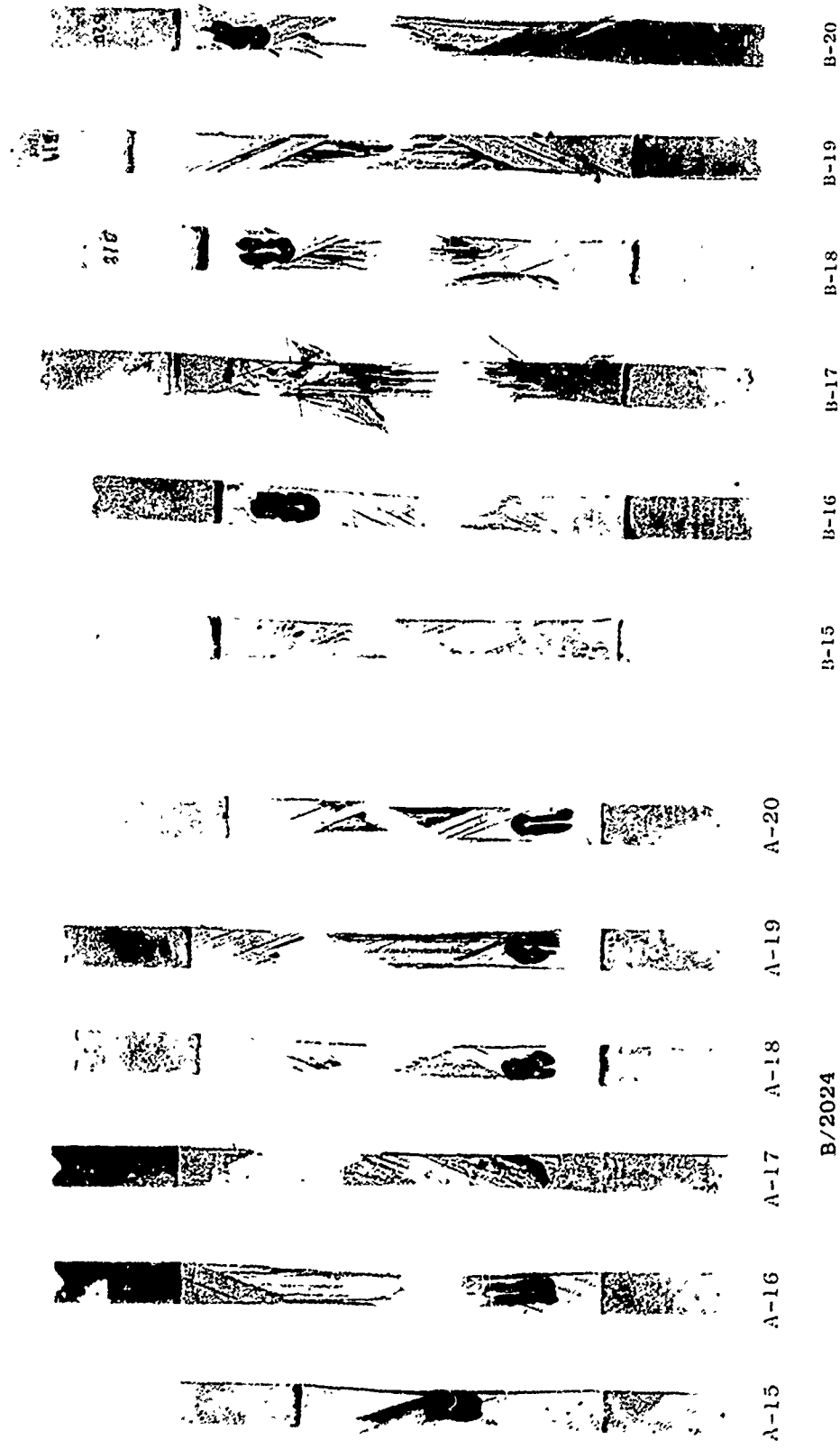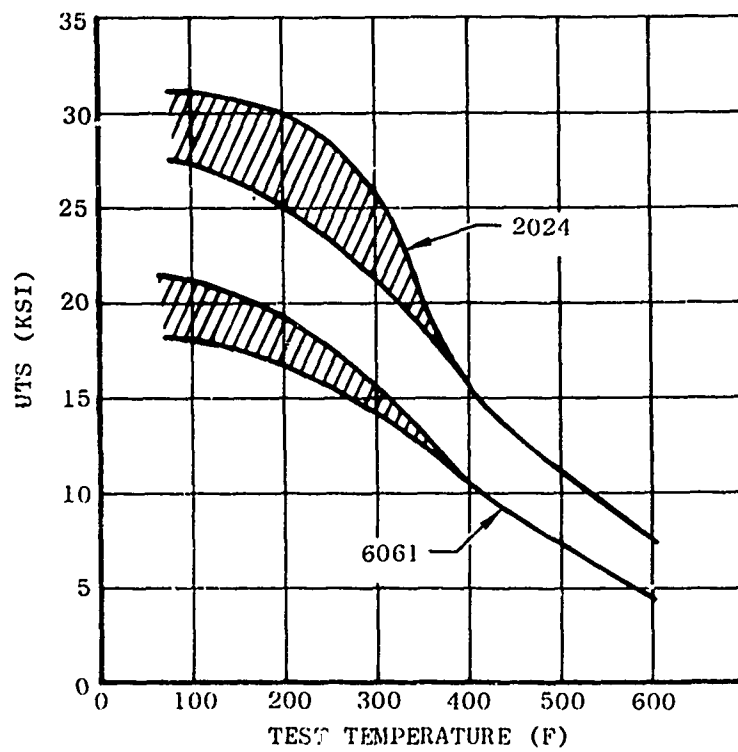
Figure 41   Tensile Strength Vs. Temperature for 2024 and 6061 Aluminum Alloys

78

TABLE XXI. AXIAL FATIGUE RESULTS OF DOUBLE EDGE NOTCHED AND BALLISTICALLY
IMPACTED B/2024 AND B/6061 COMPOSITE MATERIAL

	Specimen Number	Matrix Alloy	Test Temp(F)	Notch Depth(in)	Max. Stress [(a)]	Cycles (10^2)	a^* (in) [(b)]	UTS (ksi) [(b)] *
Double Edge Notched	A-83	2024	75	.038	60	11268	–	–
	A-84	2024	75	.038	110	2219	–	–
	A-85	2024	75	.038	125	2	–	–
	A-86	2024	600	.038	75	1002	–	–
	A-87	2024	600	.038	65	3854	–	–
	A-88	2024	600	.038	58	10005	–	–
	B-81	6061	75	.038	115	95	–	–
	B-82	6061	75	.038	104	54	–	–
	B-83	6061	600	.038	50	2638	–	–
	B-84	6061	600	.038	42	10003	–	–
Ballistically Impacted	A-33	2024	75	.091	80	0.5	.190	122
	A-34	2024	75	.046	60	109	.070	65
	A-35	2024	75	.033	50	10080	.045	52
	A-36	2024	600	.086	40	9465	.180	52
	A-37	2024	600	.046	45	10075	.070	49
	A-38	2024	600	.084	50	7625	.180	75
	B-33	6061	75	.055	60	8124	.090	67
	B-34	6061	75	.063	70	3816	.105	81
	B-35	6061	75	.048	62	10074	.075	66
	B-36	6061	600	.058	45	8680	.100	552
	B-38	6061	600	.045	50	3481	.070	54
	B-39	6061	600	.048	43	9030	.075	47

(a) Calculated Using apparant notch

(b) Calculated using effective reduction in cross-section method
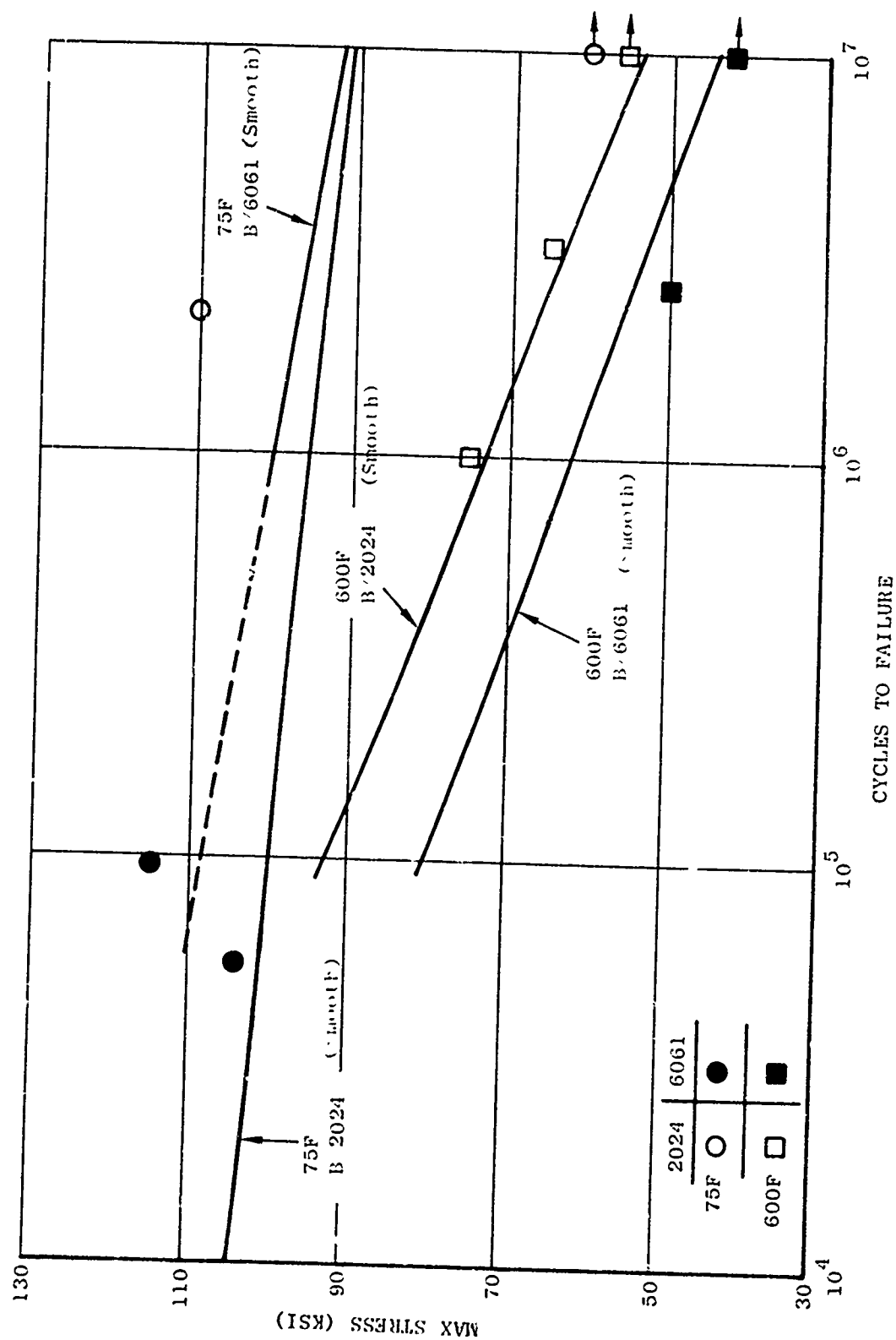
Figure 42 Axial Fatigue Results for Double Edge Notched B Al Composite Specimen
(K_t = 3) Compared to Results of Smooth Specimens

80

A-38
A-37
A-36
600F

A-88
A-87
A-86
A-35
75F
A-34
A-33

A-85
A-84
A-83
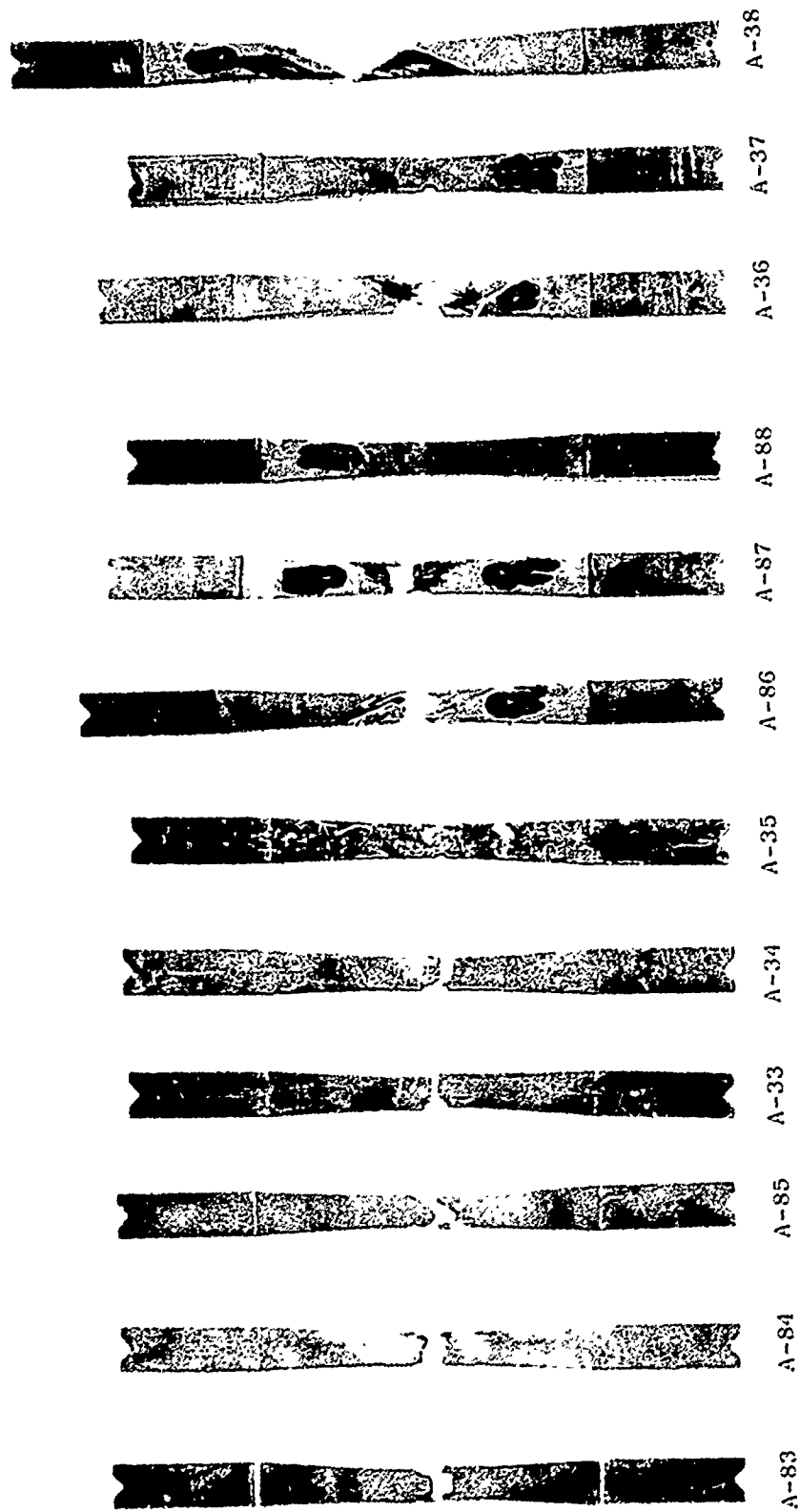
Figure 43   Double Edge Notched and Ballistically Impacted B/2024 Axial Fatigue
Specimens After Testing at 75 and 600F

81
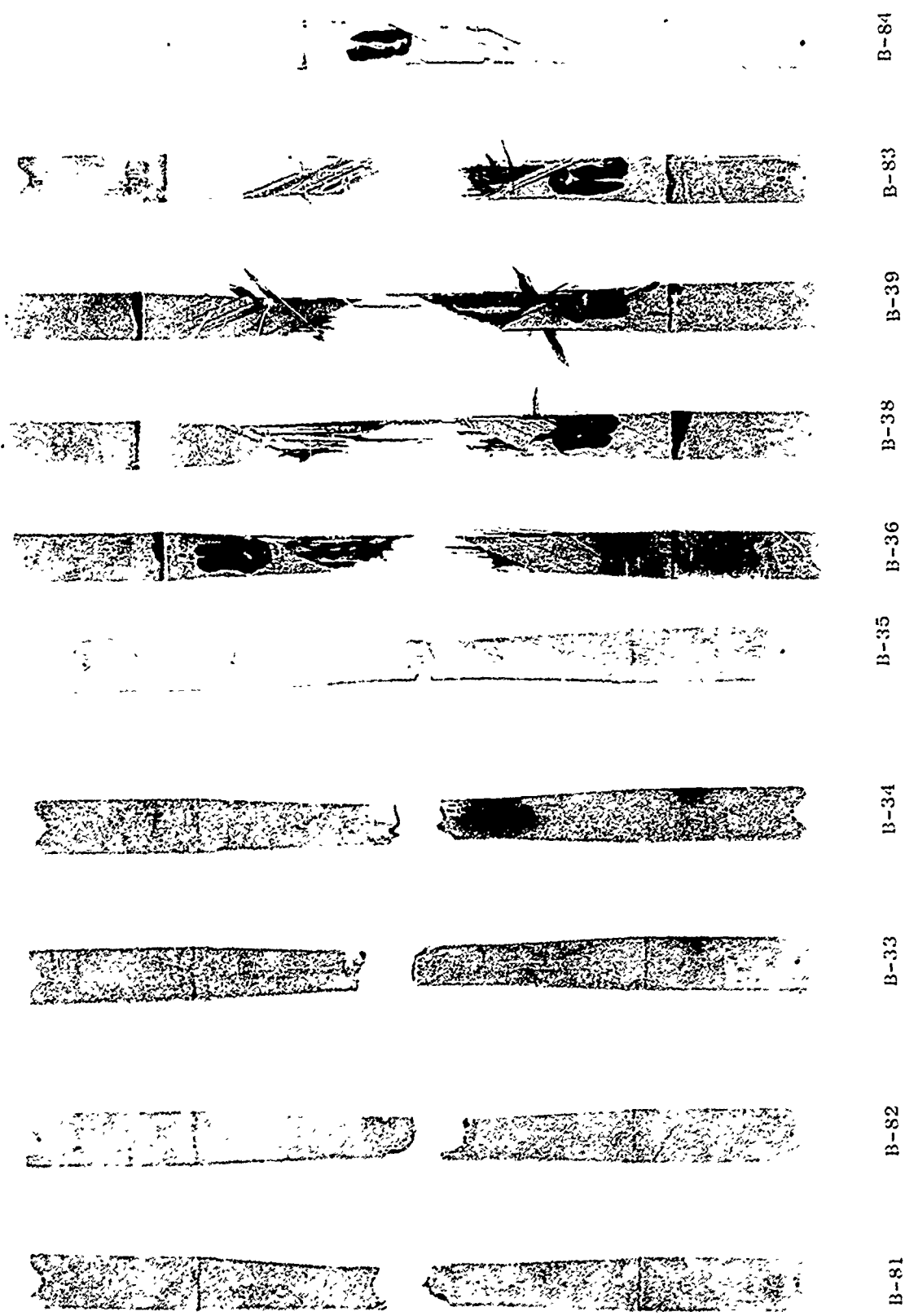
Figure 44   Double Edge Notched and Ballistically Impacted B/6061 Axial Fatigue
Specimens After Testing at 75 and 600F

82

TABLE XXII

FATIGUE LIMITS OF IMPACTED B/Al

SPECIMENS AT 10^7 CYCLES (in ksi)

Material	75F	600F
B/2024	59	54
B/6061	66	45

Using this analysis, the 600F axial fatigue strengths for both composite systems are the same as for smooth specimens, but the 75F strengths are substantially reduced. It should be noted that the 600F specimens failed in the delamination mode with the ballistic impact notch having little effect. The 75F specimens failed through the notch in a manner similar to smooth specimen tests at that temperature. The reason for the reduced 75F strength is that the damaged area adjacent to the notch is essentially a region of unreinforced aluminum, with numerous fractured filaments which are excellent sites from which fatigue cracks can initiate.

3. Effect of Cyclic Thermal Exposure on Axial Fatigue Properties

Axial fatigue test results of specimens tested after cyclic thermal exposure are presented in Table XXIII, and the data plotted in Figure 45 comparison with curves generated by standard specimens. The strengths of the specimens tested at 600F are essentially unchanged by the cyclic thermal exposure while the 75F strengths are reduced.

L, viewing the tested specimens in Figure 46, one can rationalize that the B/2024 strengths are not representative since two specimens failed near the grip and the third was a runout. The B/6061 specimens, however, exhibit the delamination failure mode, probably initiated by matrix damage caused by differential expansion of adjacent plies during thermal exposure. The 600F specimens of both systems exhibit delamination with that of the B/6061 specimens being the more severe.

Metallography of B/Al material having undergone 2000 cycles from -60F to +540F indicates there is no obvious damage, as shown in Figure 47.

4. Axial Fatigue Mechanisms

Axial fatigue failure of B/Al occurs by fatigue crack growth through the matrix. Cracks can grow parallel to the filaments, pass through at a filament fracture, and continue to grow. Crack growth continues at many locations, linking filament failures and other fatigue cracks until overload failure occurs. Figure 48 is a scanning electron micrograph of a failed fatigue specimen. The area on the left of the specimen is one of fatigue crack growth, while the area on the right of the specimen is typical of an overload tensile failure. At higher magnification it is possible to resolve fatigue striations in areas where excessive rubbing has not occurred. An example of these striations at 6800x is given in Figure 49.

Figure 50 is a photomicrograph of a B/6061 axial fatigue specimen showing the fatigue cracks emanate from the matrix/filament interface. Cracks grow between the original plies and are linked with cracks growing laterally through the specimen.

83

TABLE XXIII. AXIAL FATIGUE RESULTS OF B/A1 COMPOSITE SPECIMENS TESTED AFTER CYCLIC THERMAL EXPOSURE[a]

Specimen Number	Matrix Alloy	Test Temp. (F)	Maximum Stress (ksi)	Cycles (10^3)
A21	2024	75	95	153
A22	2024	75	90	372
A23	2024	75	70	10002
A24	2024	600	60	2477
A25	2024	600	55	6735
A26	2024	600	70	2108
B21	6061	75	85	259
B22	6061	75	90	163
B23	6061	75	70	1277
B24	6061	600	50	2787
B25	6061	600	45	5599
B26	6061	600	60	1499

(a) 2000 cycles from -60F to +540F.
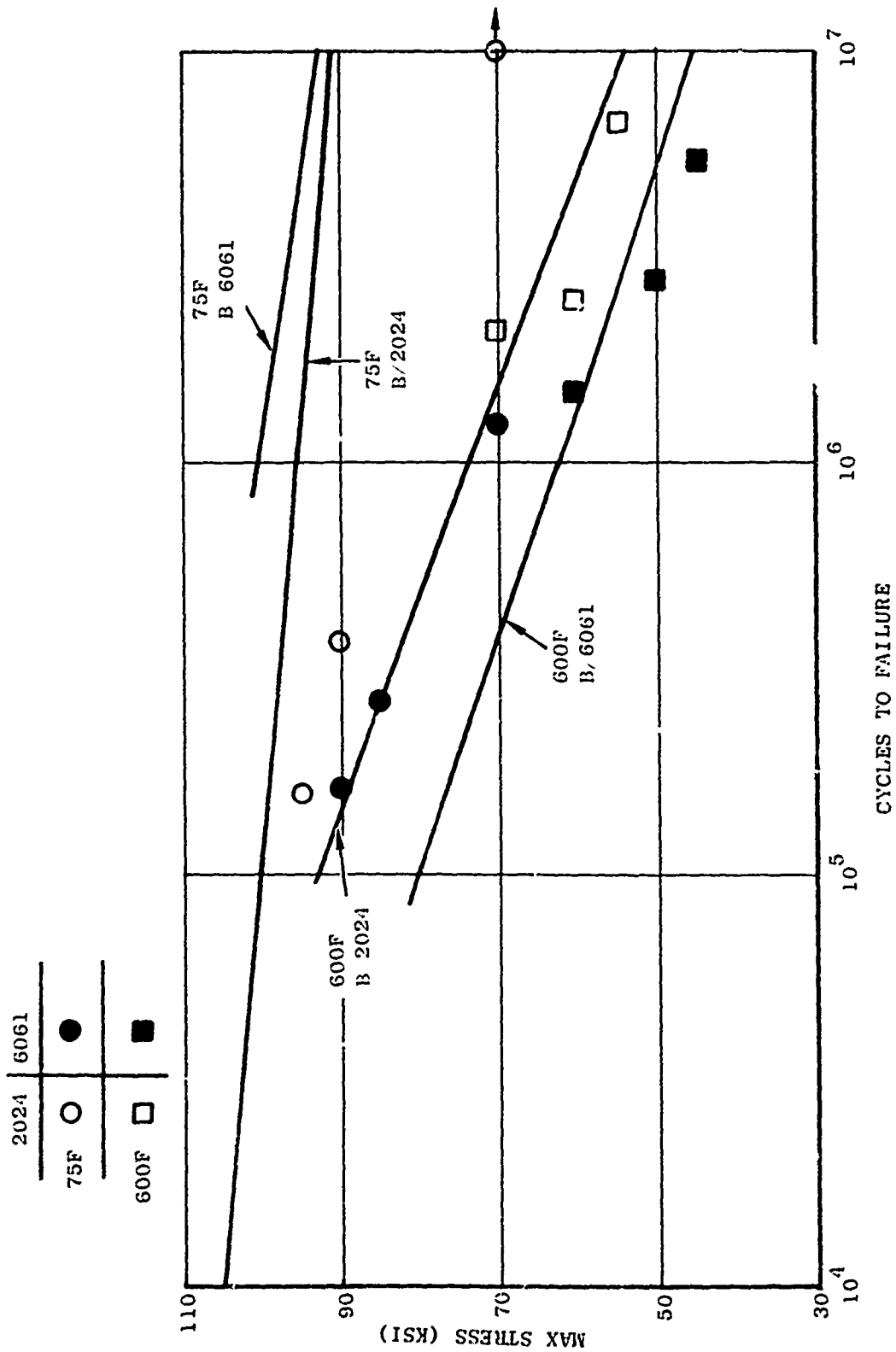
Figure 45   Axial Fatigue of B-Al Composite Specimens Thermally Cycled from – 60F
to +540F Two Thousand (2000) Times

85
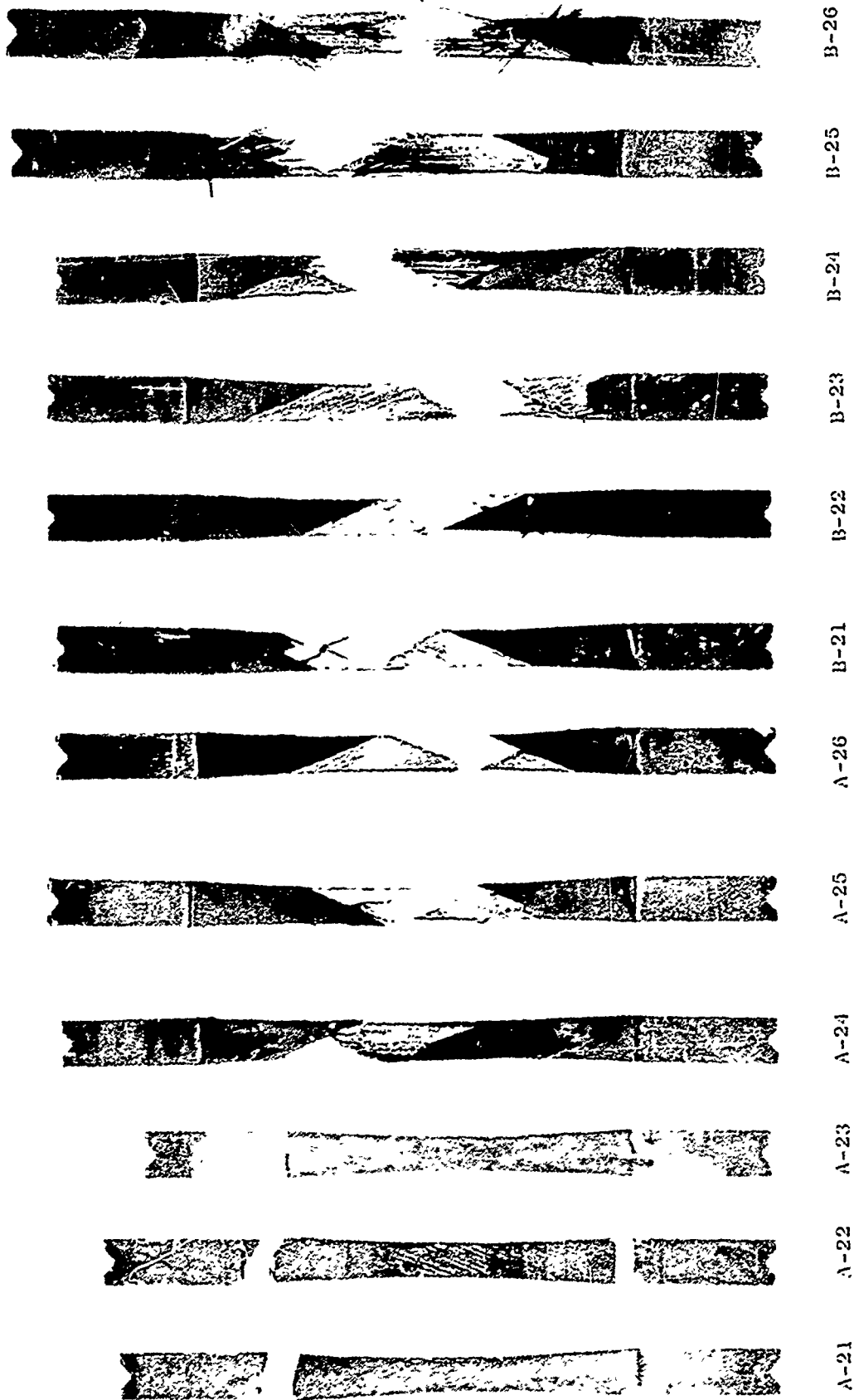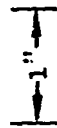
Figure 46   B/Al Axial Fatigue Specimens as Tested at 75 and 600F After Having Been
Thermally Cycled 2000 Times From -60F to +540F

86
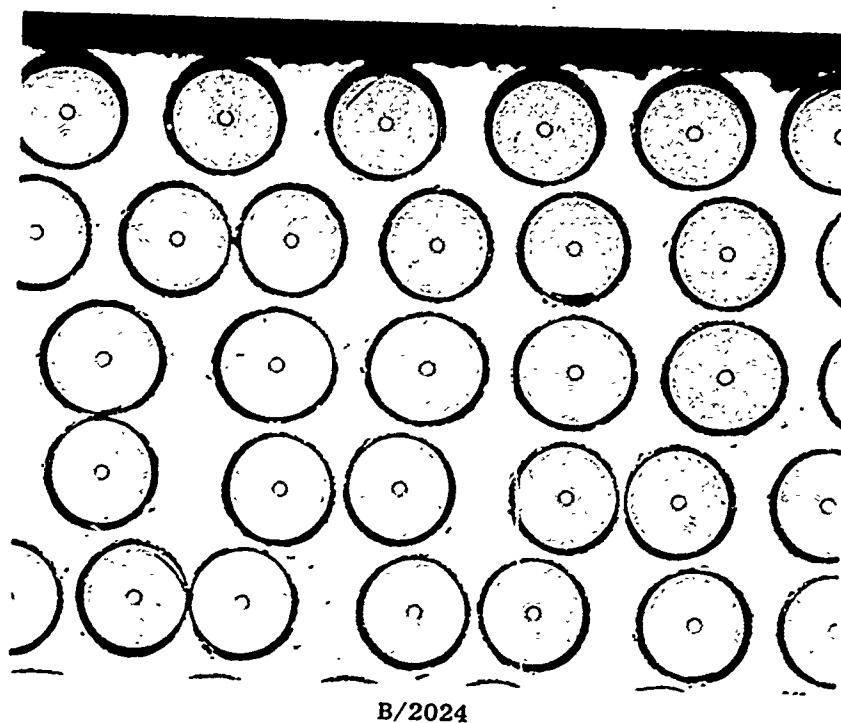
B/2024
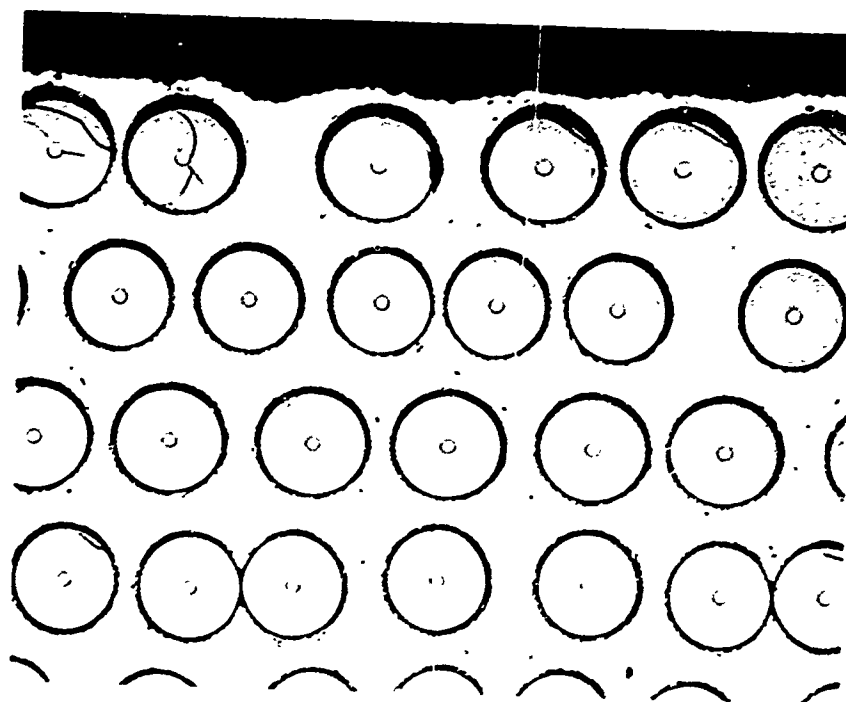
B/6061

Figure 47   Microstructure of B/Al $[22/0/-22/0]_8$ Composite Material Having Undergone Two Thousand (2000) Cycles from -60F to +540F (100X)

(b) FATIGUE   (c) OVERLOAD TENSILE
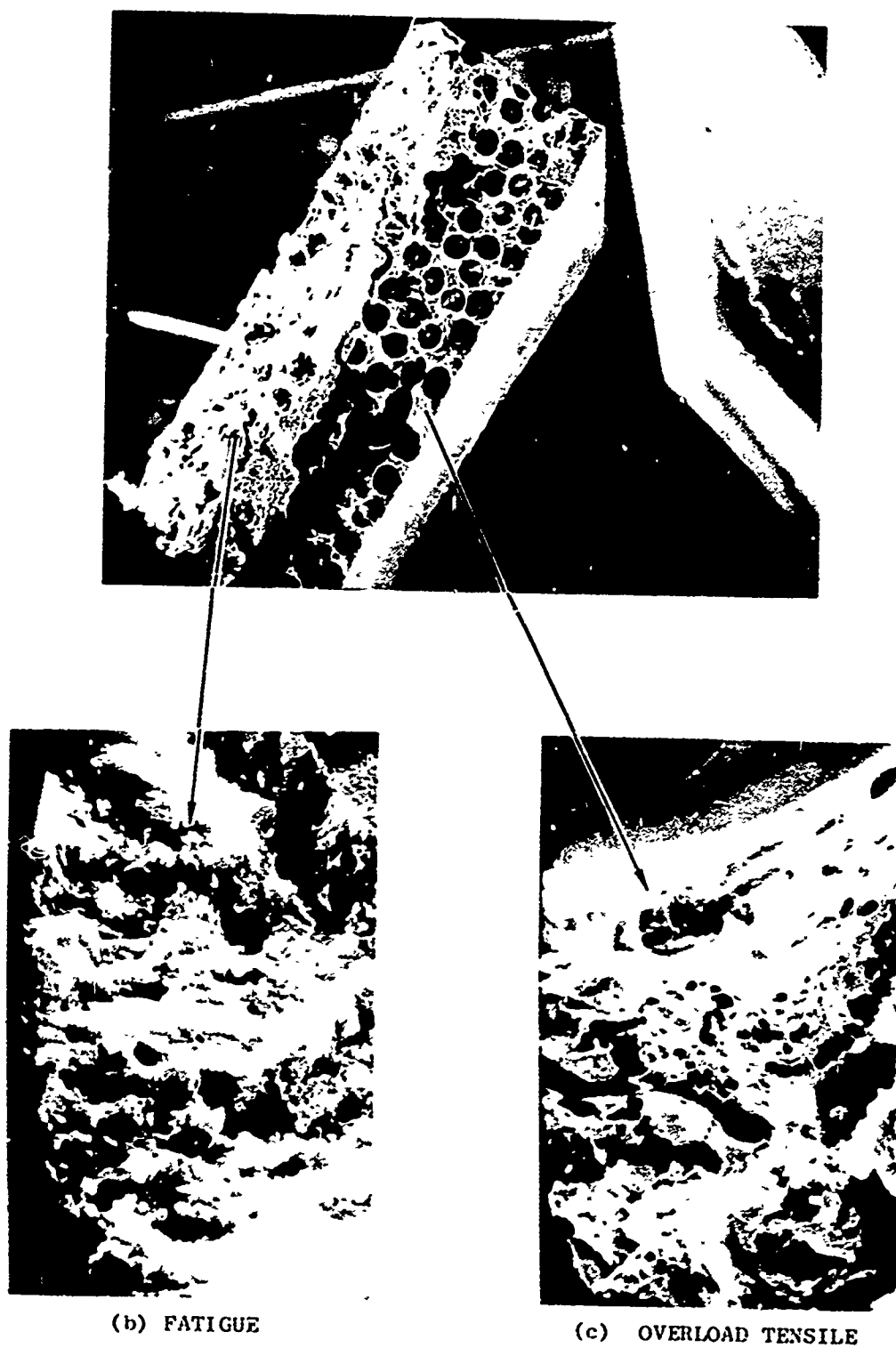
Figure 48   Fractography of an Axial Fatigue Specimen : (a) 27 X, (b) 1425X, (c) 1350X
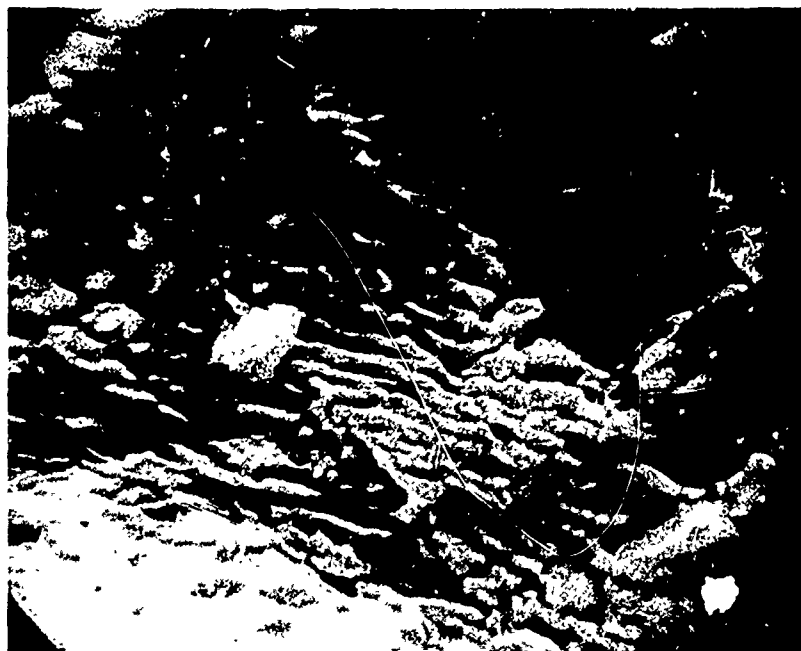
Figure 49   Fatigue Striations in Aluminum Matrix of B/2024 Specimen
Tested at 75F (6800X)
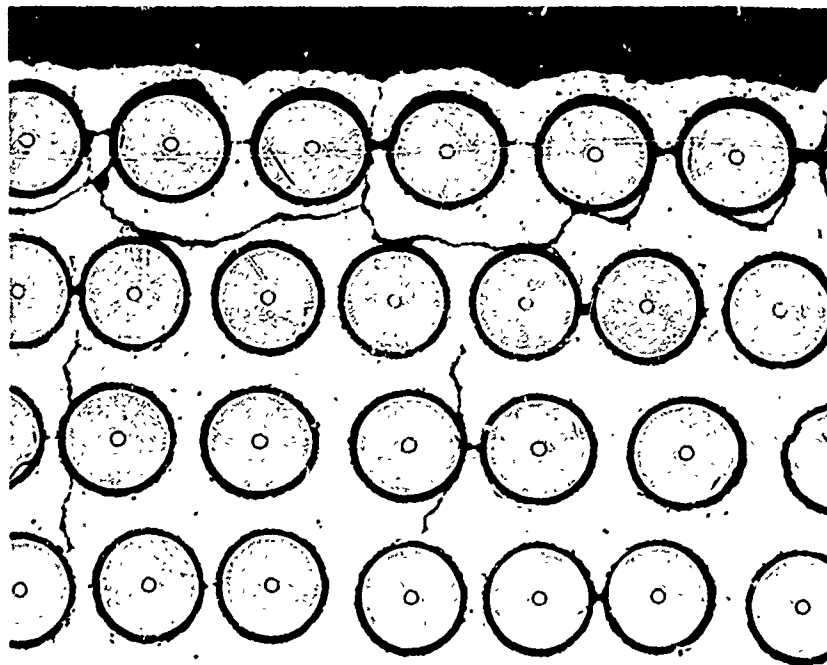
Figure 50   Fatigue Damage in a B/6061 Specimen Subjected to Axial Loading (100X)

C. Flexural Fatigue

All flexural tests were conducted on a Sonntag SF-01 Universal Fatigue Machine which has a capacity of 200 lbs static ± 200 lbs dynamic. Operating frequency is 30 Hz. The bending moment was applied to the specimen through a four point bending fixture with a 2.0" lever ratio and a 2.87" free span between grips. The test machine and fixture were calibrated prior to testing by dynamic readout of a strain gaged beam clamped in the specimen grips.

The test specimens were instrumented with chromel alumel thermocouples fixed to the specimen with RTV-106 silicon rubber. Temperatures were monitored throughout the test.

The chamber surrounding the specimen was supplied by compressed air passed through a stainless steel heat exchanger. The dynamic flow of air gave uniform temperature distribution across the gage section. The mechanical interlocks were set to automatically stop the machine when the fixture amplitude increased 15%. This was set as the failure criterion.

Flexural fatigue results are listed in Table XXIV and are plotted in Figures 51 and 52. The failure criterion was not specimen fracture but 15% change in gauge section deflection from that of cycle 1. Results are consistent and show the same trends in strength as did the axial fatigue tests. Stresses are those calculated for a beam in four point bending. Below, in Table XXV, are the estimated fatigue limits at 10^7 cycles using the above criterion for failure:

TABLE XXV. FLEXURAL FATIGUE LIMITS (ksiDa)

	B/2024	B/6061
75F	86	92
300F	77	71
600F	52	42

As can be seen in Figures 53 and 54, flexural fatigue damage occurs as fatigue cracking in the outer 22 plies. As sufficient cracks form, the compliance of the specimen increases and "failure" occurs. Damage is confined to the area of the outer most ply. Figure 55, indicates that fatigue cracks grow between the first and second layers of filaments, the region where matrix stress is greatest; reaching the surface where conditions are right. As can be seen, no damage occurs toward the interior. As mentioned in the previous section, fatigue performance is strongly a function of matrix strength, and fatigue limits follow precisely the same pattern as seen in axial fatigue. Namely, the B/6061 has a slight advantage at 75F, the B/2024 property is diminished only slightly at 300F being greater than that of the B/6061 material. At 600F, B/2024 is clearly superior.

TABLE XXIV. FLEXURAL FATIGUE RESULTS OF B/2024 AND B/6061 COMPOSITE MATERIAL SPECIMENS IN FOUR POINT BENDING

Specimen Number	Temp. (F)	Max. Calculated Stress (ksi)	Cycles (x 10^3) to 15% Increase in Deflection	Results
A-48	75	40	10,010	Runout
A-49	75	60	275	Failure
A-50	75	50	1,463	Failure
A-51	75	45	4,937	Failure
A-52	300	50	490	Failure
A-53	300	40	7,872	Failure
A-54	300	45	1,378	Failure
A-55	300	38	8,962	Failure
A-56	600	28	5,547	Failure
A-57	600	40	270	Failure
A-58	600	30	3,431	Failure
A-59	600	25	12,445	Runout
A-60	600	35	356	Failure
B-49	75	48	6,897	Failure
B-50	75	60	164	Failure
B-51	75	44	10,454	Runout
B-52	75	54	508	Failure
B-53	300	40	2,362	Failure
B-54	300	50	932	Failure
B-55	300	45	2,314	Failure
B-56	300	38	7,479	Failure
B-57	600	22	5,566	Runout
B-58	600	40	110	Failure
B-59	600	30	683	Failure
B-60	600	25	2,595	Failure
B-61	600	20	10,744	Runout
B-62	600	50	11	Failure

CYCLES TO FAILURE
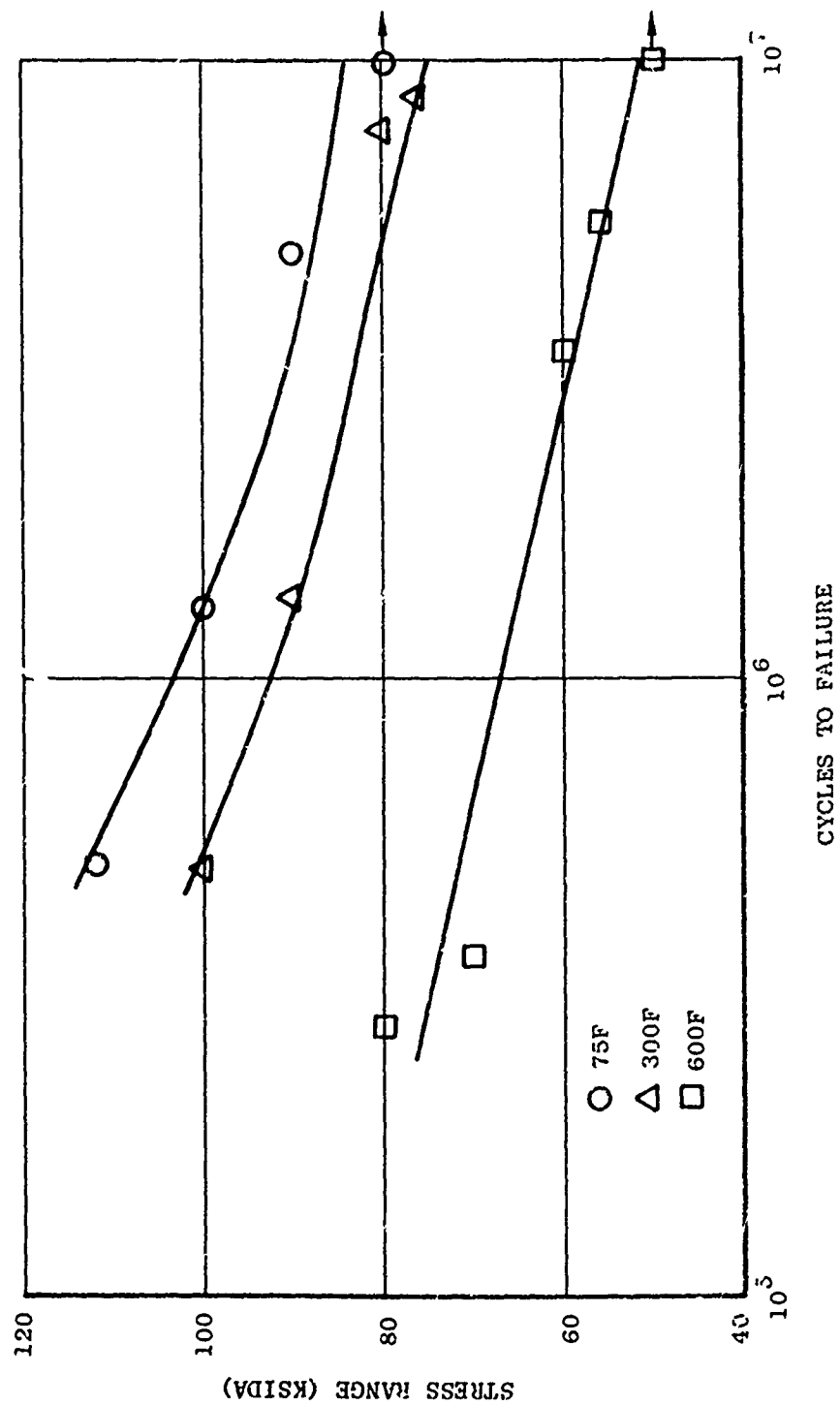
Figure 51   Flexural Fatigue Results of B/2024 Al at 75F, 300F and 600F (A=∞)

93
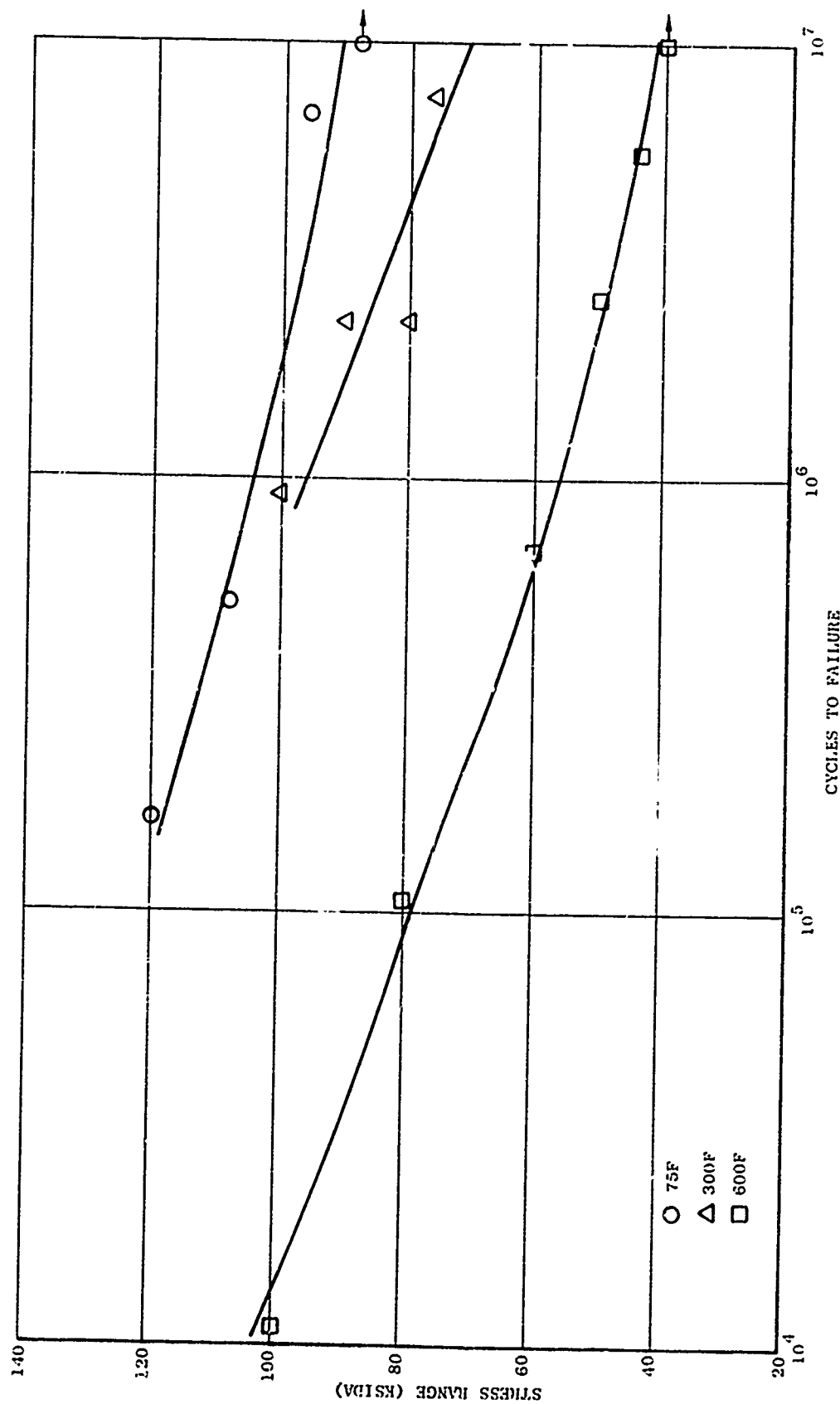
Figure 52   Flexural Fatigue Results of B/6061 Al at 75, 300 and 600F (A=∞)

94
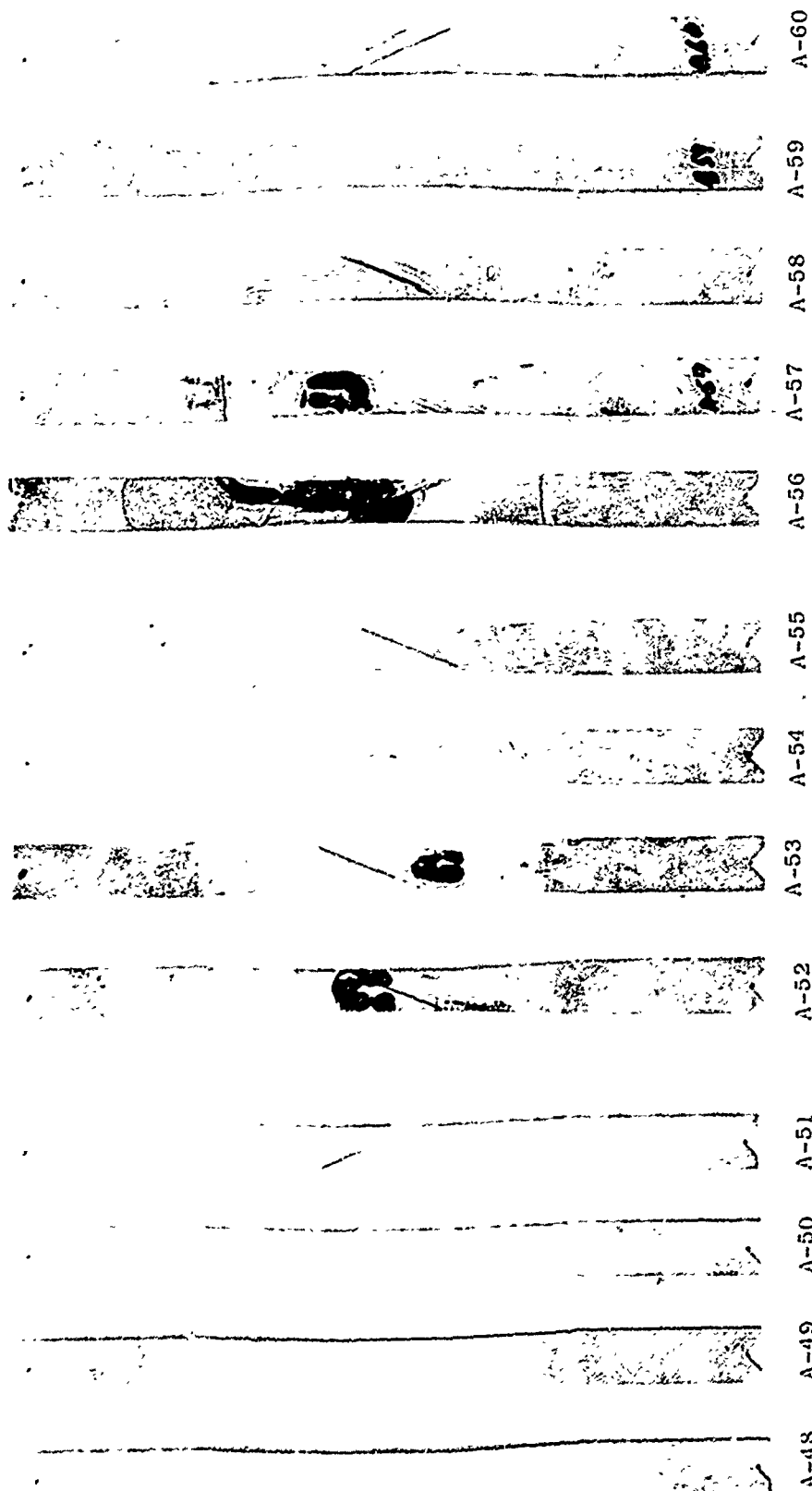
Figure 53 B/2024 [22/0/-22/0]8 Specimens After Flexural Fatigue Testing at 75, 300 and 600F

95
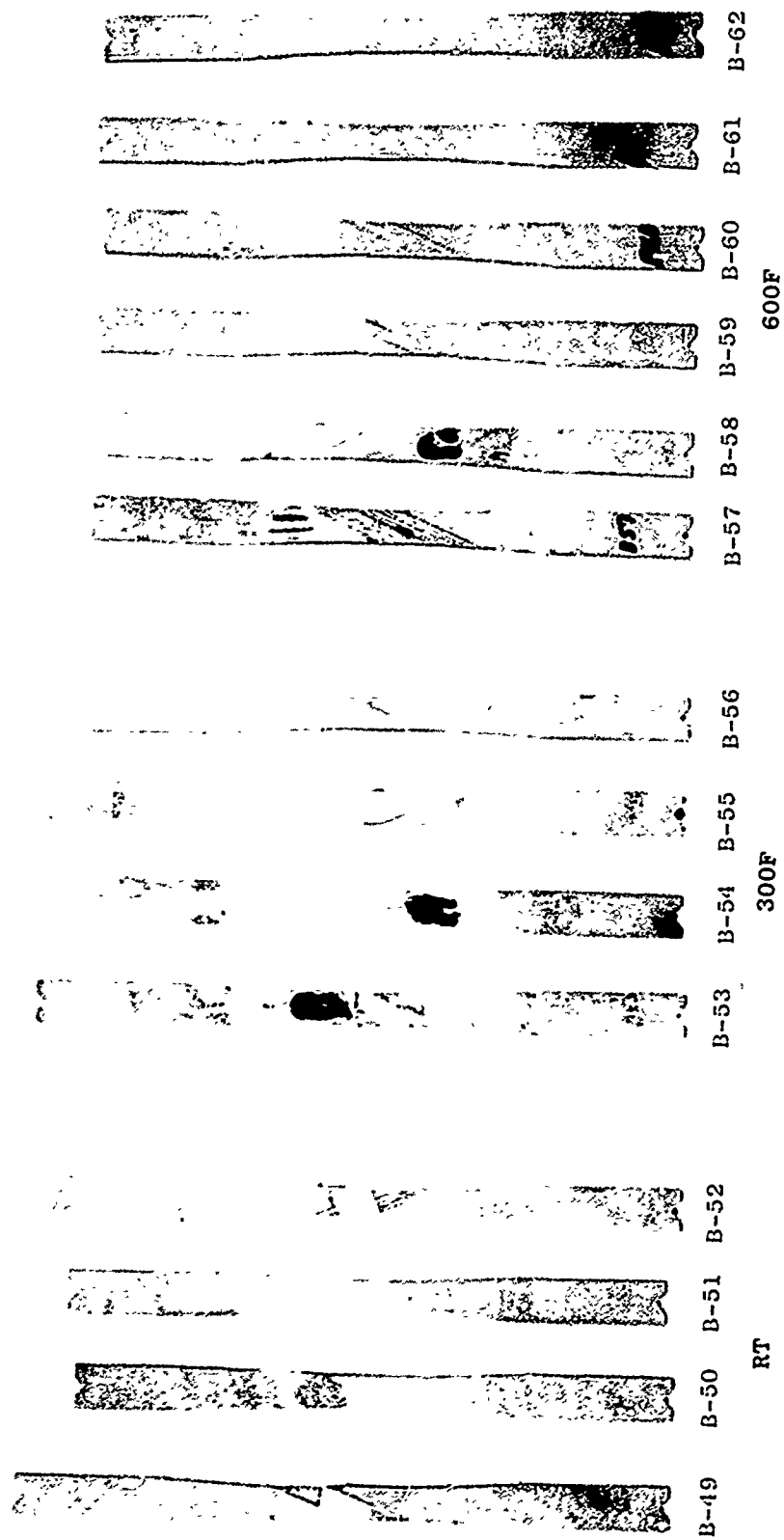
Figure 54 B/6061 [22/0/-22/0]8. Specimens After Flexural Fatigue Testing at 75, 300 and 600F

96
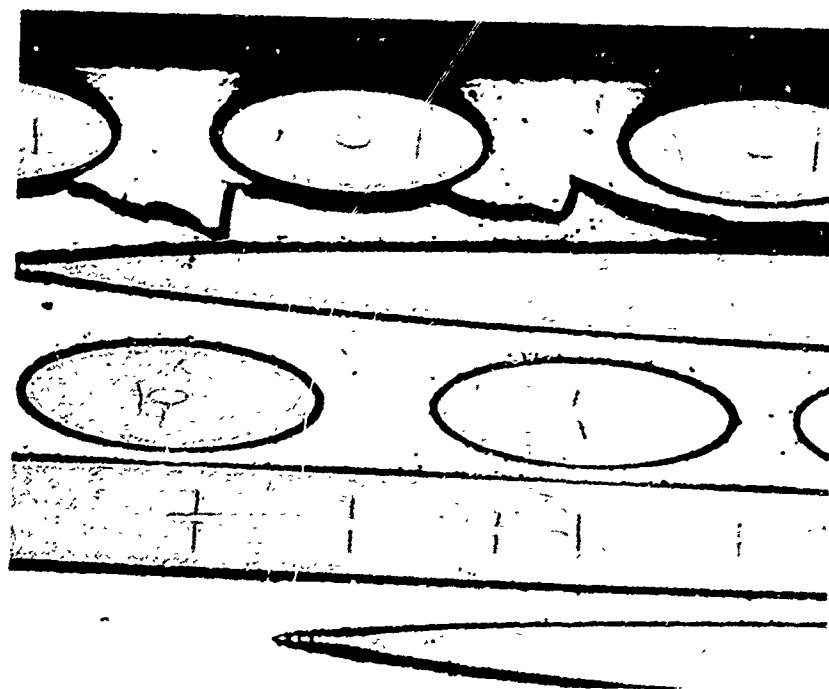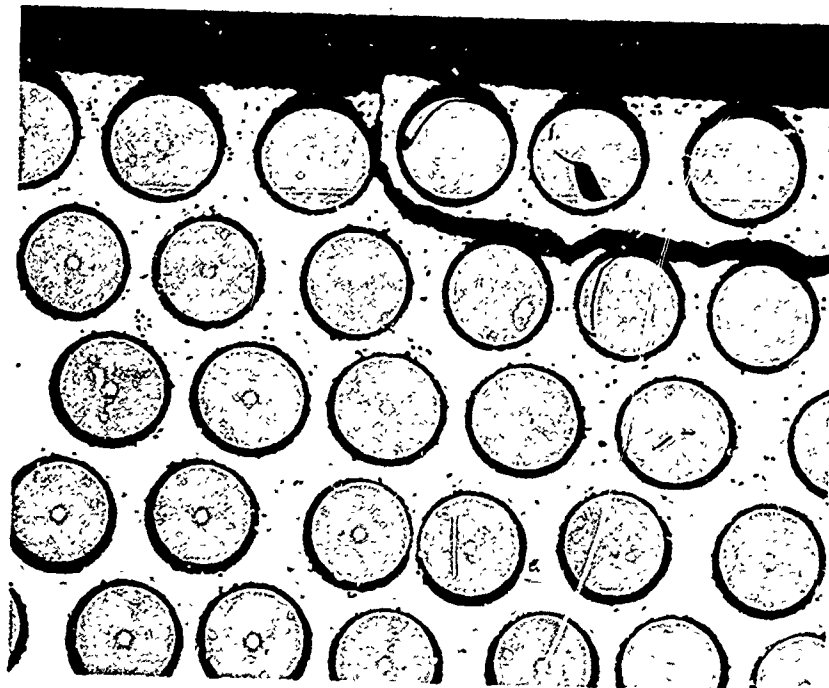
Figure 55   Photomicrographs Showing Damage Caused by Flexural Fatigue (Top Transverse Cross-Section; Bottom, Longitudinal) (100X)

D. Compression

Compression testing was conducted at 75F on B/2024 and B/6061 systems along with additional testing on 2024 Al/304 SS mesh material being used for B/Al blade dovetail bulking at GE/MPTL. Originally this portion of the program had been intended to investigate the compressive creep properties of the materials in question, but preliminary tests indicated that no significant creep would be obtained at loads of which the testing stands were capable of withstanding.

In order to obtain some information it was decided to compressively load specimens in a universal testing machine as shown in Figure 56. The specimens were oriented such that all filaments were parallel to the platens (which differs from previous work where filaments were perpendicular to the platens). Each specimen was instrumented with five (5) strain gauges on each surface perpendicular to both the platens and the [0] filament axes.

1. Compression Testing

Problems were encountered in obtaining uniform cross-sectional loading. Stress-strain curves for specimens A-1 and B-2 are plotted in Figure 57. Both materials indicated a compressive modulus of approximately 22×10^6 psi. The B/2024 specimen (A-1) deformed gradually while the B/6061 specimen (B-2) had a distinct yield point. Loading was continued until shear failure occurred in the specimens at 75 ksi for B-2024 and 50 ksi for B/6061. Metallography of failed specimens is shown in Figure 58 and 59.

The 2024 Al/304 SS mesh specimens tested, Figure 60, exhibited a lower compressive modulus, $\sim 11 \times 10^6$ psi than the B. Al specimens. Plastic instability occurred at ~80 ksi. The photomicrograph presented in Figure 61 indicates a region of little deformation caused by frictional force between specimen and platen.

2. Compression After Cyclic Thermal Explosure

B/Al and Al/SS specimens were thermally cycled from -60F to +540 two thousand times and subsequently tested in compression. Stress-strain curves, Figures 57 and 60, plotted with respect to material not exposed to the thermal cycle indicate that the thermal cycling has reduced the B/2024 compressive strength. The B/6061 compressive strength does not seem to be changed from its already low level. The failure stresses in compression of the B/2024 specimen is ~65 ksi while that of the B/6061 specimen is ~56 ksi, essentially the same as before cyclic thermal exposure. The Al/SS mesh compressive behavior is also unchanged by thermal cycling.

E. Double Lap Shear

To determine the response of B/Al and Al/304 SS mesh composite materials to shear loading at long times, the double lap shear specimen, discussed in Section III, was developed. Testing was conducted at 75 and 300F to simulate blade dovetail engine conditions.
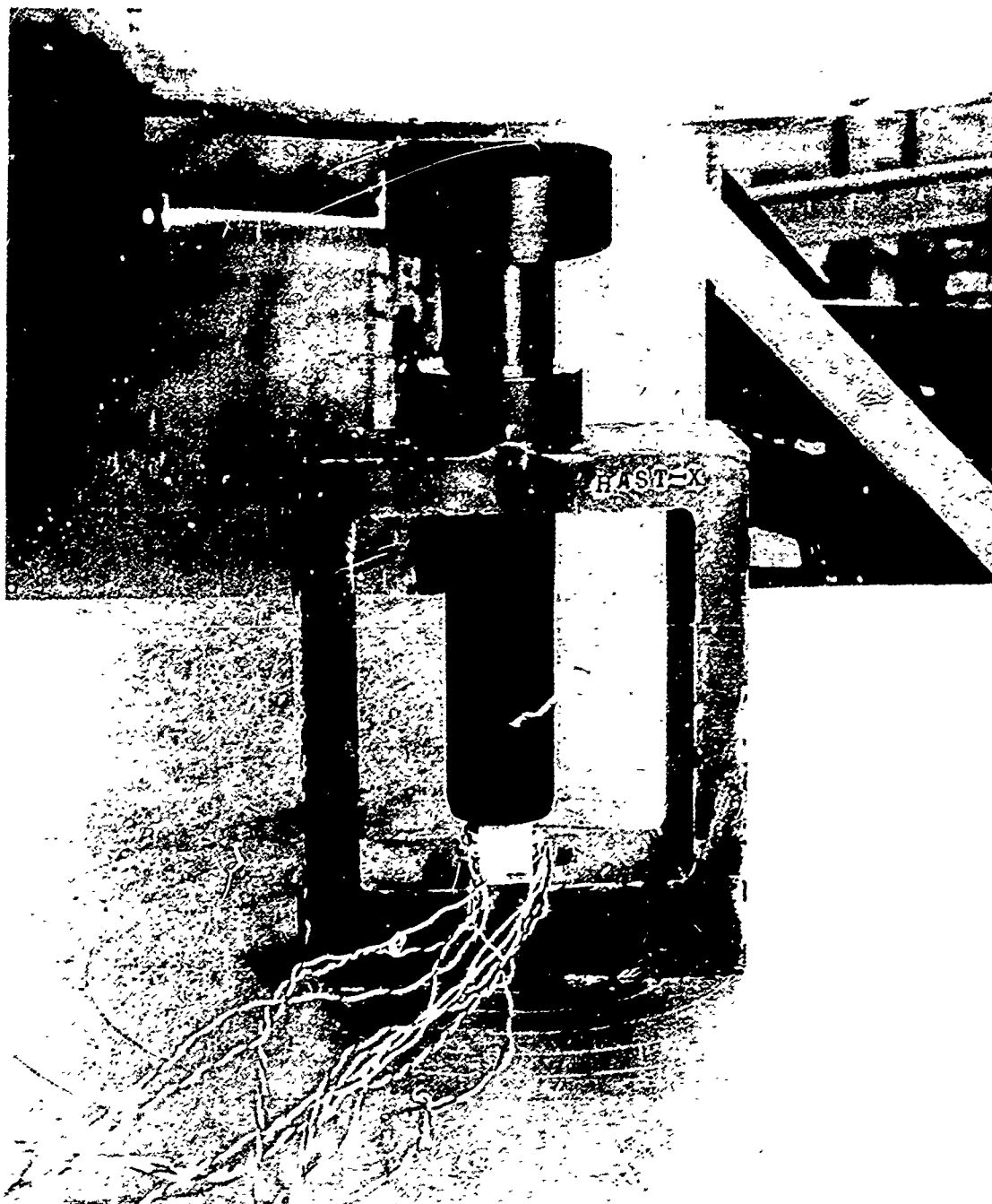
Figure 56   Compression Test Fixture

Figure 57 Comparison of B/2024 and B/6061 [22/0/-22/0]$_8$ Composite Material Behavior to Compressive Loading Before and After Cyclic Thermal Exposure, -60 to +540F Two Thousand Times

100

Figure 58   B/2024 Compression Specimen after Testing (~12X)

Figure 59   B/6061 Compression Specimen After Testing (~2X)
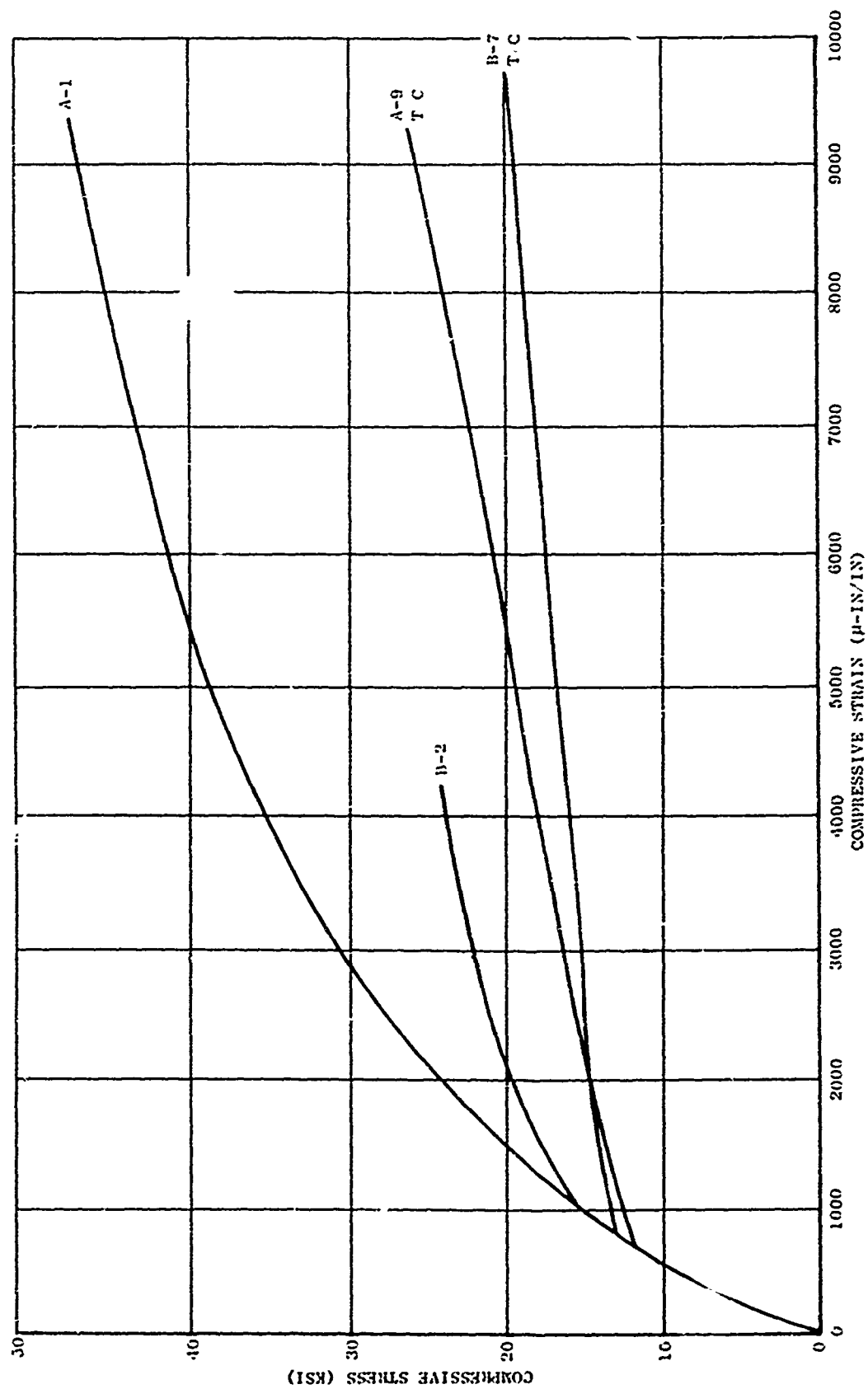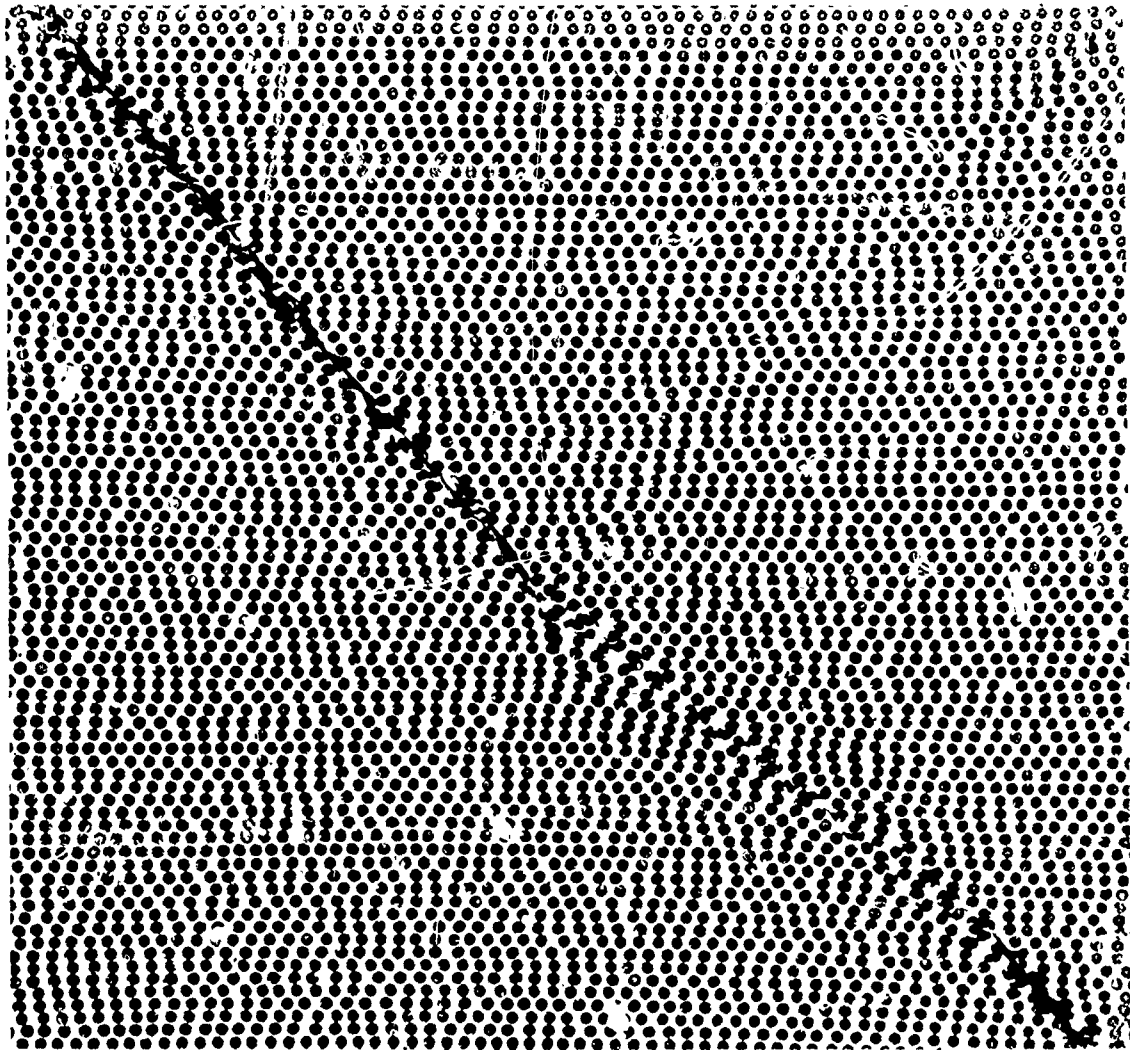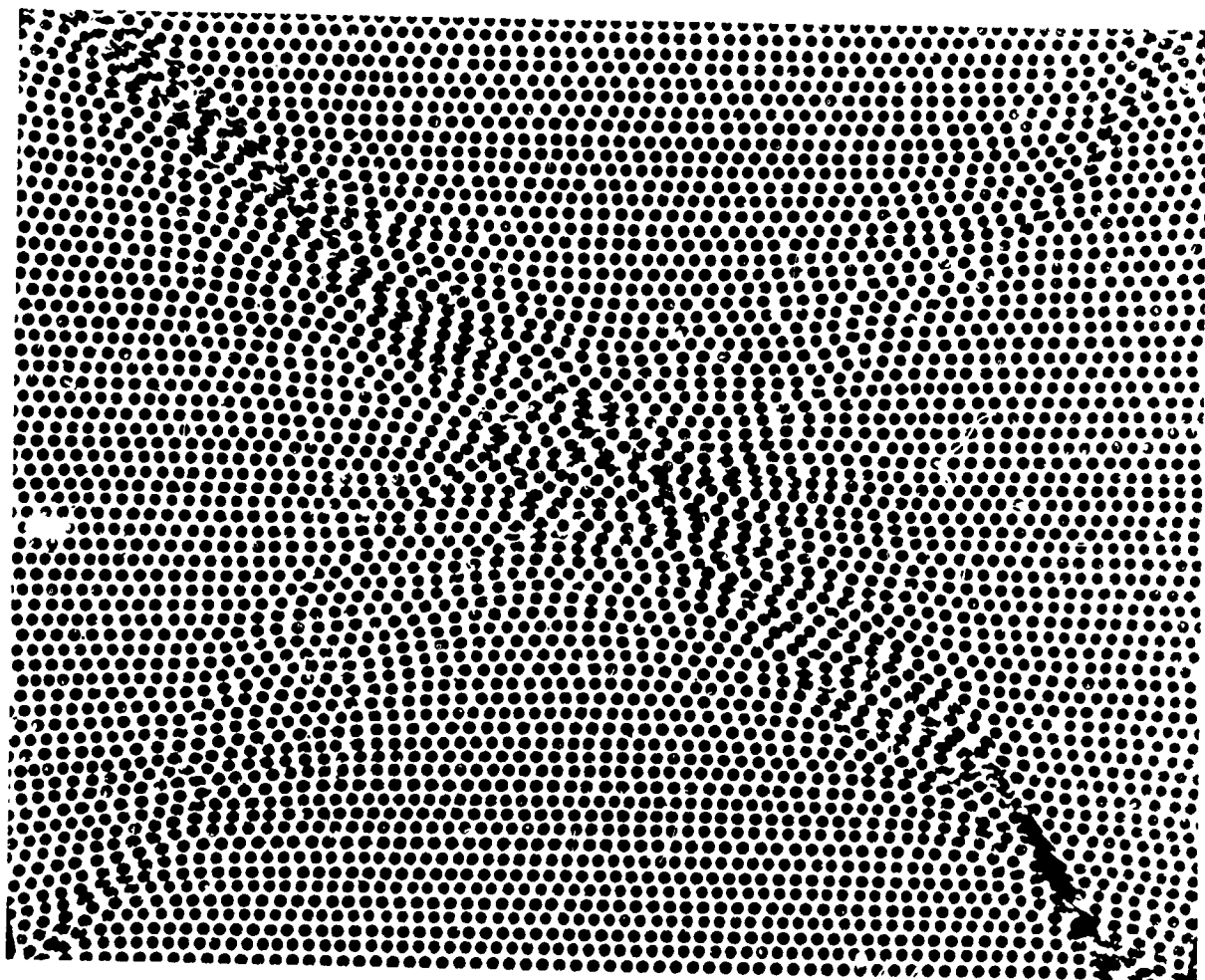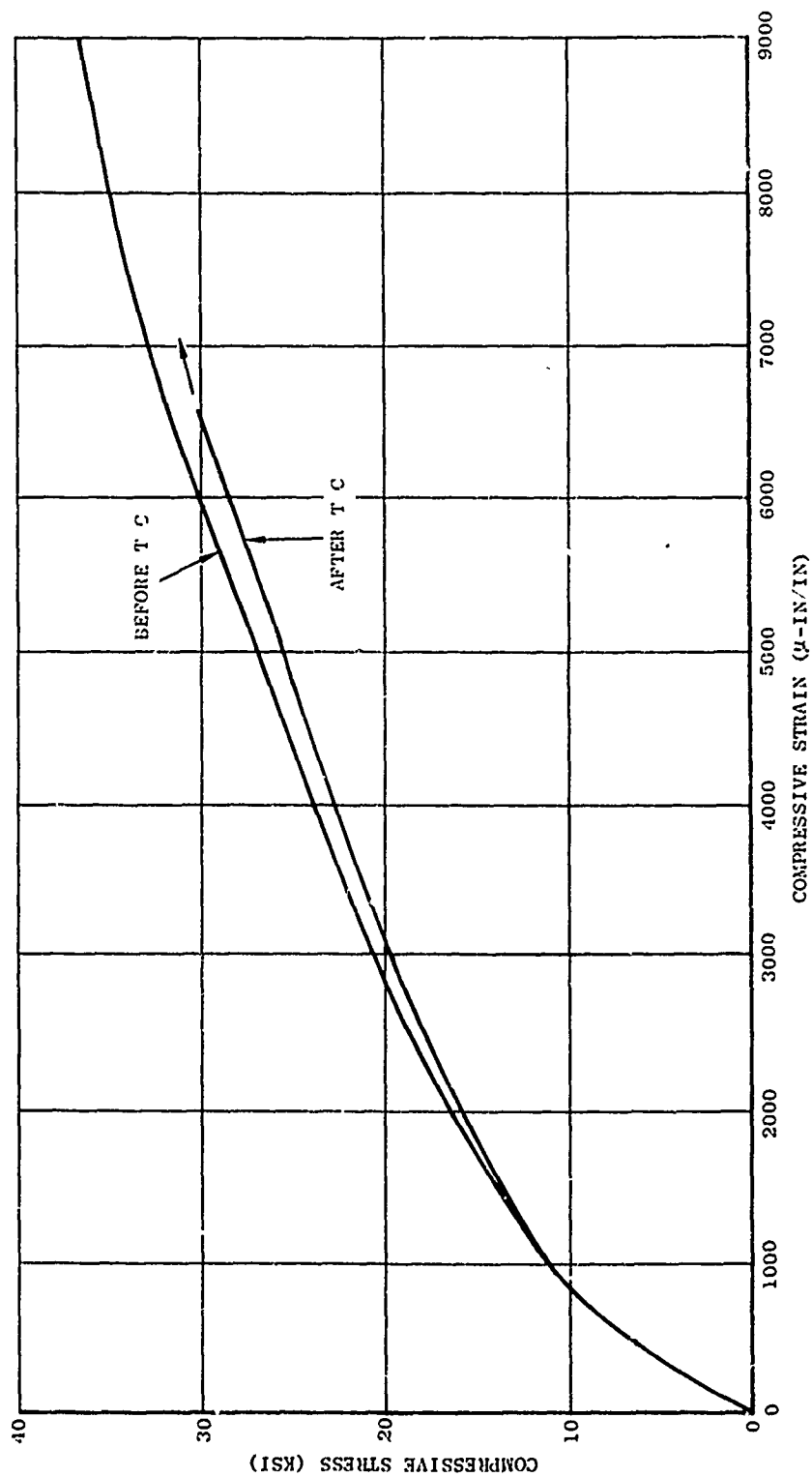
Figure 60 Comparison of 2024 Al/304 SS Mesh Composite Material Behavior to Compressive Loading Before and After Cyclic Thermal Exposure, -60F to + 540F Two Thousand Times
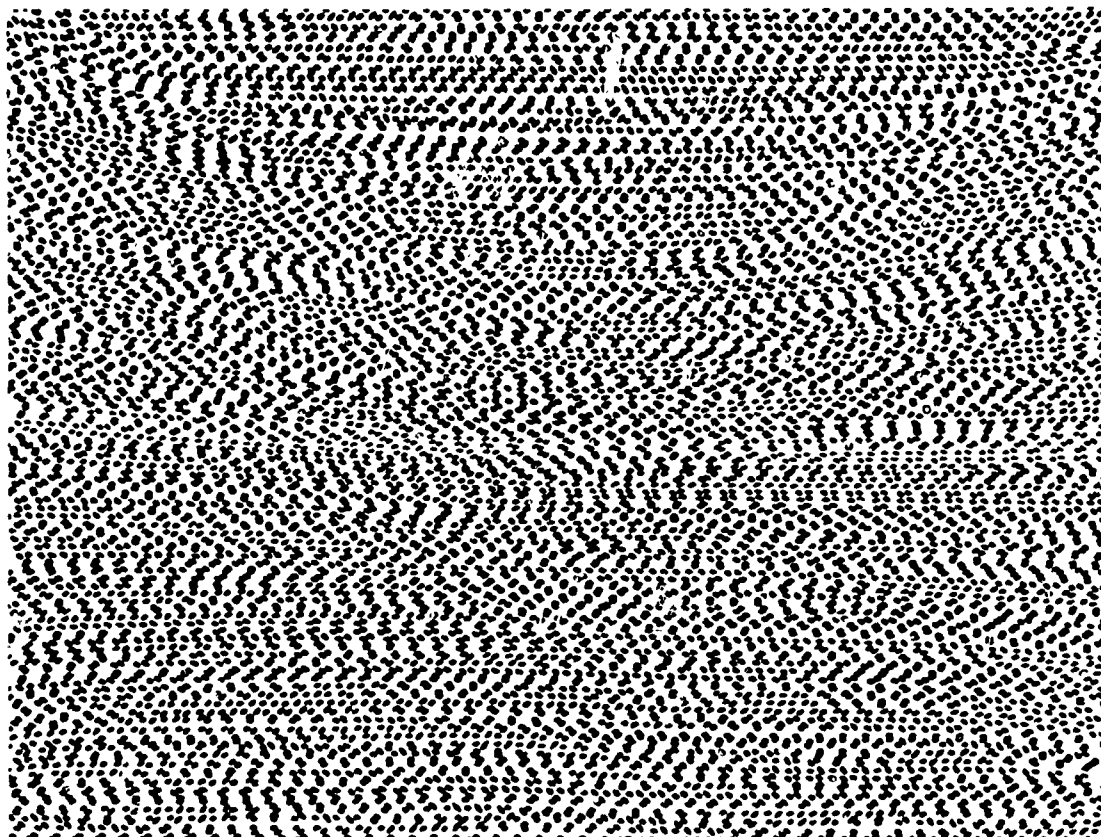
Figure 61   2024 Al/304 SS Mesh Compression Specimen After Testing (~12X)

1. Double Lap Shear Creep

Shortly after initiation of testing it was evident that obtaining meaningful creep data would be difficult. When specimens were loaded initially, they exhibited a measurable elongation which did not increase with time. Specimens were stepped to higher stresses, and failure occurred unexpectedly with little or no creep. A summary of the test data obtained is presented in Table XXVI.

2. Double Lap Shear (Short-Time)

In order to possibly obtain some useful data from the remaining specimens originally designated for creep testing; they were pulled to failure in a universal testing machine. The data obtained is presented in Table XXVII.

3. Conclusions

By examining data for both types of tests, it is clearly evident that the B/2024 has nearly twice the resistance to interlaminar shear than does the B/6061 material at 75 and 300F. The approximate values for interlaminar shear for the materials evaluated are presented in Table XXVIII.

F. Torsion Creep

To determine the relative resistance of the two B/Al composite systems under evaluation to creep caused by torsional loading, a standard torsional fatigue fixture was modified to perform the tests. The modified fixture is shown in Figure 62. The fixture consists of one fixed end and a bearing housing with sleeve ball bearings to allow free rotation at the opposite end An 8" diameter drum was fitted to the movable end. The weight was applied at the end of a cable wrapped around the drum, while the specimen was clamped between a free span of 2.85 inch. The loading drum was scribed at zero load and at various time intervals during the test. In testing, the chord length, measured between scribe lines, was used to calibrate the angle twist.

The specimen was heated by compressed air fed through a stainless steel heat exchanger. Temperatures were measured and controlled by chromel alumel thermocouples held to the gage section with RTV-106 silicone rubber.

In order to obtain baseline data, one specimen of each system was step loaded to failure at 300 and 600F. The torque-twist curves given in Figure 63 show that a surprisingly high degree of twist was obtained without apparent specimen damage. The remaining specimens were statically loaded and allowed to creep at elevated temperature. A summary of these tests is given in Table XXIX.

TABLE XXVI. CREEP TESTING OF B/Al DOUBLE LAP SHEAR SPECIMEN

Specimen Number	Material	Temp. (°F)	Test Stress (ksi)	Failure Stress (ksi)	Test Duration (hours)
A1	B/2024	R.T.	12.5	12.1	F.O.L. [a]
A2	B/2024	R.T.	8.2	11.5	193.8
A3	B/2024	R.T.	10.5	12.0	22.0
B1	B/6061	R.T.	10.0	8.8	F.O.L. [a]
B3	B/6061	R.T.	6.5	7.0	15.6
C1	Al/SS	R.T.	8.5	11.5	47.9
A5	B/2024	300	10.0	11.5	25.0
B4	B/6061	300	6.5	4.4	F.O.L. [a]
C2	Al/SS	300	10.0	6.5	F.O.L. [a]
C5	Al/SS	300	5.0	7.0	71.5

(a) Failed on Loading

TABLE XXVII. SHORT TIME DOUBLE LAP SHEAR TESTING

Specimen Number	Material	Test Temp (F)	Stress (ksi)
A4	B/2024	75	14.8
A7	B/2024	75	15.0
A6	B/2024	300	11.2
A8	B/2024	300	12.6
B5	B/6061	75	7.7
B6	B/6061	300	7.1
C3	Al/304 SS mesh	75	7.3
C4	Al/304 SS mesh	75	5.2
C6	Al/304 SS mesh	300	9.9
C7	Al/304 SS mesh	300	3.1
C8	Al/304 SS mesh	300	4.6

TABLE XXVIII. ESTIMATED[a] VALUES OF INTERLAMINAR SHEAR STRENGTH
OF B/Al AND Al/304 SS MESH MATERIAL

Material	Temperature (F)	Strength (ksi)
B/2024	75	14.5
	300	12.0
B/6061	75	7.5
	300	6.0
Al/304 SS Mesh	75	6-11
	300	3-7

[a] Based on engineering judgment from data presented in Tables
XXV and XXVI.

TABLE XXIX. SUMMARY OF TORSION CREEP TESTING OF $[22/0/-22/0]_s$ B/2024
AND B/6061 STANDARD TEST SPECIMENS AT ELEVATED TEMPERATURE

| Specimen Number	Matrix Alloy	Temp. (F)	Torque (in-lbs)	Duration (hrs)	Twist (Degrees)
A-62	2024	300	Step Loaded to Failure		107.0
A-63	2024	300	8	150.	14.6
A-64	2024	300	10	64.5	24.1
A-65	2024	300	14	89.5	39.7
A-66	2024	600	Step Loaded to Failure		101.0
A-67	2024	600	8	115.8	55.2
A-68	2024	600	6	50.2	31.2
A-69	2024	600	10	53.1	73.3
B-63	6061	300	Step Loaded to Failure		83.0
B-64	6061	300	8	101.5	11.5
B-65	6061	300	10	50.3	29.4
B-66	6061	600	Step Loaded to Failure		135.0
B-72	6061	600	8	111.4	52.9
B-73	6061	600	6	65.6	24.5
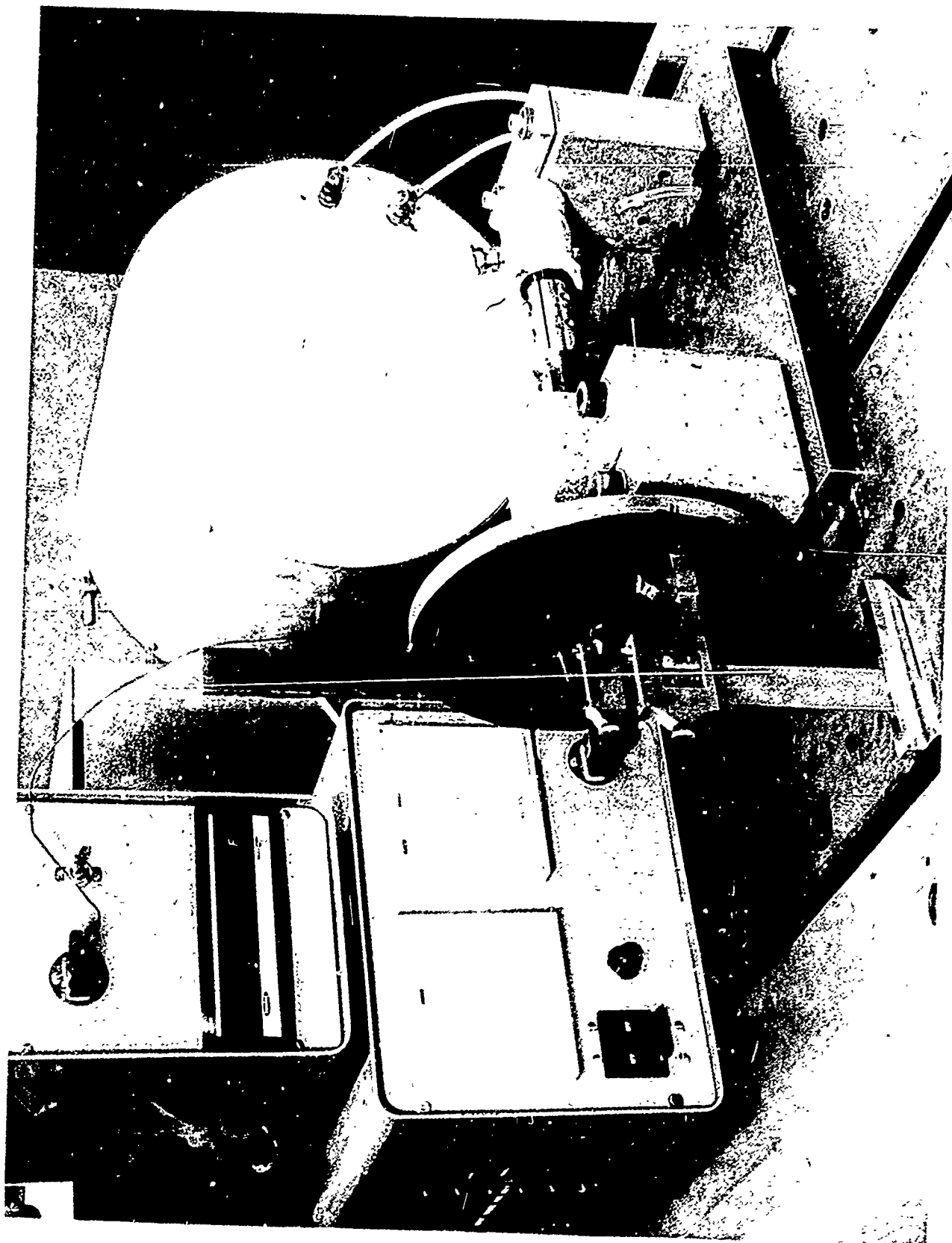
Figure 62   Torsion Creep Test Fixture
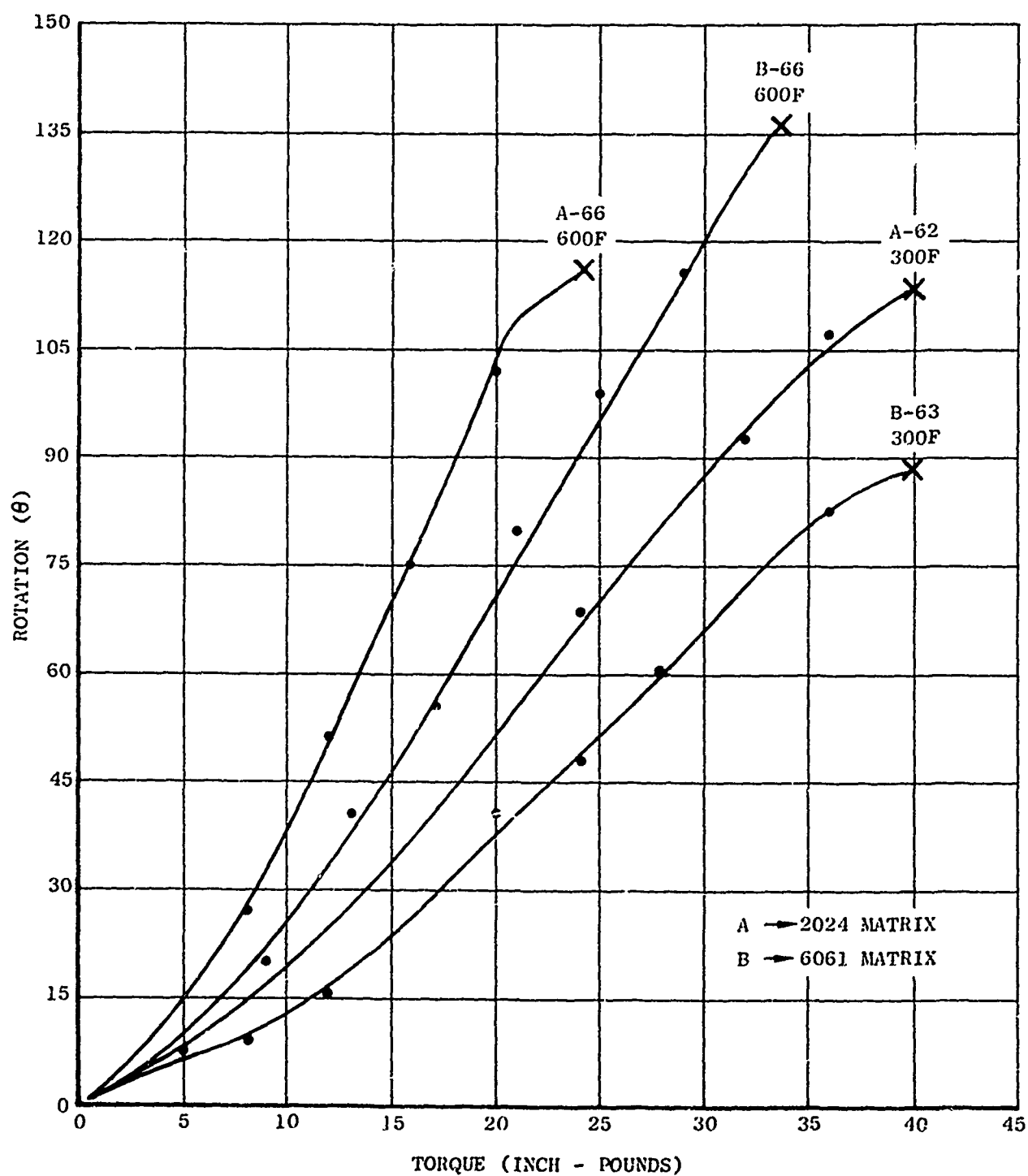
Figure 63   50 v/o [22/0/-22/0]₈ 5.6 Mil B/Al Specimens
Loaded in Torsion at 300F and 600F

One difficulty in evaluating this data is the fact that torsional stiffness in rectangular shafts is a strong function of thickness. In these specimens, the B/2024 specimens are 0.050 inches thick while B/6061 specimens are 0.059 inches. Torsional Stiffness (7) in a long rectangular shaft is

$$\frac{M_t}{\phi} \ C \ \frac{G\,ab^3}{L} \qquad \text{where}$$

M_t = Torsional moment

ϕ = Angle of twist

C = Coefficient of torsion, function of width/thickness

G = Shear Modulus

a = Width

b = Thickness

L = Length

In order to account for thickness differences in the two systems, a ratio of torsional stiffnesses yields

$$\frac{\phi A}{\phi B} = \frac{M_{tA}}{M_{tB}} \ \frac{C_B b_B^3}{C_A b_A^3} \qquad \text{where}$$

A refers to B/2024 and B to B/6061 specimens. Introducing actual dimensions.

$$\frac{\phi A}{\phi B} = \frac{M_{tA}}{M_{tB}} \ 1.65$$

At small torques and short time the B/2024 data can be normalized by using the ratio of 1.65 and then compared with B/6061. This relationship does not apply at higher torques capable of causing plastic deformation since it is based on elastic theory.

Torsion creep data of individual specimens are given in Tables XXX, XXXI and XXXII, and are plotted in Figures 64, 65, and 66. A comparison of twist at short and long times (50 hrs) is given in Table XXXIII. As can be seen, at the applied torques at 300F, all of the twist occurs shortly after load application with negligible increase at long times. At 600F a major portion of the twist occurs at short times but the creep rate does not decrease nearly as fast as at 300F.

110

TABLE XXX. TORSION CREEP DATA FOR 50 v/o B/2024 Al [22/0/-22/0]$_8$ COMPOSITE SPECIMENS AT 300F

Specimen No. A-63 Torque: 8 in/lb		Specimen No. A-64 Torque: 10 in/lb		Specimen No. A-65 Torque: 14 in/lb	
Test Duration (hours)	Angle (deg.)	Test Duration (hours)	Angle (deg.)	Test Duration (hours)	Angle (deg.)
Initial Load	4.8	Initial Load	22.9	Initial Load	36.0
4.0	12.9	0.90	23.7	0.02	36.5
27.4	13.6	14.70	24.1	1.88	37.9
45.1	14.4	25.10	24.1	3.20	37.9
120.0	14.6	39.10	24.1	16.80	38.2
150.0	14.6	48.80	24.1	27.20	38.9
		64.50	24.1	39.20	39.2
				45.60	39.3
				89.50	39.7
		Unloaded	9.7	Unloaded	19.9

111

TABLE XXXI. TORSION CREEP DATA FOR 50 v/o B/2024 Al $[22/0/-22/0]_4$ COMPOSITE SPECIMENS AT 600F

Specimen No. A-68 — Torque: 6 in/lb

Test Duration (hours)	Angle (deg.)
Initial Load	19.1
3.40	24.6
5.90	25.6
21.40	28.1
30.70	29.3
44.40	30.5
49.40	31.0
50.20	31.2
Unloaded	19.1

Specimen No. A-67 — Torque: 8 in/lb

Test Duration (hours)	Angle (deg.)
Initial Load	24.3
0.8	34.3
2.3	36.4
5.6	39.8
19.3	43.6
29.7	46.7
44.0	49.3
51.8	50.6
67.7	50.8
73.9	52.2
115.8	55.2
Unloaded	38.9

Specimen No. A-69 — Torque: 10 in/lb

Test Duration (hours)	Angle (deg.)
Initial Load	34.8
0.02	38.2
0.04	40.3
0.05	42.8
0.20	47.2
0.35	48.8
0.70	52.4
1.10	53.6
1.95	56.6
4.40	59.8
6.10	61.9
8.20	63.0
11.40	64.2
24.00	67.9
33.00	70.2
46.60	71.9
53.10	73.3
Unloaded	48.5

TABLE XXXII. TORSION CREEP DATA FOR 45+ v/o B/6061 Al [22/0/-22/0]$_s$ COMPOSITE SPECIMENS AT ELEVATED TEMPERATURE

Specimen No. B-64 Temperature: 300F Torque: 8 in/lb		Specimen No. B-65 Temperature: 300F Torque: 10 in/lb		Specimen No. B-73 Temperature: 600F Torque: 6 in/lb		Specimen No. B-72 Temperature: 600F Torque: 8 in/lb	
Test Duration (hours)	Angle (deg.)	Test Duration (hours)	Angle (deg.)	Test Duration (hours)	Angle (deg.)	Test Duration (hours)	Angle (deg.)
Initial Load	8.8	Initial Load	26.3	Initial Load	10.7	Initial Load	14.9
3.5	9.9	2.85	27.8	0.60	15.7	1.0	21.2
19.8	10.6	6.85	28.1	18.20	22.0	1.7	23.1
30.2	10.7	22.30	28.5	41.70	23.8	15.8	28.9
43.5	11.2	32.00	28.9	47.60	24.2	26.0	30.5
53.2	11.2	46.25	29.4	54.00	24.5	39.8	41.6
67.9	11.5	50.30	29.4	65.60	24.5	47.?	44.8
77.8	11.5	Unloaded	15.8	Unloaded	15.7	50.7	45.5
91.9	11.5					63.8	47.9
101.5	11.5					73.3	49.4
Unloaded	4.2					89.3	51.2
						97.6	51.9
						111.4	52.9
						Unloaded	40.0
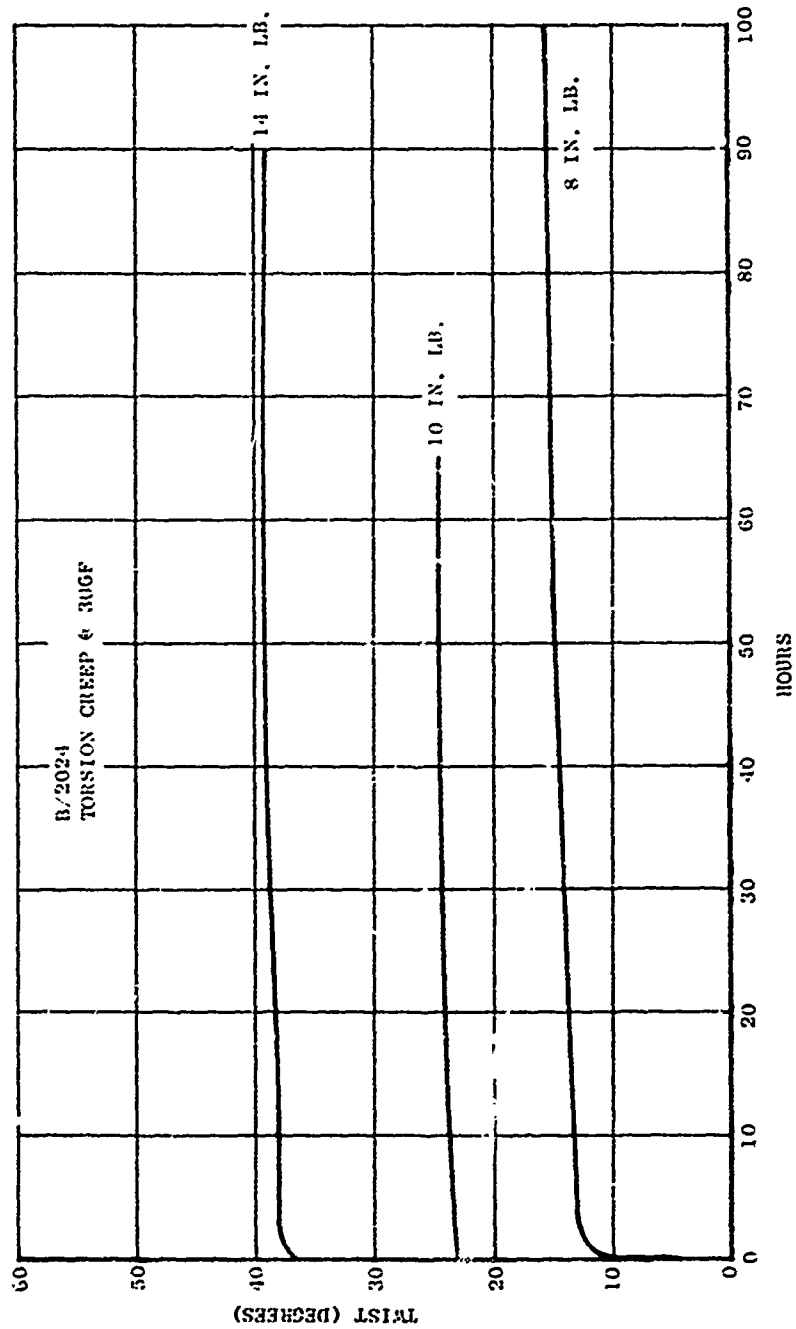
Figure 64   Torsion Creep of B/2024 [22/0/-22/0]₈ Standard Specimens at 300F

114
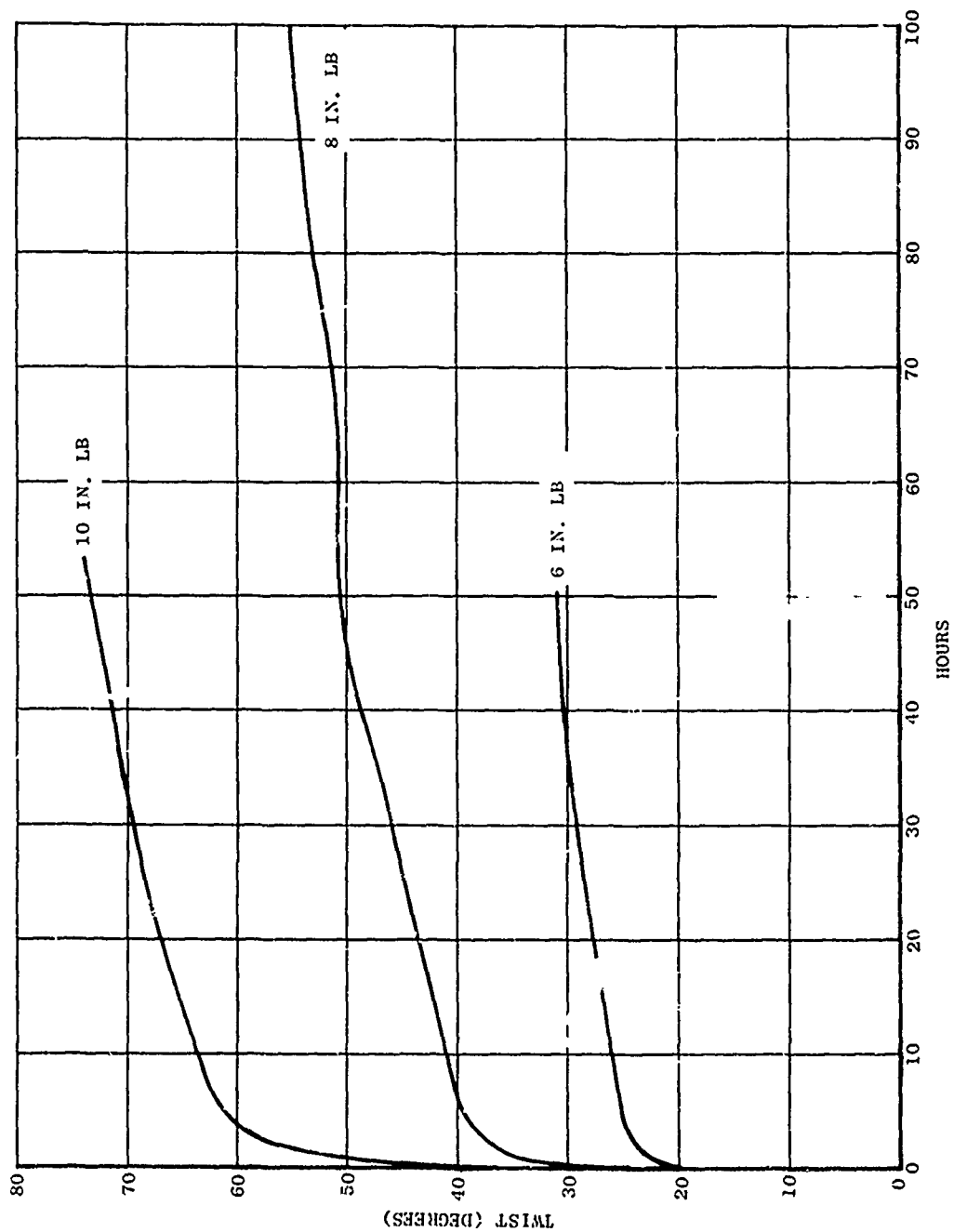
Figure 65   Torsion Creep of B/2024 [22/0/-22/0]₈ Standard Specimens at 600F

115
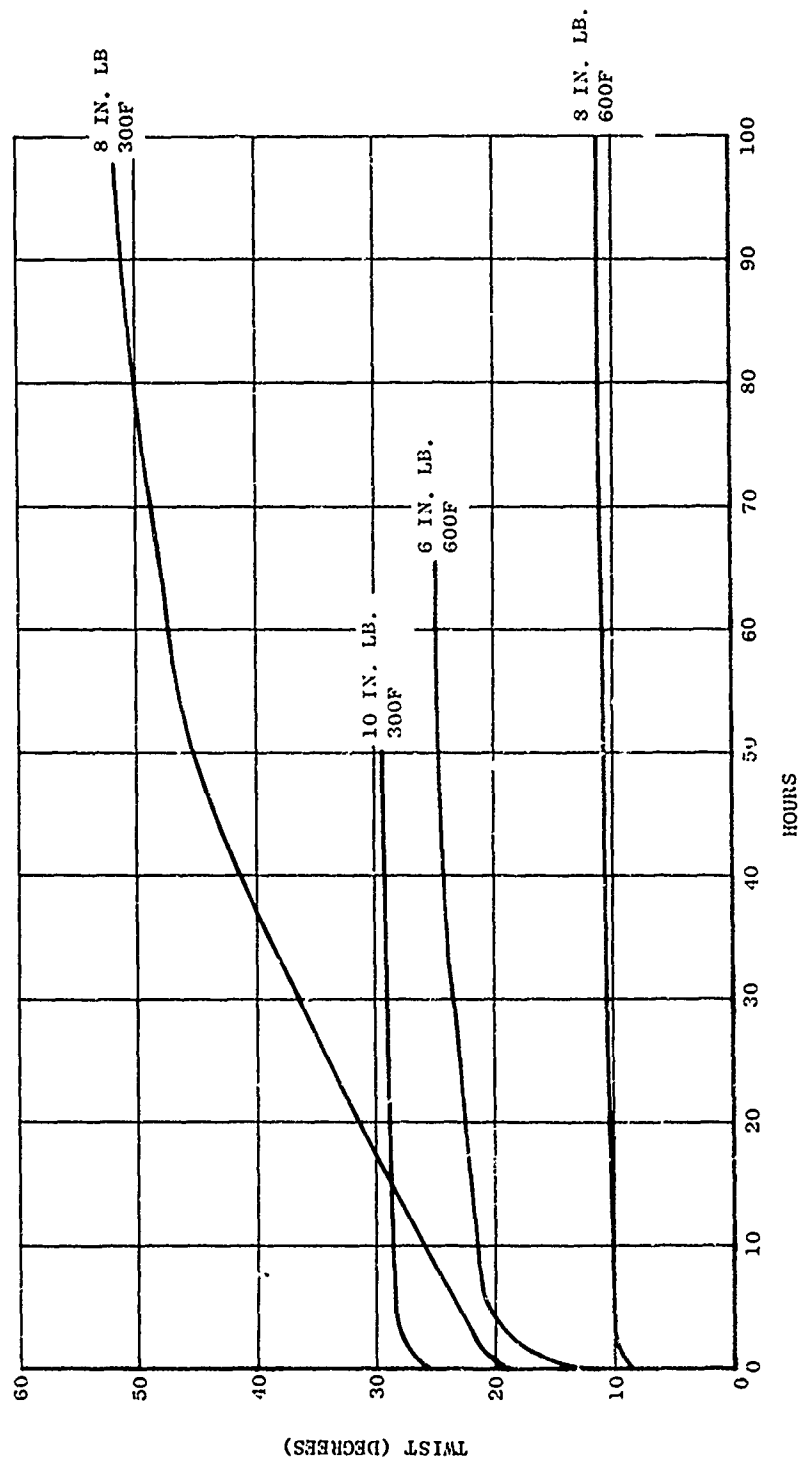
Figure 66   Torsion Creep of B/2024 and B/6061 [22/0/-22/0]₈ Standard Specimens
at 300F and 600F

116

TABLE XXXIII. COMPARISON OF TWIST FOR SHORT AND LONG TIMES AT 300F AND 600F UNDER A GIVEN TORQUE

Temperature	Torque	B/2024		B/6061	
		Static	50 Hrs	Static	50 Hrs
300F	8	13.5	14.5	9.5	11.0
300F	10	19.5	24.5	13.5	29.5
300F	14	30.0	39.0	-	-
600F	6	19.5	32.0	12.0	24.5
600F	8	27.0	50.5	18.0	45.5
600F	10	39.0	72.5	-	-

G. Stress-Rupture

Testing was conducted on standard specimens of each system using grips identical to those for tensile testing. Utilizing tensile results, test parameters were chosen to obtain 100-hour rupture lives at 300F and 600F.

Testing was conducted in a circulating hot air furnace, temperature being controlled with ± 5°F of test temperature. Temperature was measured using one control and three record thermocouples.

Stress-rupture results are presented in Table XXXIV as well as being plotted in Figure 67. It can be seen that some difficulty was encountered in testing the B/6061 material at 600F, most of the rupture lives were of short duration. The tests of the B/2024 material at 600F yield excellent results indicating a large stress sensitivity. Using this result along with that obtained by Breinan, (8), the approximate stress-rupture curves were drawn.

It is reasoned that the stress-rupture results should to some extent resemble the tensile results of each respective system. Both systems should have equivalent room temperature strengths, and at 600F, the B/2024 system should exhibit superior properties over the B/6061 system, as in fact it does. The stress for rupture at 100 hours at 600F is well defined in the B/2024 system to be 120 ksi. The analogous stress for the B/6061 system is approximately 90 ksi. The 300F case is not clear, due to the limited number of tests planned. It is thought that the B/2024 should have a longer rupture life at a given stress, but data gathered in this study does not indicate that conclusively. A selected stress of 150 ksi could be considered to be the stress necessary to cause rupture at 100 hours at 300F in both B/Al systems investigated.

118

TABLE XXXIV.   STRESS RUPTURE RESULTS OF $[22/0/-22/0]_8$ B/Al COMPOSITE SPECIMENS AT 300 AND 600F

Specimen Number	Matrix Alloy	Test Temp(F)	Stress (ksi)	Life (hr)	Failure Type
A-39	2024	300	145	216.7	(a)
A-40	2024	300	120	213.7	(b)
A-41	2024	300	170	59.7	(b)
A-42	2024	600	124	199.0	(c)
A-43	2024	600	150	FOL*	(a)
A-44	2024	600	130	10.4	(c)
A-45	2024	600	125	7.8	(a)
A-46	2024	600	122	121.2	(d)
A-47	2024	600	120	105.6	(a)
B-40	6061	300	150	11.5	(a)
B-42	6061	300	145	58.9	(c)
B-41	6061	600	50	211.9	(d)
B-43	6061	600	115	0.3	(a)
B-44	6061	600	105	1.5	(a)
B-45	6061	600	112	0.2	(c)
B-46	6061	600	130	FOL	(a)
B-47	6061	600	125	FOL	(a)
B-48	6061	600	120	0.1	(a)

(a)   Center of Gauge Section
(b)   In Grip Area
(c)   Pulled out of Grips
(d)   Unloaded without failure
 *   Failed on Loading

119

Figure 67   Stress Rupture Results of B/2024 and B/6061 [22/0/-22/0]$_8$ Composite
Material at 300 and 600F

o B/2024   300F
□ B/2024   600F
● B/6061   300F
■ B/6061   600F

120

VI CONCLUSIONS

Delineation of the fracture mechanisms and failure responses in boron/aluminum composites with regard to jet engine blading has been a prime objective of this program. The following are salient observations made during the performance of this program.

- Tensile strengths at both room temperature and 600F of the two metal matrix systems for the [0] orientation are about 185 ksi while for the [22/0/-22/0] orientation the strengths are about 150 ksi. These strengths are only slightly effected by a machined notch ($K_t = 3$). The material moduli generally follow the rule of mixture.

- Tensile failure in B/Al composites appears to occur, to a large degree, in a non-cumulative manner.

- Axial fatigue failure occurs by the process of matrix fatigue cracks linking filament failures and other fatigue cracks, thus precipitating overload failure. No macroscopic cracks were observed.

- Axial fatigue failure exhibits more delamination as the strength of the matrix is decreased.

- Flexural fatigue damage occurs as delamination of the outer plies by interlaminar and interfilamentary fatigue crack growth and the lower strengths attributable to the off axis (22°) outer ply panels.

- B/Al composites can withstand substantial torsional strain at elevated temperatures, apparently without harming properties.

- Stress-rupture curves exhibit a shallow slope with the stresses necessary to cause failure in the B/2024 material being in the neighborhood of the UTS.

- Cyclic thermal exposure damage appears to be a function of matrix fatigue resistance. The exposure to 2000 cycles from -60F to 540F apparently lowers the fatigue strength.

- Acoustic emission by filament damage in B/Al does not completely describe tensile failures, but this technique does provide some insight on the failure mechanism.

- B/Al materials can withstand compressive stress in excess of 50 ksi in the short transverse direction before failing in shear.

- Hard body ballistic impact causes internal filament damage in addition to the apparent surface damage and reduces the fatigue strength more than the static strength.

- The two composite systems, B/2024 and B/6061, show essentially equal tensile, axial fatigue and flexural fatigue properties at room temperature. The higher temperature properties of the B/2024 system are superior to those of the B/6061 System.

- Evaluation of the basic raw material tapes indicates that the continuous roll bonded (CRB) tape is equivalent, if not superior to the commercially available B/Al tapes.

121/122

VII RECOMMENDATION

Based on these conclusions, it is recommended that additional testings be performed on blades and blade elements to further extend our knowledge of failure mechanisms. Also it is recommended that 50 v/o 5.6 mil B/2024 Al be selected over the equivalent B/6061 system for further engine blade evaluation. Additional areas that require evaluation include the effect of various layup configurations and orientations and the effect of larger B filament diameters on the behavior of these metal composites. More extensive work is necessary on blade elements and actual compressor blading to optimize material properties to withstand both hard and soft body ballistic impact.

VIII. REFERENCES

(1) Peterson, R.E., *Stress Concentration Design Factors*, John Wiley & Sons, N.Y., 1953.

(2) Young, J.H., Carlson, R.G., AFML-TR-70-140, 1970.

(3) Herring, H.W., NASA - TR-R-383, 1972.

(4) Rizzo, R.R., J. Comp. Mat. 3, 202 (1969).

(5) Tsai, S.W., AFML-TR-66-149, I & II, 1966.

(6) Edmonson, R.E., and Harrison. R.W., F33615-71-C-1646, 1973.

(7) Crandall and Dahl, *Introduction to the Mechanics of Solids*, McGraw-Hill, (1959) New York

(8) Breinan and Kreider, Met. Trans., 1970, Vol. 1, p. 930.

APPENDIX A

QUALITY ASSURANCE PLAN DATA SHEET

Part A: Monolayer Tape

Vendor Tape No. _____

MPTL-GE Tape No. _____

Item No.	Description	Vendor Evaluation	MPTL-GE Evaluation
Raw Material			
1.	Aluminum – type	x	
2.	Aluminum – vendor	x	
3.	Aluminum – Specification	x	
4.	Aluminum – thickness (mils)	x	
5.	Boron filament – vendor	x	
6.	Boron filament – lot No.	x	
7.	Boron filament – diameter (mils)	x	
8.	Boron filament – tensile strength (ksi)	x	
9.	Boron filament – diameter check (mils)		x
Tape			
10.	Width (inches)	x	x
11.	Length (inches)	x	x
12.	Thickness (mils)	x	x
13.	Visual examination	x	x
NDT of Tape			
14.	Low energy x-ray radiography		x
15.	Filament uniformity		x
16.	Filament count (fil/inch)		x
17.	Volume % – boron		x
Destructive Evaluation of Tape			
18.	Tape tensile test	x	x
19.	Boron filament extraction		x
20.	Avg. filament tensile strength (ksi)		x
21.	Mean filament tensile strength (ksi)		x
22.	Standard deviation		x
23.	Coefficient of variation		x
24.	Metallographic evaluation		x
25.	Area measured		x
26.	No. of Filaments		x
27.	Volume % boron		x

Part B: 8 Ply Panels

Vendor Panel No. _____

MPTL-GE Panel No. _____

| Item No.	Description	Vendor Evaluation	MPTL-GE Evaluation
Raw Material			
1.	Aluminum – type	x	
2.	Aluminum – vendor	x	
3.	Aluminum – specification	x	
4.	Thickness (mils)	x	
5.	Boron filament – vendor	x	
6.	Boron filament – Lot No.	x	
7.	Boron filament – diameter (mils)	x	
8.	Boron filament – tensile strength (ksi)	x	
9.	Boron filament – diameter check (mils)		x
Panel			
10.	Width	x	x
11.	Length	x	x
12.	Thickness (inches)	x	x
13.	Avg. ply thickness (mils)	x	x
14.	Visual examination	x	x
NDT of Panel			
15.	Thru-transmission ultrasonic C-scan (gran scale)		x
16.	Ultrasonic thickness direction velocity		x
Destructive Evaluation of Panels			
17.	Panel tensile tests	x	x
18.	Boron filament extraction		x
19.	Avg. filament tensile strength (ksi)		x
20.	Mean filament tensile strength (ksi)		x
21.	Standard deviation		x
22.	Coefficient of variation		x
23.	Metallographic evaluation		x
24.	Area measured		x
25.	Volume % boron		x

APPENDIX B
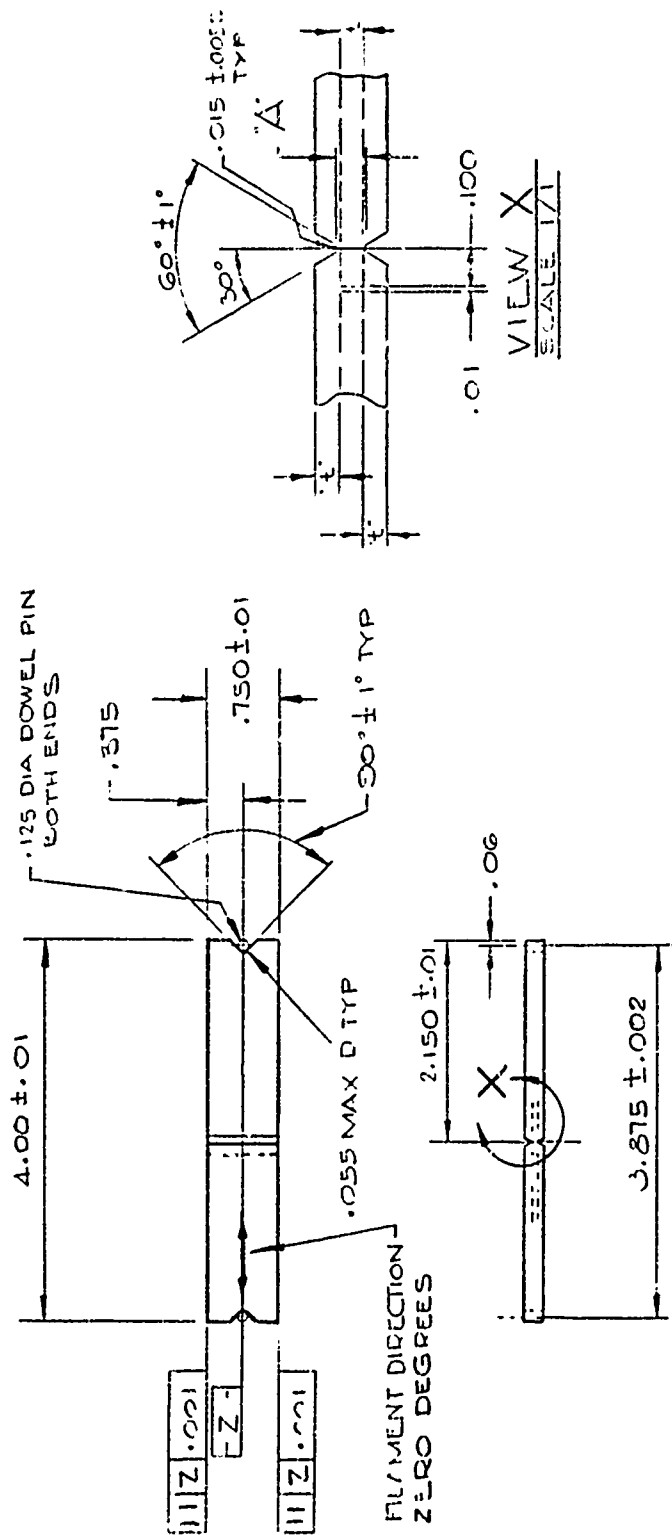
Test Specimen Configurations

130
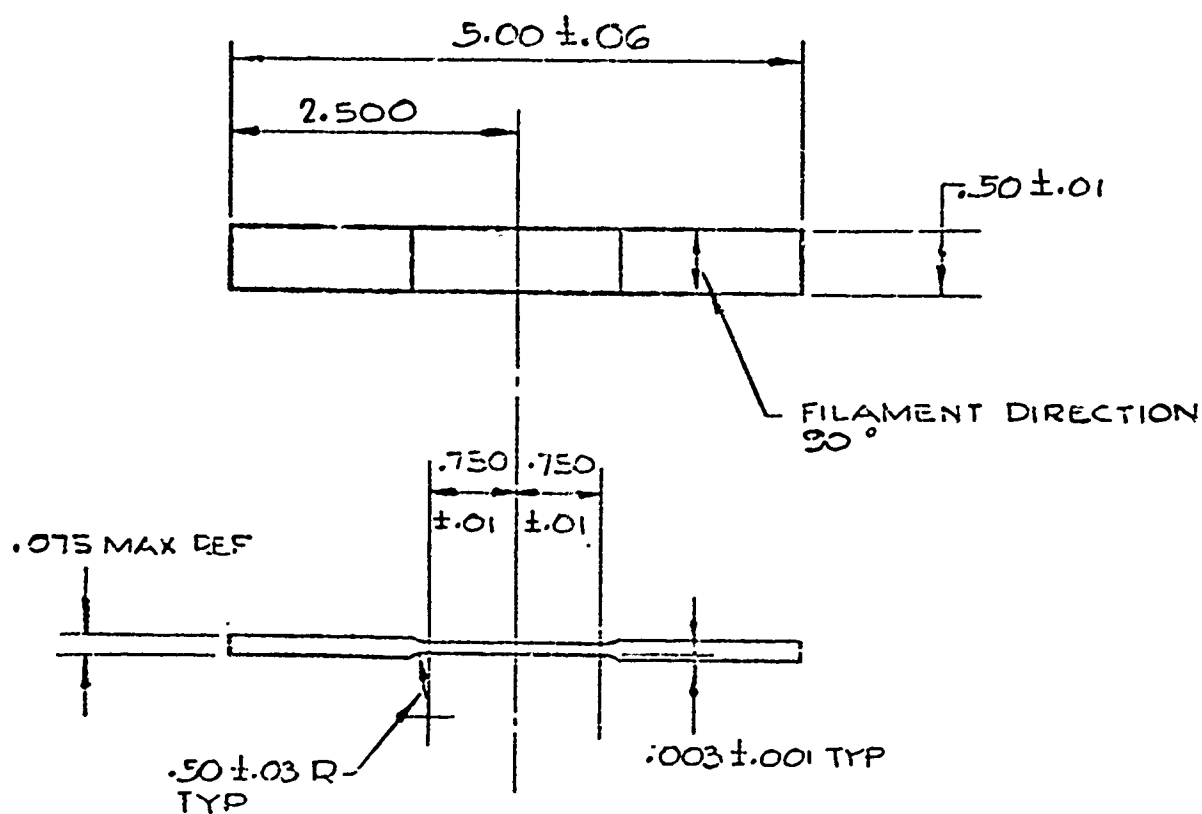
Transverse Tensile Test Specimen Configuration to be used for
Baseline Data Acquisition. Design Assumes Presence of Protective
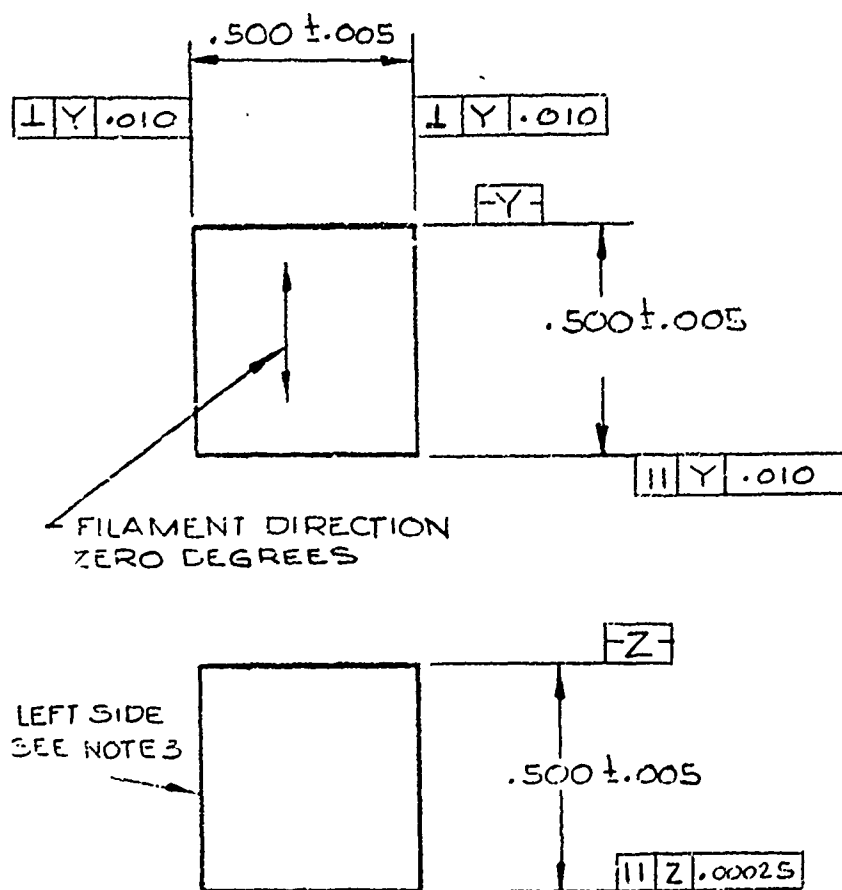Outer Surface of Stainless Steel Mesh.
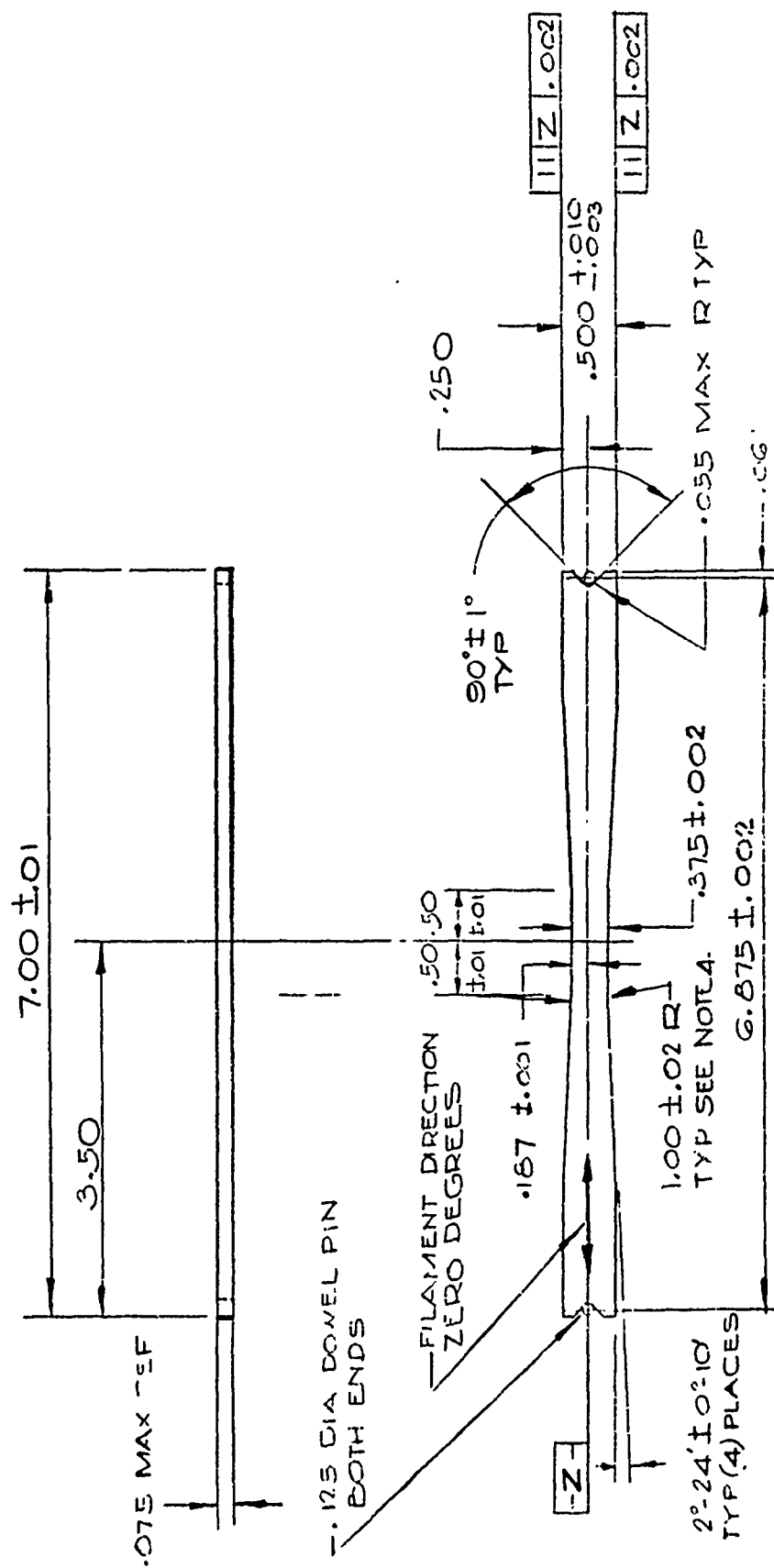
Tensile, Tensile Fatigue, and Stress Rupture Test Specimen Configuration. Design Assumes No Protective Outer Surface of Stainless Steel Mesh.

132

Notched Tensile & Notched Tensile Fatigue Test Specimen Configuration.

133

Double Lap Shear Creep Test Specimen Configuration.

Compressive Creep Test Specimen Configuration.

DISCLAIMER NOTICE

THIS DOCUMENT IS BEST QUALITY PRACTICABLE. THE COPY FURNISHED TO DTIC CONTAINED A SIGNIFICANT NUMBER OF PAGES WHICH DO NOT REPRODUCE LEGIBLY.